UCRL-TR-219380

LAWRENCE
LIVERMORE
NATIONAL
LABORATORY

Final Report: Stroke Sensor Development Using Microdot Sensor Arrays

J. C. Carter, T. S. Wilson, R. M. Alvis, C. N. Paulson, U. S. Setlur, M. T. McBride, S. B. Brown, J. P. Bearinger, and B. W. Colston

November 15, 2005

Disclaimer

Auspices Statement

This work was performed under the auspices of the U. S. Department of Energy (DOE) by the University of California, Lawrence Livermore National Laboratory (LLNL) under Contract No. W-7405-Eng-48. The project (01-ERD-101) was funded by the Laboratory Directed Research and Development Program at LLNL.

FY04 LDRD Final Report
Stroke Sensor Development Using Microdot Sensor arrays
LDRD Project Tracking Code: 01-ERD-101
J. Chance Carter, Principal Investigator

Co-Investigators
T. S. Wilson, R. M. Alvis, C. N. Paulson,
U. S. Setlur, M. T. McBride, S. B. Brown,
J. P. Bearinger, and B. W. Colston

Introduction/Background

Stroke is a major cause of mortality and is the primary cause of long-term disability in the United States. A recent study of Stroke incidence, using conservative calculations, suggests that over 700,000 people annually in this country will have a stroke.[1] Of these 700,000, approximately 150,000 will die and 400,000 will be left with a significant deficit; only one quarter will return to an independent – although not necessarily baseline – level of functioning. The costs of caring for victims of stroke in the acute phase, chronic care, and lost productivity amount to 40 billion per year.[2] Of all strokes, approximately 20% are hemorrhagic and 20% are due to small vessel disease. Thus, the number of people with large vessel thromboembolic disease and the target population of this research is greater than 400,000.

Currently, the only approved therapy for treatment of acute ischemic stroke is intravenous thrombolytic drugs. While stroke patients who receive these drugs are more likely to have better outcomes than those who do not, their improvement is highly dependent on the initiation of treatment within three hours of the onset of symptoms, with an increased risk of intracranial hemorrhage if the medication is begun outside this time window.[3] With this rigid temporal limitation, and with the concern over intracranial hemorrhage, only 2-3% of people with acute stroke are currently being treated by these means.[4]

There is ongoing research for a second treatment methodology involving the use of mechanical devices for removing the thrombus (clot) in stroke victims. Two recent reports[5,6] of a mechanical removal of thrombus, with subsequent improved patient outcome, highlight the potential of this developing technology. Researchers in the MTP are responsible for one of the photomechanical devices under FDA trials.[7,8] It is conceivable that in the near-term, a second approved therapy for treatment of acute ischemic stroke will involve the mechanical removal of the thrombus.

Stroke is a major thrust area for the Medical Technology Program (M-division). Through MTP, LLNL has a sizable investment and recognizable expertise in stroke treatment research. The proposed microdot array sensor for stroke will complement this existing program in which mechanical devices are being designed for removing the thrombus. The following list of stroke projects and their relative status shows that MTP has a proven track record of taking ideas to industry:

The goal of this LDRD funded project was to develop and demonstrate a minimally invasive optical fiber-based sensor for rapid and *in-vivo* measurements of multiple stroke biomarkers (e.g. pH and enzyme). The development of this sensor also

required the development of a new fabrication technology for attaching indicator chemistries to optical fibers. A benefit of this work is to provide clinicians with a tool to assess vascular integrity of the region beyond the thrombus to determine whether or not it is safe to proceed with the removal of the clot. Such an assessment could extend the use of thrombolytic drug treatment to acute stroke victims outside the current rigid temporal limitation of 3 hours. Furthermore, this sensor would also provide a tool for use with emerging treatments involving the use of mechanical devices for removing the thrombus. The sensor effectively assesses the risk for reperfusion injury.

Results/Technical Outcome

This report is divided into 5 individual sections, which are outlined below according to subject matter. Each section is written as a separate paper and contains results, discussions, and conclusions:

1. **Section 1: Introduction to Optical fiber-Based Sensors**
   This section provides an introduction to optical fiber-based sensing with and emphasis on photopolymerization/photodeposition fabrication methods for making multianalyte sensors.

2. **Section 2: Fabricating Optical Fiber Imaging Sensors Using Inkjet Printing Technology: A pH Sensor Proof-of-Concept**
   Inkjet printing technologies were developed and evaluated for fabricating optical fiber imaging sensors. This section describes the proof-of-concept demonstration using a non-contact (i.e. piezo-based microjet system) microdispensing technology. [J. Chance Carter et al, Biosensors and Bioelectronics 21, 1359-1364 (2006)].

3. **Section 3: Development and Evaluation of an Automated, Microdispensing Platform for Printing Sensing Arrays on Optical Fiber Image Guides** A custom contact-based microdispensing system for fabricating optical fiber imaging sensors was developed in-house. This section describes the development and evaluation of this system for fabricating optical fiber imaging sensors. [Although not included in this report, additional information on this subject may be found in (IL-10490) J. Chance Carter et.al. Method for creating chemical sensors using contact-based microdispensing technology, April 5 2004, US patent application serial number 60-559834].

4. **Section 4: Chemistry Development for Contact-based Inkjet Printing**
   Custom polymer-based indicator chemistries were developed for sensing pH and enzymes in solution. This section describes the development of acrylamide-based hydrogels, and a new class of FRET-based indicators for detecting enzymes in solution.

5. **Section 5: Development of a FRET-based Enzyme Sensor**
   Single and Multianalyte optical fiber-based FRET enzyme sensors were fabricated using the contact-based microdispensing system described in Section 3.

6. **Appendix A: Optical Fiber Preparation for Printing/Polymerization**
   A 5-step procedure is described for preparing optical fiber image guides for printing/polymerization of sensor arrays. Also included is a discussion of custom fixtures designed for preparing batches of optical fiber image guides.

7. **Appendix B: Pictures of Contact-based Microdispensing Platform**
   This section includes pictures of the contact-based platform described in Section 3.2.

Exit Plan

1. A work-for-others (WFO) project entitled "Multiplexed High-Density Bio-Agent Arrays" is now in its second year of follow-on funding [TSWG, Broad Agency Announcement 20-Q-4655, Mission Area Number and Title: Field Confirmatory Biological Analysis Requirement Number: 415/ ATL-415-TUFTSU-3470]. This project aims to develop a battery-powered, portable, array reader imaging-based system to process and analyze small volume aqueous samples for the presence of and to identify viable or dead known biological warfare agents. The array format consists of either an optical fiber or beadchip array, containing bead sensors in individual wells. The beads contain both DNA probe molecules as well as optical encoding indicators that serve as identifiers for the probe type on each bead.

2. The data obtained through this LDRD project will support an NIH-RO1 grant with expected submission in FY06/07. The proposal will focus on one of two possible applications, stroke sensors or periodontal disease sensors.

References

[1] Broderick J, Brott T, Kothari R, et al. The greater Cincinnati/Northern Kentucky stroke study: Preliminary first-ever and total incidence rates of stroke among blacks. Stroke 1998, 29:415-421.

[2] Gorelick PB, Sacco, RL, Smith DB, et al. Prevention of first stroke: A review of guidelines and a multidisciplinary consensus statement from the National Stroke Association. JAMA 1999, 281:1112-1120.

[3] The National Institute of Neurological Disorders and Stroke (NINDS) rt-PA Stroke Study Group. Tissue plasminogen activator for acute ischemic stroke. NEJM 1995, 333:1581-1587.

[4] Katzan I, Furlan A, Lloyd L, Frank J, et al. Use of tissue-type plasminogen activator for acute ischemic stroke: The Cleveland area experience. JAMA 2000, 283:1151-1158.

[5] Cerebral Embolism Task Force. Cardiogenic brain embolism: The second report of the Cerebral Embolism Task Force. Arch Neurol 1989, 46:727-743. Chopko BW,

Kerber C, Wong W, Georgy B. Transcatheter snare removal of acute middle cerebral artery thromboembolism: Technical case report. Neurosurgery 2000 Jun;46(6):1529-31.

[6] Hama Y, Kaji T, Iwasaki Y, Naeshiro H, Higo R, Shima T, and Kusano, S. Transfer of internal carotid artery thrombus to the external carotid artery using a balloon microcatheter. Neuroradiol 2000, 42:775-777.

[7] US Patent 6,022,309, Opto-Acoustic Thrombolysis, P. Celliers, L. Da Silva, M. Glinsky, R. London, D.J. Maitland, and D. Matthews, filed April 24, 1996.

[8] US Patent 5,944,687, Opto-Acoustic Transducer for Medical Applications, W. Bennet, P. Celliers, L. Da Silva, M. Glinsky, P. Krulevich, A. Lee, R. London, D. Maitland, and D. Matthews, filed April 24, 1996.

Section 1

Introduction to Optical Fiber-Based Sensors

1.1 Introduction

The combination of optical fiber technologies with conventional sensing techniques [1], [2] such as colorimetric and fluorescence methods of analysis, has led to the present day field of fiber optic chemical sensors [2-7]. The key attributes of optical fibers include their small physical size, efficient light transmitting capability, and immunity to electromagnetic interference, which allows for in-situ, remote, and real-time measurement of target analytes.

Fiber based chemical sensing has evolved into two distinct categories of intrinsic versus extrinsic sensors [8]. Intrinsic sensors utilize changes in the waveguiding (i.e. light transmitting) characteristics of an optical fiber, in response to the chemical environment surrounding the fiber. For example, in the most common types of intrinsic fiber based sensors (Figure 1.1 (a), the evanescent wave generated during total internal reflection of light along the fiber core interacts with the chemical species surrounding the core, thereby affecting the optical properties (e.g. refractive index) of the fiber. Extrinsic fiber based sensors are fundamentally different in that these utilize the fiber as a simple "light pipe" for transmitting and collecting light only. In fact, extrinsic fiber based sensors utilize fibers which have been designed to reduce or eliminate the affect of the environment on the waveguiding characteristics of the fiber. An example of the most common type of extrinsic sensor is shown in Figure 1.1 (b) in which an indicator

chemistry layer or membrane has been attached to the polished surface of an optical fiber. The indicator chemistry contains at least one light energy absorbing dye whose optical characteristics (e.g. absorption, fluorescence) changes in response to the target analyte. In this example, light is transmitted through the fiber toward the distal end where the indicator chemistry is attached. In most cases, the presence of the target analyte, alters the indicator chemistry optical properties which is transmitted via the fiber back to the proximal end where a detector monitors the signal. Alternatively, some extrinsic sensors utilize indicator chemistries, which react with the target analyte producing a biproduct with detectable optical properties [9]. The sensors developed for this project are the extrinsic type fiber based sensors, utilizing an indicator-based chemistry to indirectly measure the presence of an analyte or multiple analytes of interest. This chemistry is attached at the distal end of an optical fiber image guide (i.e. fiber bundle).

1.2 Photopolymerization/Photodeposition

Photopolymerization methods are among the earliest methods used for fiber-based sensor fabrication. In recent years, Walt et al advanced this method by demonstrating that unique patterns of indicator chemistries could be covalently attached directly to the tips of optical fiber bundles, comprised of thousands of densely packed fibers [30-31]. Specifically, these polymerized arrays of indicator chemistries were produced by immersing the optical fiber tip in a polymerizable indicator chemistry and selectively "growing" the indicator chemistries on the end of the optical fiber strands via ultraviolet radiation photopolymerization (Figure 1.4). These sensor arrays were then spatially discriminated using simple imaging techniques. Multianalyte sensors can be fabricated

by immersing the fiber tip sequentially in different polymerizable solutions followed by photopolymerization. However, the order in which the sensing elements were added to the fiber surface was critical because of cross sensitivity issues [32]. Furthermore, these arrays are non-uniform, resulting from the lack of control during the photopolymerization step. This leads to sensors that are not reproducible in their response.

Building upon Walt's work, Sections 2 and 3 of this report describe the use of inkjet printing technologies, both contact and non-contact microdispensors (Figure 1.5), for fabricating optical fiber imaging sensors by printing an array of photopolymerizable sensing elements on the surface of an optical fiber image guide.

1.3 References

[1] Angel, S.M., Kulp, T.J., Myrick M.L., Langry, K.C., 1991. "Chemical Sensor Technology Vol.3: Development and applications of fiber optic sensors." Edited by Noboru Yamazoe. Elsevier, Kodansha Ltd. P. 163-183.

[2] Hirschfeld, T., Callis, J.B., Kowalski, B.R., year?. "Chemical Sensing in Process Analysis," Science,

[3] Alder, John F., 1986. "Optical fibre chemical sensors," Fresenius Z Anal. Chem 324: 372-375.

[4] Boisde G. and Perez J.J., 1987. "Miniature chemical optical fiber sensors for pH measurements." SPIE Vol. 798 Fiber Optic Sensors II.

[5] Peterson, John, 1988. "Fiber optic chemical sensor development," SPIE Vol. 990, Biochemical and Environmental Applications of Fibers (invited paper.)

[6] Arnold, Mark A., 1992. "Fiber-optic chemical sensors," Analytical Chemistry, Vol. 64, No. 21: 1015A-1024A.

[7] Roe, Jeffrey N., 1992. "Biosensor Development," Review, Pharmaceutical Research, Vol. 9, No. 7: 835-844.

[8] O. S. Wolfbeis, Ed., *Fiber-optic Chemical Sensors and Biosensors,* (CRC press, Boca Raton, FL, 1991). vol. 1.

[9] Panova, A. A., Pantano, P., Walt, D. R., 1997. In-situ fluorescence imaging of localized corrosion with a pH sensitive imaging fiber. Anal. Chem. 69, 1635-1641.

[10] Peterson, J.I., Goldstein, S.R., Fitzgerald, R.V., Buckhold, D.K., 1980. Fiber optic pH probe for physiological use. Anal. Chem. 52, 864-869.

[11] Saari, L.A., Seitz, W.R., 1982. pH sensor based on immobilized fluoresceinamine. Anal. Chem. 54, 821-823.

[12] Gehrich, J.L., Lubbers, D.W., Opitz, N., Hansmann, D.R., Miller, W.W., Tusa, J.K., Yafuso, M., 1986. Optical fluorescence and its application to an intravascular blood-gas monitoring system. IEEE Trans. Biomed. Eng. 33, 117-132.

[13] Munkholm, C., Walt, D.R., Milanovich, F.P., Klainer, S.M., 1986. Polymer modification of fiber optic chemical sensors as a method of enhancing fluorescence signal for pH measurements. Anal. Chem. 58, 1427-1430.

[14] Jordan, D.M., Walt, D.R., 1987. Physiological pH fiber optic chemical sensor based on energy-transfer. Anal. Chem. 59, 437-439.

[15] Nivens, D.A., Zhang, Y., Angel, S.M., 1998. A fiber optic pH sensor using base-catalyzed organo-silica sol-gel. Anal. Chim. Acta 376, 235-245.

[16] Zhujun, Z., Seitz, W.R., 1984. A fluorescence sensor for quantifying pH in the range from 6.5 to 8.5. Anal. Chim. Acta 160, 47-55.

[17] Nivens, D.A., Schiza, M.V., Angel, S.M., 2002. Multilayer sol-gel membranes for optical sensing applications: single layer pH and dual layer CO_2 and NH_3 sensors. Talanta 58(3), 543-550.

[18] Brian G. Healey, Stacy E. Foran, David R. Walt, 1995. Photodeposition of micrometer-scale polymer patterns on optical imaging fibers. Science, Vol. 269, 1078-1079.

[19] Peterson, J.I., Goldstein, S.R., Fitzgerald, R.V., Buckhold, D.K., 1980. Fiber optic pH probe for physiological use. Anal. Chem. 52, 864-869.

[20] Saari, L.A., Seitz, W.R., 1982. pH sensor based on immobilized fluoresceinamine. Anal. Chem. 54, 821-823.

[21] Gehrich, J.L., Lubbers, D.W., Opitz, N., Hansmann, D.R., Miller, W.W., Tusa, J.K., Yafuso, M., 1986. Optical fluorescence and its application to an intravascular blood-gas monitoring system. IEEE Trans. Biomed. Eng. 33, 117-132.

[22] Zhujun, Z., Seitz, W.R., 1984. A fluorescence sensor for quantifying pH in the range from 6.5 to 8.5. Anal. Chim. Acta 160, 47-55.

[23] Nivens, D.A., Zhang, Y., Angel, S.M., 1998. A fiber optic pH sensor using base-catalyzed organo-silica sol-gel. Anal. Chim. Acta 376, 235-245.

[24] Munkholm, C., Walt, D.R., Milanovich, F.P., Klainer, S.M., 1986. Polymer modification of fiber optic chemical sensors as a method of enhancing fluorescence signal for pH measurements. Anal. Chem. 58, 1427-1430.

[25] Jordan, D. M., Walt, D. R., 1987. Physiological pH fiber optic chemical sensor based on energy-transfer. Anal. Chem. 59, 437-439.

[26] Ming-Ren, S. Fuh, L. W. Burgess, T. Hirschfeld, G. D. Christian and F. Wang, 1987. Single fibre optic fluorescence pH probe, The Analyst, 112 (8), 1159-1163.

[27] O. S. Wolfbeis, Ed., *Fiber-optic Chemical Sensors and Biosensors,* (CRC press, Boca Raton, FL, 1991). vol. 1.

[28] D. A. Nivens, M. V. Schiza, and S. M. Angel, 2002. Multilayer sol-gel membranes for optical sensing applications: single layer pH and dual layer CO_2 and NH_3 sensors, Talanta, 58 (3): 543-550.

[29] M. V. Schiza, M. P. Nelson, M. L. Myrick and S. M. Angel, 2001. Use of a 2D to 1D dimension reduction fiber-optic array for multiwavelength imaging sensors, *Appl. Spectrosc*., 55 (2), 217-226.

[30] S. M. Barnard and D. R. Walt, 1991. A fiberoptic chemical sensor with discrete sensing sites, Nature, 353 (6342) 338-340.

[31] B. G. Healy, S. E. Foran, D. R. Walt, 1995, Photodeposition of Micrometer-Scale Polymer Patterns on Optical imaging Fibers, Scinece, 269, 1078.

[32] J. A. Ferguson, B. G. Healy, K. S. Bronk, S. M. Barnard and D. R. Walt, 1997. Simultaneous monitoring of pH, CO_2, and O_2 using an optical imaging fiber., *Anal. Chim, Acta* 3400, 123-131.

1.5 Figures for Section 1

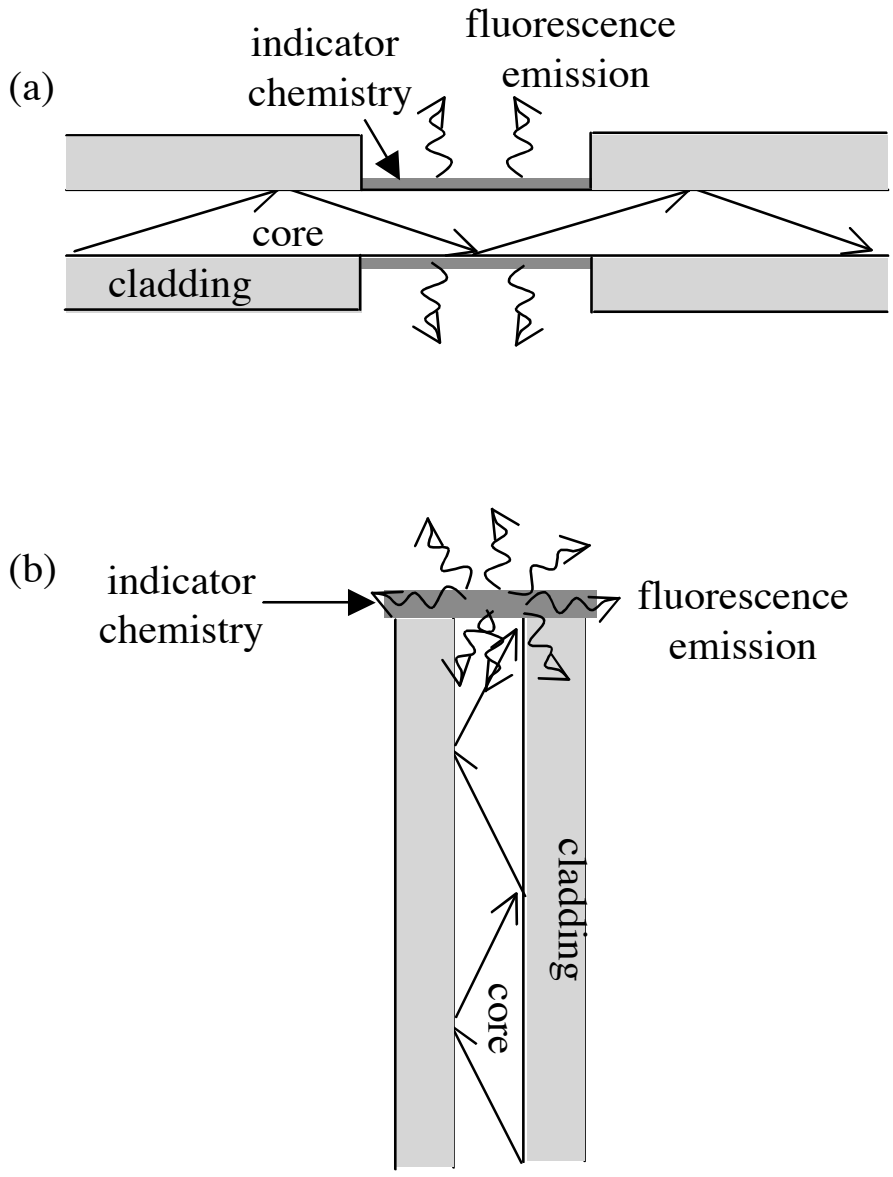

Figure 1.1: (a) As light waveguides through the optical fiber, the evanescent wave can excite an indicator chemistry (e.g. fluorescence based indicator) coated on the fiber core. In another configuration, light absorption or refractive index changes can be monitored. or absorption and/or refractive index changes can be measured. (b) Light waveguideing in an optical fiber can be used to excite an indicator chemistry (e.g. fluorescence based) immobilized on the distal tip of the fiber. A portion of the resulting fluorescence emission is collected by the same fiber and can be used to monitor the presence of a target analyte.

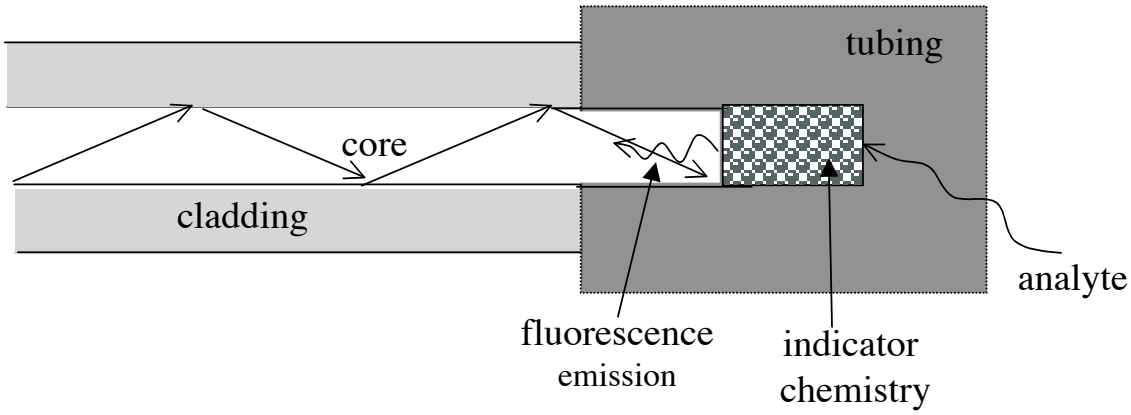

Figure 1.2: Indicator chemistries (fluorescence based) can be housed in tubing or some other device, which is mechanically attached to the distal portion of the optical fiber. The tubing allows certain analytes (e.g. gas molecules) to diffuse to the indicator chemistry resulting in, for example, a change in the optical properties of the indicator and/or the formation of a colorimetric product via a chemical reaction. Such changes are then monitored via the optical fiber.

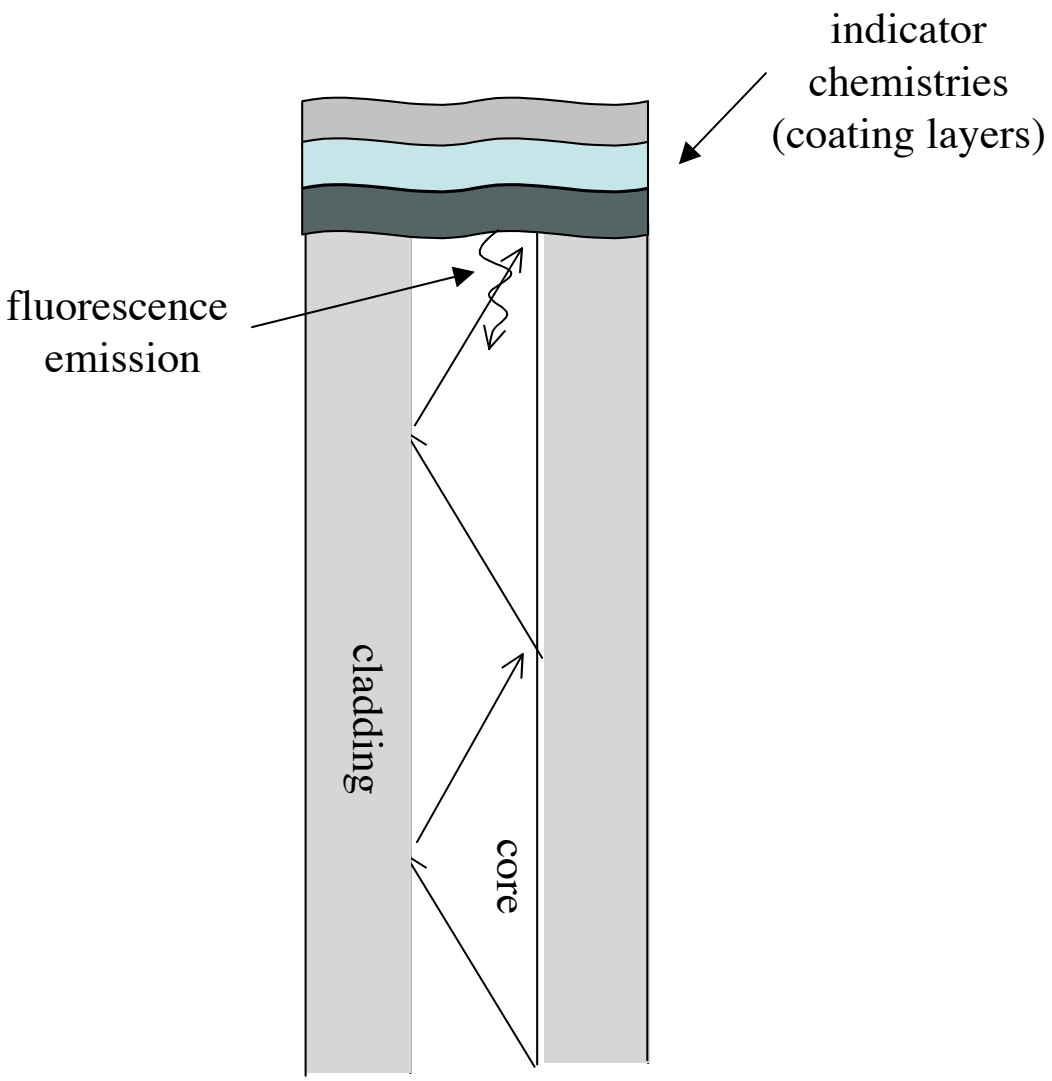

Figure 1.3: Multianalyte sensors can be prepared by dip or spin coating multiple layers of indicator chemistries, immobilized in a suitable matrix (i.e. polymer), on the fiber tip target. The target analyte(s) diffuse through the layer(s) and interact with the indicator chemistry of a particular layer and produce an optically distinct signal (e.g. fluorescence or absorption).

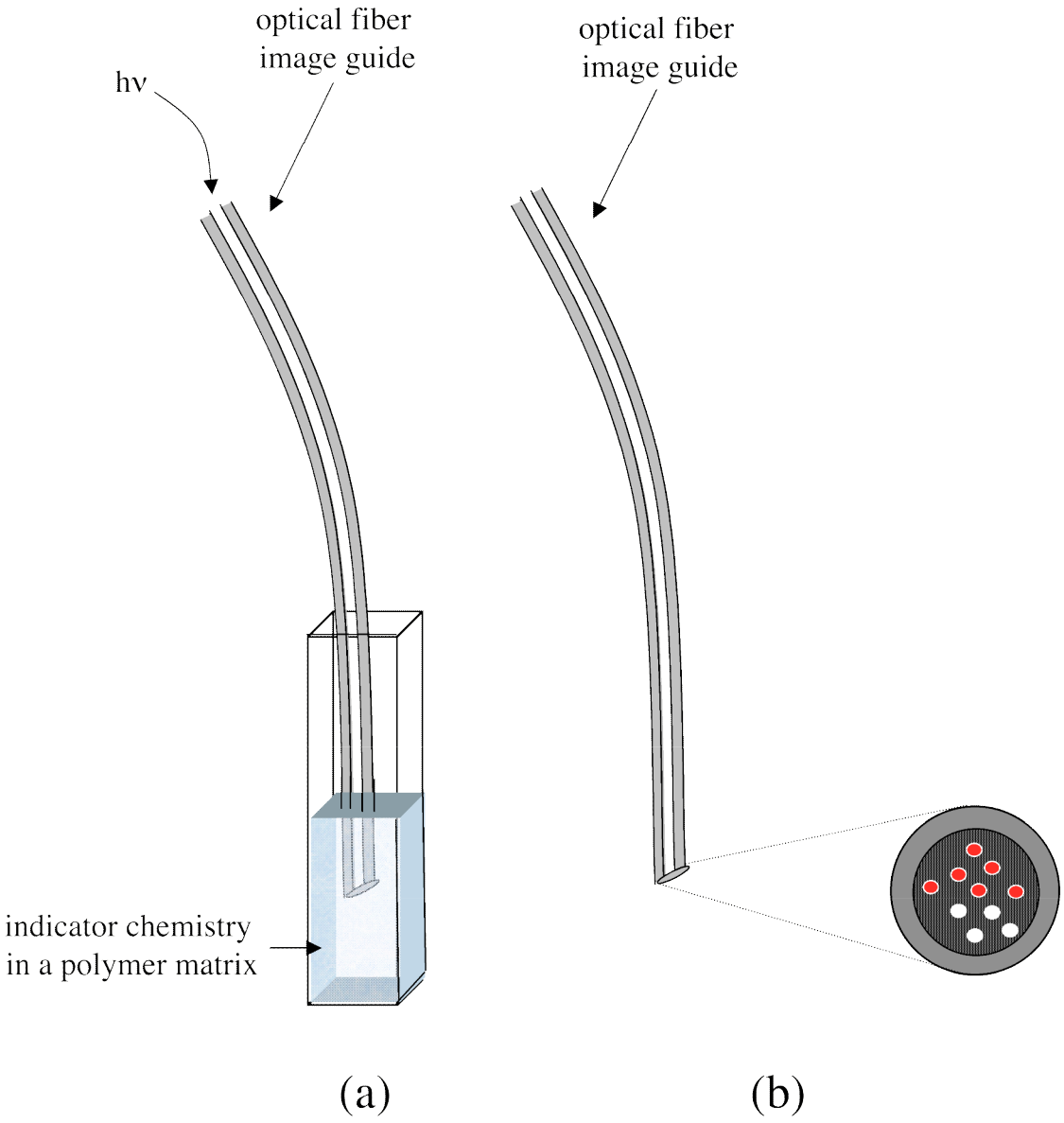

Figure 1.4: a) Photopolymerization involves (a) placing the distal portion of a polished optical fiber in a reagent solution containing both the indicator chemistry and a photopolymerizable matrix followed by light input via the proximal end of the fiber, (b) resulting in polymerization of the reagent on the distal end of the fiber. This procedure can be repeated several times using different reagents, resulting in a multianalyte sensor.

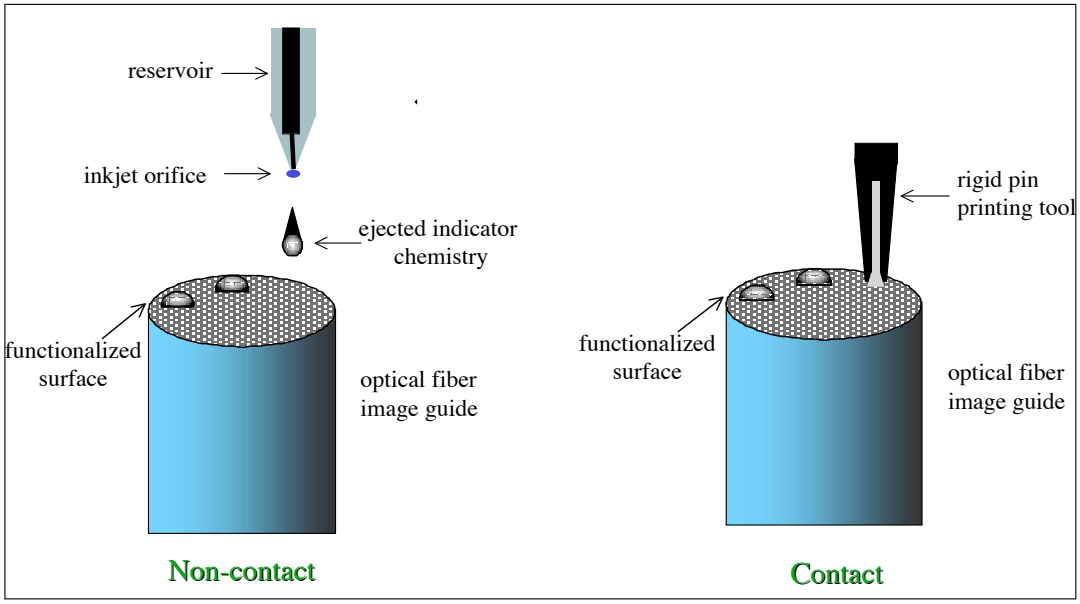

Figure 1.5: Inkjet printing technologies include both non-contact and contact microdispensing designs. (a) Non-contact devices typically utilize a piezo to eject droplets of indicator reagent, whereas (b) contact devices utilize rigid capillary printing tools that "stamp" the chemistry onto the surface of the fiber or other device.

Section 2

Fabricating Optical Fiber Imaging Sensors Using Inkjet Printing Technology: a pH Sensor Proof-of-Concept

2.1 Introduction

The most promising approach to fiber-based pH sensing has been the confinement (e.g. covalent [1-6], electrostatic [7,8]) of pH sensitive indicators in substrates attached to the fiber surface. Traditional methods for fabricating fiber-based pH sensors involve attachment of the substrate through mechanical [1-3, 7], dip coating [6]), or photopolymerization methods [4-5]. Mechanical methods vary but most designs utilize tubing (e.g. capillary) filled with indicating reagent. In some cases, the substrate is directly bound [9] (e.g. epoxy) to the fiber surface. Sensors of this type are typically fabricated in two principal steps. The steps involve immobilizing the indicator chemistry on a solid support material, and subsequently attaching this to the fiber. This method gives better reproducibility and is widely used [10]). However, a survey of the literature shows that sensors fabricated in this manner are limited to single analyte measurements. Dip coating methods are commonly used in many sol-gel sensor preparations and typically produce micron-thick sensing membranes per dip, with the resulting membrane(s) covering the entire surface of the fiber. Unlike mechanical methods, the sensing layer can be produced in one step since the fiber tip is dipped in a formulation containing both the indicator chemistry and the solid support chemistry. Multiple coatings of different indicating chemistries can be sequentially added to the same fiber, producing multianalyte sensors [8, 11]. Such multianalyte sensor designs can suffer from

issues of chemical compatibility and cross sensitivity. Sensors fabricated by dip coating have not been shown to be reproducible and do not offer spatial discrimination of the individual sensing layers, since each target analyte must interact with the indicator chemistry of a particular layer and produce an optically distinct signal (e.g. fluorescence or absorption).

Photopolymerization methods are among the earliest methods used for fiber-based sensor fabrication. In recent years, Walt et al advanced this method by demonstrating that unique patterns of indicator chemistries could be covalently attached directly to the tips of image guide fibers, comprised of thousands of densely packed fibers [12-14]. Specifically, these polymerized arrays of indicator chemistries were produced by immersing the optical fiber tip in a polymerizable indicator chemistry and selectively "growing" the indicator chemistries on the end of the optical fiber strands via ultraviolet UV) radiation photopolymerization. These sensor arrays were then spatially discriminated using simple imaging techniques. Multianalyte sensors can be fabricated by immersing the fiber tip sequentially in different polymerizable solutions followed by photopolymerization. However, the order in which the sensing elements were added to the fiber surface was critical because of cross sensitivity issues (Ferguson et al., 1997 [15]). Furthermore, these arrays are non-uniform, resulting from the lack of control during the photopolymerization step. This leads to sensors that are not reproducible in their response.

Building upon Walt's work, we demonstrate the feasibility of using Drop-on-Demand microjet printing technology [16] for fabricating imaging sensors by printing an array of photopolymerizable sensing elements on the surface of an optical fiber image guide. The microjet printing process produces highly reproducible droplets via a piezoelectric driven orifice, resulting in a very uniform sensor array. For these initial studies, a pH sensitive indicator was immobilized in a polymeric support and tested using a fluorescence imaging apparatus. Several key optical and physical properties of the microdot sensor array are evaluated in terms of morphology, response time, and pH sensing reproducibility.

2.2 Experimental

The printed indicator chemistry was comprised of a proprietary optical polymer (i.e. epoxy) that was photopolymerized from a mixture of glycidyl ethers of dihydroxy compounds including cyclohexanedimethanol diglycidyl ether, glycerol diglycidyl ether, butanediol diglycidyl ether, and ethylene glycol diglycidyl ether, in which a pH sensitive dye, fluorescein (Sigma-Fluka), was dissolved at 0.6%w/w. The concentration of fluorophore in the polymer was based on prior experience of one author. Reactive materials were purchased from Aldrich Chemical Co. and Monomer-Polymer Laboratories, and used as received. All photopolymerization was performed using the Green Spot™ (300-480nm) from UV Source, Inc. The Lewis acid initiator species SbF_6- was created in situ by UV photolysis (2000mW) from a commercial triaryl compound present at a 0.5%w/w level. Buffered solutions were prepared using Hydrion buffers.

Optical fiber image guides (Sumitomo, IGN-05/06) were polished (1 micron finish) and cleaned with acetone. After evaporation of solvent, image guides were dipped in a commercially available fluoroaliphatic copolymer solution (3M Inc., FC-724 proprietary formulation), which also contains a low concentration of alkyltrialkyloxysilane coupling agent. The image guides were then baked for ~45 min at 140∞C, resulting is a single micrometers-thick, optically transparent coating on the fiber surface with a surface energy expected to be ~15 dynes/cm as reported in the 3M literature. Adhesion of the coating to the optical fiber is presumed to be a combination of mechanical adhesion, van der Waals attraction, and some covalent bonding through condensation of surface silanol groups on the optical fiber with the alkyloxysilane groups of the coating during the baking process. Adhesion of the subsequently polymerized microdot sensors (epoxy chemistry) to the fluoropolymer coating is presumed to be a combination of mechanical interlocking and van der Waal's forces. The fluoroaliphatic copolymer likely contains polyfluoroacrylate, which would allow hydrogen bonding between carbonyl groups and the hydroxyl groups of the epoxy. Although rigorous adhesion characterization was not performed, the microdots remained intact on the fiber surface after repeated cycles of exposure to aqueous environments with subsequent drying.

Figure 2.1 shows the custom fluorescence imaging system, a similar system previously described [17]), utilizes a liquid nitrogen cooled, charge-coupled device (Princeton Instruments, Model LN/CCD-512TKB/1) photodetector and a high intensity blue light-emitting-diode (LED) for excitation. The imaging system was designed to magnify the distal portion of the optical image guide 10 fold. The resulting image of the fiber tip

covered 203 pixels of the CCD (no pixel binning). For all fluorescence measurements, 7x7 on-chip pixel binning was used. This resulted in a 29x29 grid of superpixels in which there was no overlap in signal from adjacent microdot sensing elements. The images used to calculate the calibration curve shown in Figure 3 were acquired with 10 coadditions, 25 sec exposures each. Images used to calculate the response time data shown in Figure 4 were acquired with 12 sec exposures.

pH measurements below pH 6 were hindered by matrix effects. The relative error for the pH 6 and pH 3-5 (not shown) measurements was greater by a factor of 3-4 compared to the relative error for all data points from pH 6.8 to 9. The pooled relative error for data between pH 6.8 and 9 was 1.3%. When the data for pH 6 was included in the calculation, the pooled relative error was 2.2%. The 2% variation we report in the text is actually on the high end of the measurement.

2.3 Results and Discussion

The process for inkjet printing indicator chemistries on an optical substrate is similar to that used to produce micro-optical components [18-20]. This technology, known as Drop-on-Demand microjet printing, is a process that utilizes a piezo driven orifice, which emits a highly reproducible droplet (i.e. indicator chemistry) each time an appropriate driving pulse produces a displacement of the piezoelectric element surrounding the orifice. Figure 2.2a shows an image of droplet emission from the piezo driven orifice. With the aid of stroboscopic illumination, this image is actually the superposition of ~1000 individual droplets. The clarity of the monomer droplet in Figure 2.2a indicates the time

and spatial precision of the microjet process. Other key features of the microjet system (Fig 2.2b) include motion control actuators for accurate positioning of the substrate (i.e. optical fiber) during printing, a UV light pipe for photopolymerizing printed monomers, and a clean-air/exhaust system for preventing airborne contamination.

The microjet system was used to print microdot arrays of indicator chemistries on the tips of optical fiber image guides. The capabilities of the microjet process for printing chemistries on an optical image guide are shown in the darkfield images of Figure 2.3a-d. The top-view image of Figure 2.3a shows 7 microdots 'printed' in a 6-around-1 configuration on the polished surface of a 500-□m diameter optical image guide. The diameter of the circle through the centers of the circumferentially printed microdots is 260 microns, indicating this pattern easily fits on the end of the image guide. The reproducibility of the printing process was excellent for microdot diameter, height, and roundness and is summarized in Table 2.1. The roundness is calculated by dividing the difference between maximum and minimum diameters by the average diameter. Figure 2.3b shows a side view of the seven microdots and provides visual detail about the array aspect ratio (i.e. diameter vs. height). This ratio is controllable by adjusting physical characteristics (e.g. surface tension, viscosity) of the monomer formulation using surface active materials, as example Fluorad FC171 (3M, Inc.), and temperature (75∞C) of the fluid in the printhead, by adjusting the surface energy of the optical fiber using surface modifiers (e.g. fluoroaliphatic copolymer), and by adjusting the number and diameter (orifice size) of deposited droplets. In all experiments, each microdot is a single droplet expelled from a 40-micron orifice, and all image guide fibers are treated prior to printing

in this study with a fluoroaliphatic copolymer surface modifier. Figures 2.3c and d are the expanded top view and side view, respectively, of a single microdot and clearly show the microdot symmetrical morphology. It should be noted that beneath the transparent microdot of Figure 2.3c, the individual pixels comprising the optical image guide are clearly discernable due to a lensing effect caused by the microdot morphology. In addition to morphological characteristics, the fluorescence intensity of 30 fluorescein-doped microdots were measured and compared using an imaging spectrometer and determined to vary by 2 percent or less.

Although this example of an optical sensor system uses only one indicator, it demonstrates the unique capability of inkjet technology to place multiple microdots, each possibly containing a different fluorophore, on the end of the optical image guide. Any indicator compound that will form a solid solution in a polyether or polyacrylate produced by photopolymerization is a suitable candidate.

2.3.1 Sensor calibration/variability

The pH sensing ability of the fluorescein-doped microdots was evaluated using a custom fluorescence imaging system. Sensor variability of the microdot array was minimal across the range of pH 6 to 9 as shown in Figure 2.4. In the pH range 6.8 to 8, the response is linear. Above pH 8, the change in fluorescence intensity with increasing pH is less due to the pKa of the immobilized fluorescein indicator. Though fluorescein is typically used over a wider pH range than shown, we were unable to detect significant changes in pH below pH 6. We attribute this to an undesirable residual or buffering

effect within the microdots caused by the use of the Lewis acid catalyst species, SbF_6^- ion and UV radiation for polymerizing the fluorescein-doped formulation. It is important to note that because of uneven illumination (i.e. excitation) of the individual fluorescein immobilized microdot sensors, all data for each microdot was normalized to the fluorescence intensity at pH 9 and plotted at the relative change in fluorescence intensity versus pH.

2.3.2. Sensor response time/hysteresis

The time response of the 6-around-1 microdot array to changes in pH was evaluated. For these experiments, the fiber tip was alternated between pH 9 and pH 6.8 buffered solutions while acquiring successive images. In Figure 2.5, the response curves of 7 microdots over 3 cycles of pH changes between pH 9 to pH 6.8 were identical and show a t_{100} (time to 100% of total response) response time of ~25 sec for decreasing or increasing changes. These plots were also normalized due to uneven illumination of the microdot array as previously discussed. The large spike that is evident at the edge of the transition from pH 9 to 6.8 (cycle 3) was intentional to show how these sensors respond to brief exposure to air while changing between pH buffered solutions. The lack of hysteresis in the response curves indicates no photobleaching and/or dye leaching.

2.4 Conclusions

Microjet printing technology is a viable tool for fabricating fiber-based imaging sensors. Although only pH sensing was demonstrated in this pilot study, the microjet technique is potentially amenable to fabricating multianalyte sensors to simultaneously measure other biologically important parameters such as blood/gas and other ions. Sensors fabricated in

this manner do not have issues of cross sensitivity or chemical compatibility since each indicator chemistry can be attached to the fiber surface independently (i.e. microdots are never exposed to other chemistries). This is in contrast to dip coating and other photopolymerization techniques. Multianalyte sensors, in which different indicators would be used, could greatly benefit from this technique. Another important feature of this technique is the excellent uniformity of the polymer sensor arrays on the fiber surface. Such uniformity has not been demonstrated with any of the other techniques discussed in this paper. The ability to fabricate reproducible sensors could enable large-scale production of fiber sensors without the need to calibrate each individual sensor.

2.5 References

[1] Peterson, J.I., Goldstein, S.R., Fitzgerald, R.V., Buckhold, D.K., 1980. Fiber optic pH probe for physiological use. Anal. Chem. 52, 864-869.

[2] Saari, L.A., Seitz, W.R., 1982. pH sensor based on immobilized fluoresceinamine. Anal. Chem. 54, 821-823.

[3] Gehrich, J.L., Lubbers, D.W., Opitz, N., Hansmann, D.R., Miller, W.W., Tusa, J.K., Yafuso, M., 1986. Optical fluorescence and its application to an intravascular blood-gas monitoring system. IEEE Trans. Biomed. Eng. 33, 117-132.

[4] Munkholm, C., Walt, D.R., Milanovich, F.P., Klainer, S.M., 1986. Polymer modification of fiber optic chemical sensors as a method of enhancing fluorescence signal for pH measurements. Anal. Chem. 58, 1427-1430.

[5] Jordan, D.M., Walt, D.R., 1987. Physiological pH fiber optic chemical sensor based on energy-transfer. Anal. Chem. 59, 437-439.

[6] Nivens, D.A., Zhang, Y., Angel, S.M., 1998. A fiber optic pH sensor using base-catalyzed organo-silica sol-gel. Anal. Chim. Acta 376, 235-245.

[7] Zhujun, Z., Seitz, W.R., 1984. A fluorescence sensor for quantifying pH in the range from 6.5 to 8.5. Anal. Chim. Acta 160, 47-55.

[8] Nivens, D.A., Schiza, M.V., Angel, S.M., 2002. Multilayer sol-gel membranes for optical sensing applications: single layer pH and dual layer CO_2 and NH_3 sensors. Talanta 58(3), 543-550.

[9] Fuh, M.R.S., Burgess, L.W., Hirschfeld, T., Christian, G.D., Wang, F., 1987. Single fibre optic fluorescence pH probe. Analyst 112 (8), 1159 – 1163.

[10] Wolfbeis, O. S., (Ed.), 1991. Fiber-Optic Chemical Sensors and Biosensors Volume 1, CRC Press, Boca Raton, FL, pp. 77.

[11] Schiza, M.V., Nelson, M.P., Myrick, M.L., Angel, S.M., 2001. Use of a 2D to 1D dimension reduction fiber-optic array for multiwavelength imaging sensors. Appl. Spectrosc. 55(2), 217-226.

[12] Healey, B.G., Foran, S.E., Walt, D.R., 1995. Photodeposition of micrometer-scale polymer patterns on optical imaging fibers. Science 269 (5227), 1078-1080.

[13] Healey, B.G., Walt, D.R., 1997. Fast temporal response fiber optic chemical sensors based on the photodeposition of micrometer-scale polymer arrays. Anal. Chem. 69, 2213-2216.

[14] Barnard, S.M., Walt, D.R., 1991. A fiber optic chemical sensor with discrete sensing sites. Nature 353 (6342) 338-340.

[15] Ferguson, J.A., Healey, B.G., Bronk, K.S., Barnard, S.M., Walt, D.R., 1997. Simultaneous monitoring of pH, CO_2 and O_2 using an optical imaging fiber. Anal. Chim. Acta 340, 123-131.

[16] Wallace, D.B., Cox, W.R., Hayes, D.J., 2002. In: Pique, A., Chrisey, D.B., (Eds.), Direct Write Using Ink-Jet Techniques, Academic Press, New York, Chapter 7.

[17] Carter, J.C., Egan, W.J., Nair, R.B., Murphy, C.J., Morgan, S.L., Angel, S.M., 1999. Fiber-optic imaging for in-situ chemical measurements. SPIE Proceed. 3540, 210-221.

[18] Cox, W.R., Hayes, D.J., Chen, T., Ussery, D.W., 1995. Fabrication of micro-optics by microjet printing. SPIE Proceed. 2383, 110-115.

[19] Cox, W.R., Chen, T., Ussery, D., Hayes, D.J., Tatum, J.A., MacFarlane, D.L., 1996. Microjetted lenslet-tipped fibers. Optics Communication 123(4-6), 492-496.

[20] Chen, T., Cox, W.R., Lenhard, D., Hayes, D.J., 2002. Microjet printing of high precision microlens array for packaging of fiber-optic components. SPIE Proc. 4652, 136-141.

2.6 Figures for Section 2

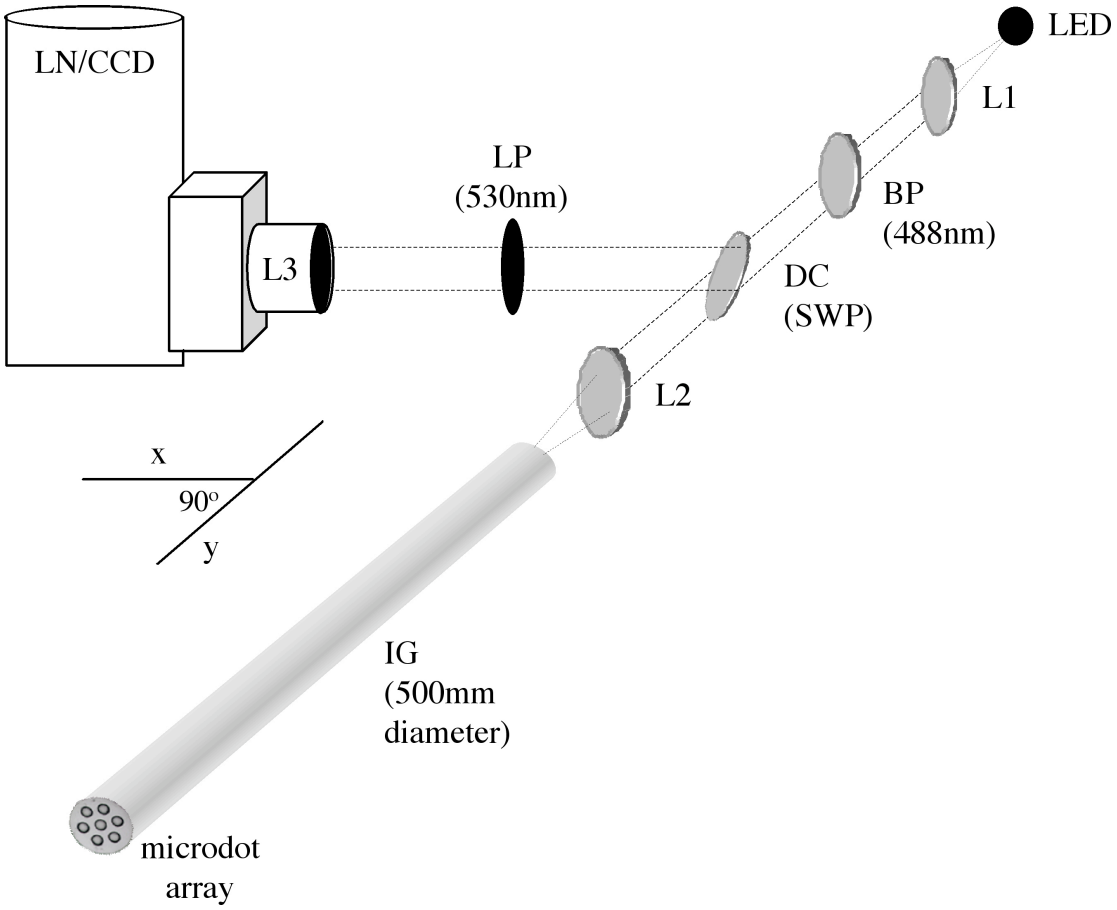

Figure 2.1: Custom fluorescence imaging system. It utilizes a liquid nitrogen cooled, charge-couple device photodetector and a blue light-emitting-diode (LED) for excitation. The imaging system was designed to magnify the distal portion of the optical image guide where the microdot array is printed.

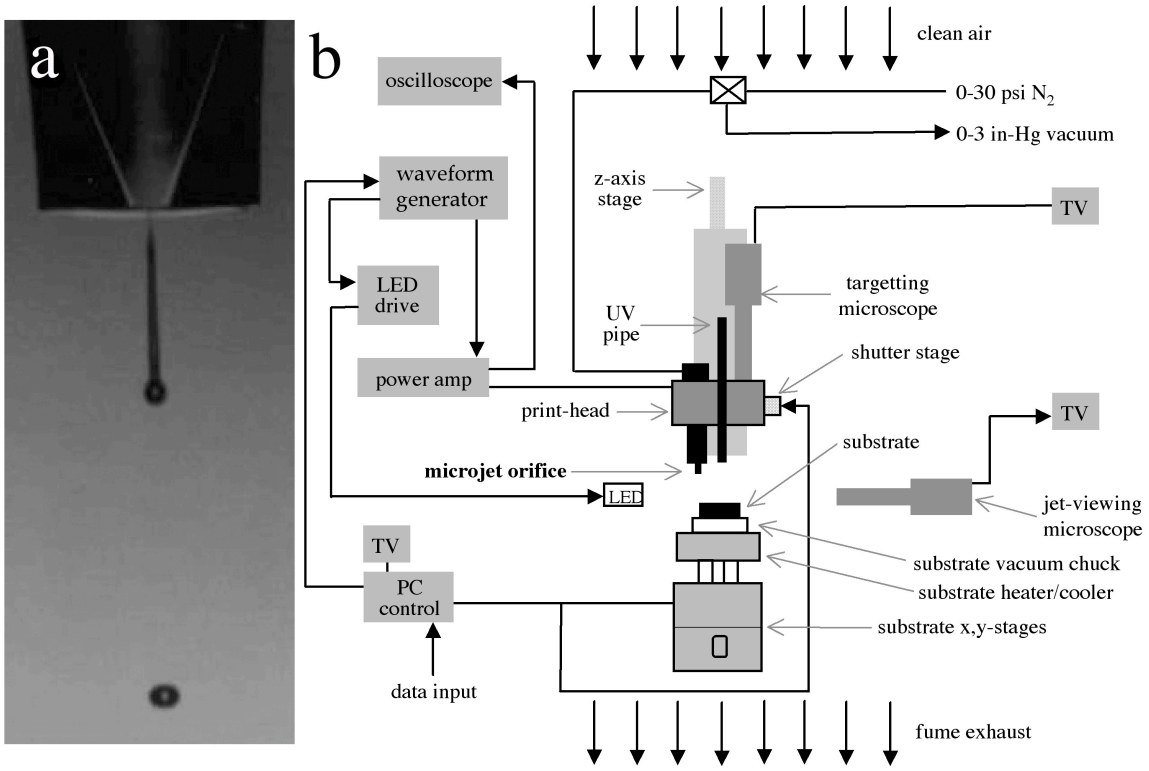

Figure 2.2: (a) A stroboscopically illuminated image of 50 micron diameter droplets (~1000 superimposed) of polymer-based indicator chemistry emitted from the piezo-driven microjet orifice, and a (b) schematic of the Drop-on-Demand microjet system used in printing patterned arrays of indicator chemistries on optical image guides.

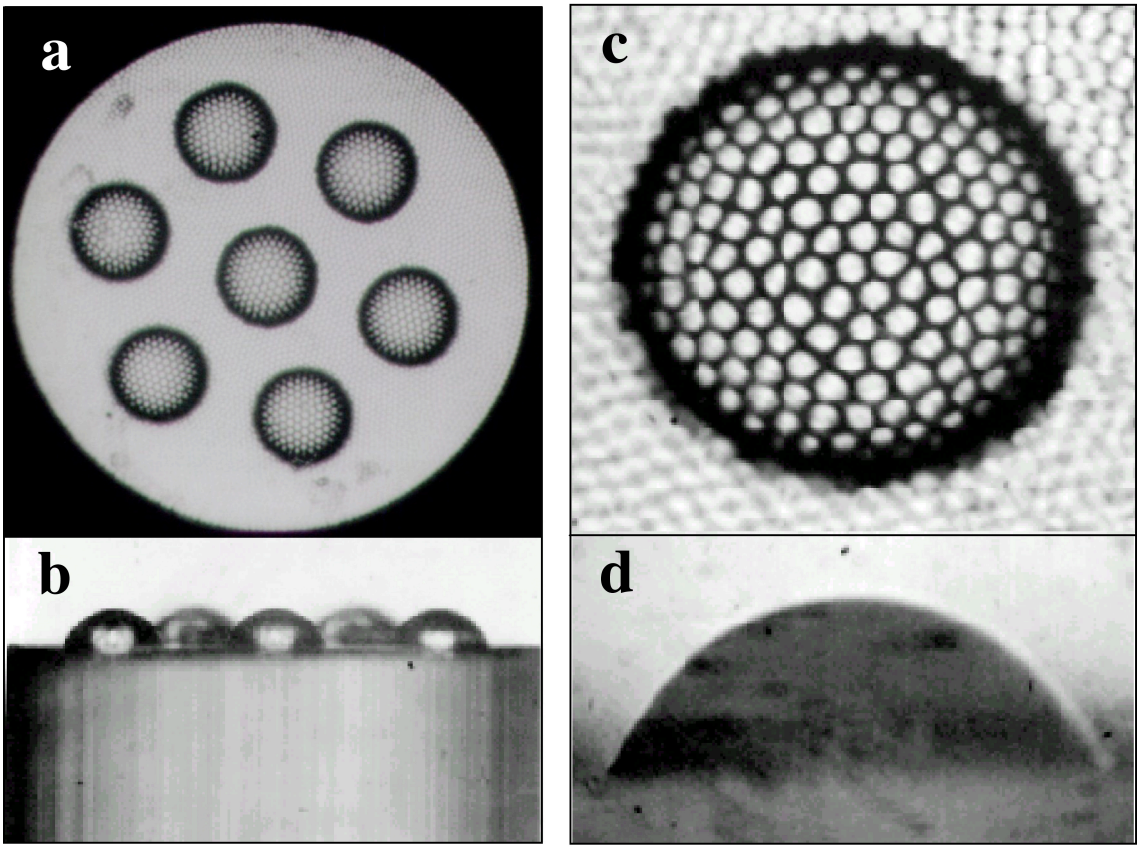

Figure 2.3: (a) Top view and (b) side view of seven 92 micron diameter microdots printed on a 500 micron diameter optical image guide and the (c) expanded top view and (d) side view of a single 92 micron diameter microdot.

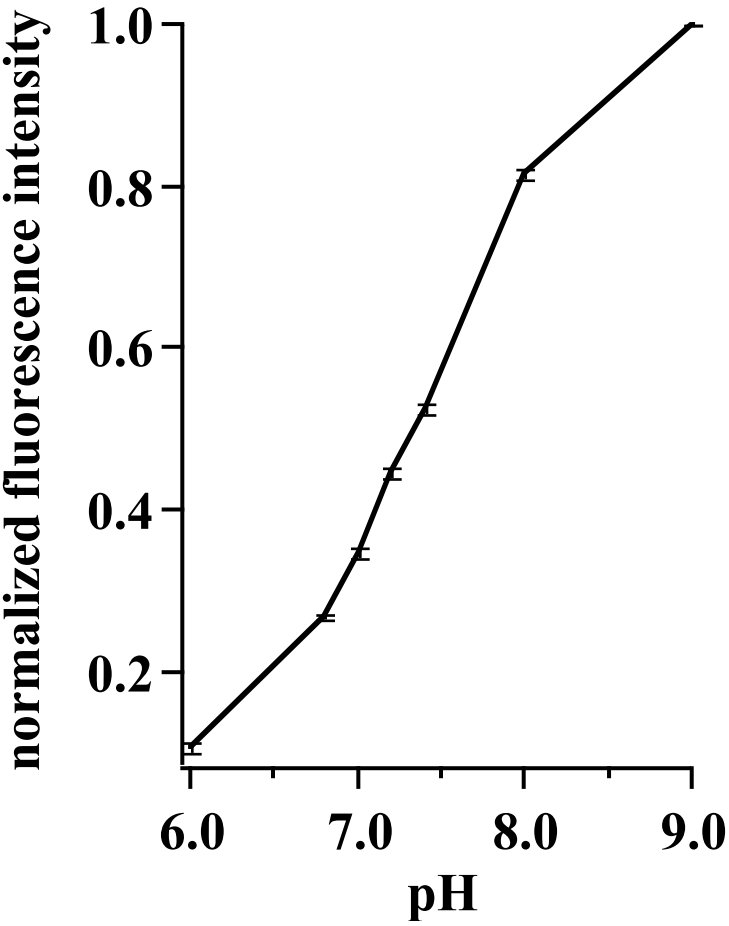

Figure 2.4: Plot of normalized fluorescence intensity vs. pH for a 6-around-1 microdot array. Error bars show ±1 standard deviation.

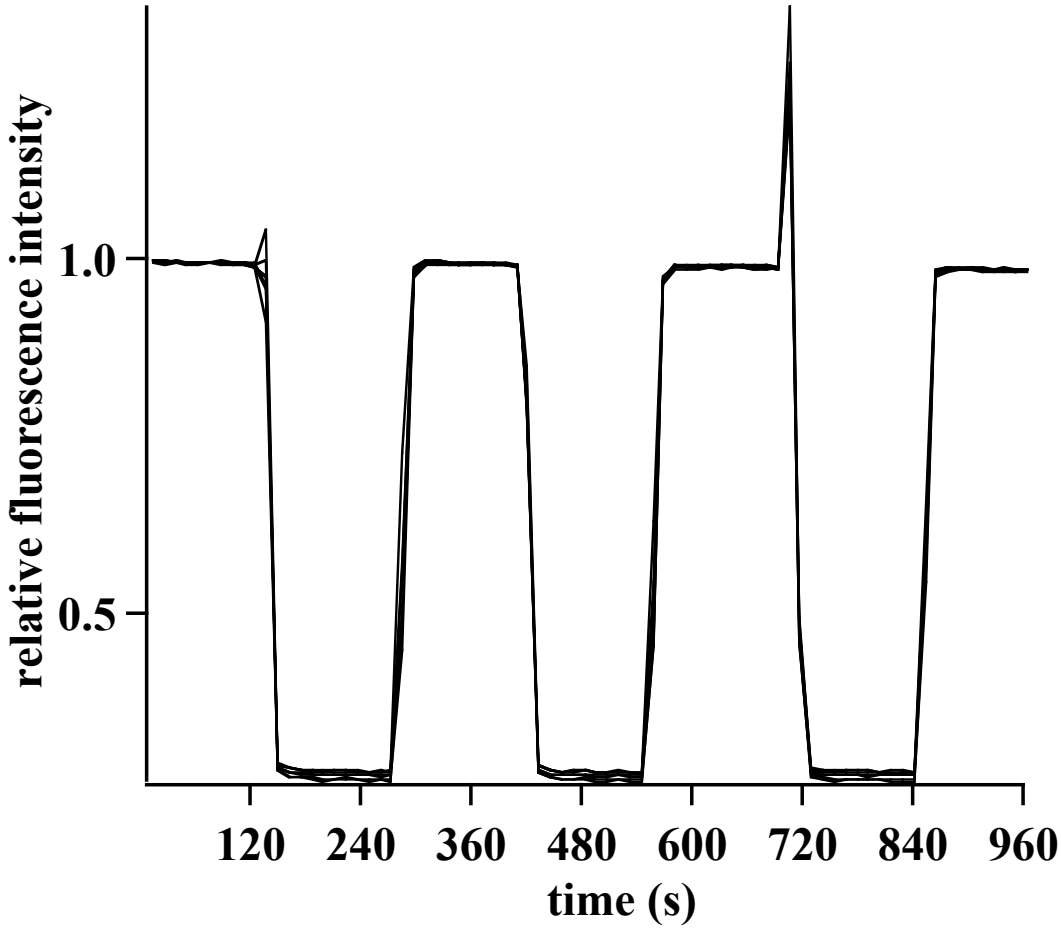

Figure 2.5: Relative pH response time curves of a 6-around-1 microdot array between pH 9 and 6.8 indicating a t_{100} response time of ~25 seconds.

microdot diameter	93.3 ± 2.2 microns
microdot height	35.0 ± 1.0 micron
microdot roundness*	0.00072 ± 0.00023
fluorescence intensity	≤ 2% (variation)

*[(max. diameter - min. diameter)/ avg. diameter]

Table 2.1: Physical and optical characteristics of microdot array sensors.

Section 3

Development and Evaluation of an Automated, Micro-dispensing Platform for Printing Sensing Arrays on Optical Fiber Image Guides.

3.1 Introduction

The most promising approach to fiber-based sensing has been the confinement (e.g. covalent[1-5,7], electrostatic[6,8]) of chemical indicators in substrates attached to the fiber surface. Traditional methods for fabricating fiber-based sensors involve attachment of the substrate through mechanical[1-3,6], dip coating[7,8], or photopolymerization methods[4,5]. Mechanical methods vary but most designs utilize tubing (e.g. capillary) filled with indicating reagent. In some cases, the substrate is directly bound[9] (e.g. epoxy) to the fiber surface. Sensors of this type are typically fabricated in two principal steps. The steps involve immobilizing the indicator chemistry on a solid support material, and subsequently attaching this to the fiber. This method gives better reproducibility and is widely used[10]. However, a survey of the literature shows that sensors fabricating in this manner are limited to single analyte measurements.

Dip coating methods are commonly used in many sol-gel sensor preparations and typically produce micron-thick sensing membranes per dip, with the resulting membrane(s) covering the entire surface of the fiber. Unlike mechanical methods, the sensing layer can be produced in one step since the fiber tip is dipped in a formulation containing both the indicator chemistry and the solid support chemistry. Multiple coatings of different indicating chemistries can be sequentially added to the same fiber,

producing multianalyte sensors[8,11]. Such multianalyte sensor designs can suffer from issues of chemical compatibility and cross sensitivity. Sensors fabricated by dip coating have not been shown to be reproducible and do not offer spatial discrimination of the individual sensing layers, since each target analyte must interact with the indicator chemistry of a particular layer and produce an optically distinct signal (e.g. fluorescence or absorption).

Photopolymerization methods are among the earliest methods used for fiber-based sensor fabrication. In recent years, Walt et al advanced this method by demonstrating that unique patterns of indicator chemistries could be covalently attached directly to the tips of optical fiber bundles, comprised of thousands of densely packed fibers[12-13]. Specifically, these polymerized arrays of indicator chemistries were produced by immersing the optical fiber tip in a polymerizable indicator chemistry and selectively "growing" the indicator chemistries on the end of the optical fiber strands via ultraviolet radiation photopolymerization. These sensor arrays were then spatially discriminated using simple imaging techniques. Multianalyte sensors can be fabricated by immersing the fiber tip sequentially in different polymerizable solutions followed by photopolymerization. However, the order in which the sensing elements were added to the fiber surface was critical because of cross sensitivity issues[14]. Furthermore, these arrays are non-uniform, resulting from the lack of control during the photopolymerization step. This leads to sensors that are not reproducible in their response.

In this Section we present a novel approach for attaching polymer-based indicator chemistries (i.e. microdot arrays) directly to the tips of optical fiber image guides. The approach involves the use of a contact-based microdispensing system, which was modified to allow for "printing" microdots arrays on the fiber surface and for subsequent photopolymerization of the array. The discussion that follows details the design of the system hardware and software including the concept of operation. The overall system capabilities were tested and optimized for printing and polymerization of select indicator chemistries immobilized in a polymeric support in a 6-around-1 configuration on test slides and optical fiber image guide sensors.

3.2 System Description

A schematic illustration of the system (see Appendix B for system pictures) for fabricating optical fiber-based imaging sensors is shown in figure 1. The major components of the system include a microdispensing printing platform **1**; an imaging vision system **2**; a polymerization chamber **4**; and a computer **5** with custom software.

3.2.1 Concept of operation

Sensor fabrication begins by loading the distal end of a functionalized optical fiber image guide (i.e. image guide fiber) **6**, onto a translational (i.e. shown with directional arrows) platform **11.** The vertical translating platform **11** (as shown with directional double arrows) and a linear horizontal translation stage **3** (also shown with directional arrows) are configured to translate the distal portion of the image guide fiber **6** into position within the microdispensing printing platform **1** for printing the predetermined patterns of

microdots on the tip of the image guide fiber **6.** This is accomplished via a computer **5** having custom software (e.g., a graphical interface control means **15**). A fixture **7** is used to connect the proximal end of the same optical fiber to the imaging vision system **2** (shown enclosed in a dashed box) having, a charge coupled device (CCD) **9** with an attached lens **10** and a collimating optic **8**. A ring light illumination source **20**, provides uniform illumination of the optical image guide **6**, while printing a selected pattern of microdots on the tip of the image guide fiber **6**. Such an arrangement allows images to be acquired via the imaging vision system **2** during printing, for real-time inspection and quality control purposes.

Once the distal end of the image guide fiber is in the printing position **12** within the microdispensing printing platform **1**, a print head **13,** which contains at least one rigid pin printing tool **14**, is then directed via the graphical user interface **15** control means to a homing position via a robotic positioner (i.e., X, Y, Z translation stages **16**, **17**, **18** - shown with accompanying directional arrows). The rigid pin printing tool **14** is directed to load a sample from a well plate, blot the tip of the printing tool, and dispense the sample onto the tip of the image guide fiber **6**. The printing tool is then directed to a cleaning station to remove any remaining sample before loading a new sample.

Once the predetermined pattern of microdots have been printed on the image guide fiber tip, the vertical translating platform **11** and linear horizontal translating stage **3** will move the distal end of the image guide fiber **6** to a positon under the photo-polymerization chamber **4** for processing as detailed below.

An ultraviolet (UV) light source **22** is used to direct predetermined wavelengths along a liquid light guide **21**, to the photo-polymerization chamber **4**. The Photo-polymerization chamber **4** is configured to house the distal portion of the liquid light guide **21** in addition to housing a probe **23** for monitoring the humidity and an inlet **24** for purging the photo-polymerization chamber **4** with humidified N_2 gas.

3.2.2 Microdispensing printing platform

The most complex component of the fabrication system is the microdispensing printing platform, which handles most of the operations during fiber sensor fabrication. The platform is an environmentally controlled chamber that houses the robotic x,y,z translational arm. Attached to this arm is a fixture for holding the printhead, a rigid pin printing tool(s). The programmable robotic arm directs the printing tool to stations (Figure 2) within the chamber for performing various tasks including sample loading, pin blotting, sample dispensing, and pin cleaning.

For developing the microdispensing platform, the options of (1) building a robotic system in house or (2) modifying a commercially available robotic system were considered and the latter chosen as the more cost and time effective. A commercially available microdispensor (Virtek, Canada) designed for biological microarray printing and analysis (e.g. gene expression, genotyping) was acquired and modified in-house. The major modifications to the Virtek system involved adaptations to allow for printing on fibers since the system is only designed to print on slides or membranes. This involved the addition of a new base, which raised the overall height of the instrument 7 inches,

providing sufficient space for translating an optical fiber fixture via horizontal (Newport Inc., IMS Series 300mm high-performance linear stage) and linear (Newport Inc., LTA series coupled to a 426 series translation stage), stages into the printing position. A clear channel for horizontally translating the optical fiber fixture beneath the system was created by relocating various vacuum and fluidic lines and removing sheet metal from the right side of the system base. The orifice for vertically translating the optical fiber fixture into the chamber such that the optical fiber is flush with the chamber surface was created by removing a heater (see Figure 2d), which was part of the original Virtek system design.

3.2.3 Imaging vision system

Figure 1 shows the custom imaging vision system (shown enclosed in a dashed box) for viewing in real time the printing process on optical fiber image guides. The vision system consists of a charge-coupled device (CCD, Roper scientific, CoolSnap CS) with attached zoom lens (Nikon, 175 mm lens) and a microscope objective (Olympus, UMS 10x, • -corrected). The image of the distal portion of the fiber (i.e. nearest the printing tool) is transmitted via thousands of individually clad fibers that form the coherent image guide; the microscope objective transmits this image to the CCD, which is displayed in real time on a monitor. In addition, a light guide coupled ring light, located in the microdispensing chamber, provides even illumination of the distal portion of the optical fiber image guide during printing so that real-time images may be acquired using the vision imaging system.

3.2.4 Polymerization chamber

After samples are printed on an optical fiber, the fiber fixture is translated linearly and then vertically until the fixture rests against the bottom edges of the polymerization chamber, which is an open bottom cube (1x1x1in.) suspended above the horizontal linear stage. The chamber is designed with several ports through which a liquid light guide, (5mm diameter) a humidity probe, and gas tubing are secured. The light guide is attached to a high intensity tungsten-halogen uv-vis light source (Exfo, Novacure 2100) which provides the excitation energy for photo-induced polymerization of the monomer-based indicator chemistries to the fiber surface. During photo-induced polymerization, the atmosphere in the chamber is maintained at ~90% relative humidity (RH) N_2 gas via a two-stage N_2 humidifier. The N_2 gas is fed into the two-stage humidifier at a rate of ~15 standard ft^3/hour (SCFH). When the fiber fixture is positioned against the bottom edges of the chamber so as to form a seal (non airtight), the chamber reaches 90% RH in ~20sec.

3.2.5 Custom software/interface

Although the Virtek system contains most of the necessary hardware required for our printing needs, the manufacturers software was only designed to allow dispensing of linear arrays, rather than patterns (this is the case with similar microarray devices). To optimize the number density of microdots printed on the surface of an optical fiber, more complex geometrical printing patterns are required (for example, a circular pattern of 6 dots surrounding one central microdot). Therefore, custom user interface and software

architecture were developed in LabVIEW (National Instruments, v7.0) software to control the robotics using the manufacturer's serial (RS232) command set. The custom single user interface (Figure 3) contains all the features for controlling the instrument, including positioning the rigid tool, zeroing the tool at the center of the fiber, creating a custom printing pattern, and executing an automated printing and photopolymerization routine.

A primary feature of the custom software is the pattern editor, which is displayed in the upper right corner of the user interface (see Fig. 3). The pattern editor is a user-defined template of the surface to be printed (e.g. optical fiber) and allows the user to create and visualize a to-scale pattern to be dispensed. For example, the pattern editor in Figure 3 displays a 6-around-1 pattern, as it would appear to the user prior to initiating the printing and polymerization automated routine. A mouse controlled drag-and-drop feature allows the user to select a sample from a color-coded palette, mapped to a well in the 96-well plate sample holder, and place these in any pattern on the template. The drag and drop feature is a visual aid and does not require the user to specify [x,y] coordinates, which greatly lessons the difficulty of specifying microdot geometries. The user can create new patterns, or load a previously saved pattern to the pattern editor (i.e. there are 10 predefined patterns). Figure 4 shows three different printing pattern geometries that may be chosen to print single or multiple samples (i.e. indicator chemistries) on an optical fiber. Even after a pattern has been selected, the user can move the position of a single dot in that pattern relative to other dots. For multianalyte sensor fabrication, this is useful since different indicator chemistry formulations may not wet the surface to be printed in

the same manner. This feature also allow different sized pin printing tools to be used for printing. The selection order of color-coded samples in the pattern editor determines the order in which samples are actually loaded and dispensed. When printing multiple samples on the same substrate (e.g. optical fiber), all droplets from a single sample are printed before moving to the next sample. As a general rule-of-thumb, the most volatile sample should be printed last when printing multiple indicator chemistries.

Another key feature of the user interface (see Fig. 3) is the joystick emulator, which appears in the upper left corner. The joystick emulator allows rigid pin printing tool (i.e. pin) movement in coarse (2 mm), intermediate (100 μm and 10 μm), and fine (2.5 μm) increments. This feature is primarily used to reference the center of a newly loaded optical fiber with the robot homing position (x:0, y:0, z:0) to allow precise printing on the fiber surface. Fig. 5 illustrates example techniques for positioning a pin to provide a reference coordinate. First, the pin is centered above the optical image guide fiber using the software joystick control (see Figure 3). Next, the pin can be enabled to contact the fiber surface (Fig. 5b) to set a reference coordinate that is relative to the robot homing position. As another arrangement, the pin can be brought into proximate contact (Fig 5c,d) with a fiber surface (e.g., 100 microns or less) to provide a shadow image of a pin for purposes of alignment. As the pin is brought into contact or substantially in contact with the surface of the image guide fiber, an image of the distal portion of pin is captured in real time via the vision imaging system.

Another key feature of the software is the ability to setup an automated routine. An automated routine is used to execute a single printing cycle for each indicator chemistry specified in a desired custom pattern. The printing cycle includes chemistry pickup from a specified well in a well plate, conditioning the sample delivery of the rigid pin printing tool by printing a specified number of microdots on a predetermined blotting substrate (e.g., a glass slide), printing the desired microdot configuration on an optical fiber image guide, cleaning the rigid pin printing tool according to a user specified wash cycle before the next chemistry pickup, and translating the fiber to the photopolymerization chamber where the fiber tip is exposed to a specified UV dosage. In a settings menu, a user can specify which wells are used for sample pickup, the stages in a wash cycle, the conditioning procedure, the descent speed of the rigid pin printing tool during printing, and the amount of time the tool rests on the printing surface. It is possible to pause the automated routine, make modifications to the pattern or wash cycle, realign the rigid pin tool and optical array, or manually position the rigid pin tool before resuming the routine.

Finally, the photopolymerization of dispensed samples (i.e. monomer based indicator chemistries) on the optical fiber is software controlled. Once printing on the fiber is complete, the fiber fixture is translated as part of the automated routine to the polymerization chamber. When translated into the correct position, the fixture rests against the bottom edges of the polymerization chamber and acts as a seal (not completely air tight), allowing the humidity to increase within the chamber. A liquid light guide located in the top of the chamber directs a controlled dose of uv light onto the

fiber surface where the monomer droplets rest. Once photopolymerization is complete, the fiber is translated back to the original loading position for removal.

3.3 Results

3.3.1 Printing evaluation on slides

The printing capabilities of the system were initially tested using an acrylamide-based hydrogel formulation (see Chap 4) printed on microscope slides. These initial formulations did not include a fluorescent indicator dye such as, for example, fluorescein dye for measuring changes in pH. Before printing, the pre-cleaned slides (Gold Seal, Portsmouth, NH) were dipped in a 5% (w/w) solution of polystyrene in toluene and dried in a vacuum oven backfilled with dry nitrogen and operated at 120 degrees C, resulting in a single microns thick polystyrene film with a surface energy of ~35 dynes/cm^2. The fabrication system was programmed to print two linear array of sensing elements on slides followed by photopolymerization (polymerizaton on slides is not automated but rather carried out off line) as shown in Figure 6a. Figure 6b shows the same linear array of microdots exposed to a droplet of water, verifying successful polymerization (i.e. microdots did not dissolve). The size of each microdot is ~100 microns each, which is determined by the size of the rigid pin printing tool (~90 um stamp), the surface energy of the polystyrene film and the surface tension (20-22 dynes/cm^2) of the indicator chemistry formulation. The photopolymerization conditions in the chamber were ~90 % RH with a UV (320-390 nm bandpass filter) dosage of 1000 mW for 40 seconds.

Figure 7a,b shows a 6-around-1 pattern of sensing elements printed and subsequently polymerized on a glass slide using the same procedures described above. The image in Figure 6b was acquired after exposing the sensing elements to a droplet of water. The photopolymerization conditions in the chamber were ~90 % RH with a UV (320-390 nm bandpass filter) dosage of 500 mW for 1 min 15 seconds.

3.3.2 Printing evaluation on optical fiber image guides

3.3.2.1 Single analyte sensor fabrication

Fig. 8 shows a bright-field image of a 6-around-1 microdot array printed on a polished optical fiber image guide (distal end) having a diameter of 500 microns. Before printing, the image guide fibers were cleaned and functionalized according to the procedures described in Appendix A. Briefly, the fibers were functionalized with allyltrichlorosilane, which provides a carbon-carbon double bond "handle" for covalently linking the microdot to the fiber surface during the photopolymerization step. The surface energy of the functionalized fiber surface is expected to be ~35 dyn/cm^2 and the surface tension of the formulation is 20-22 dyn/cm^2. Each microdot is about 100 microns in diameter and is comprised of an acrylamide-based polymer formulation containing immobilized, pH sensitive, acryloylfluorescein dye. The pH sensing capabilities are described in Section 5.

3.3.2.2 Multi-analyte sensor fabrication

Fig. 9 shows a bright-field image of the polished surface of the distal end of an optical fiber image guide onto which a 6-around-1 microdot array of multianalyte polymer

immobilized indicator chemistries have been printed. The two largest microdots (~110 microns in diameter) of similar size are acrylamide-based hydrogels that contain acryloyfluorescein indicator chemistry for sensing pH changes in solution. The remaining 5 microdots (~75 microns in diameter) of similar size are also acrylamide-based hydrogels. Of these 5, all but the central microdot contains a fluorescence resonance energy transfer (FRET) based polypeptide sequence [5-FAM-Lys(X)-Pro-Leu-Ala-Nva-Dap(5/6-TMR)-Ala-Arg-NH_2, where X = $COCH_2$-(OCH_2CH_2)-$NHCOCH_2CH_2CH{=}CH_2$] indicator chemistry for detecting select enzymes (e.g. matrix metalloproteinase, MMP-3 and/or chymotrypsin). The central microdot contains no indicator chemistry and serves as an experimental control. The fiber preparation procedures are the same as previously described for single analyte sensor fabrication. The polypeptide design is described in detail in Section 4. Briefly, the polypeptide sequence contains a unique "handle" [X = $COCH_2$-(OCH_2CH_2)-$NHCOCH_2CH_2CH{=}CH_2$] which provides a carbon-carbon double bond for covalently linking the peptide sequence to the polymer microdot during the photopolymerization step. The acrylamide formulations for the pH and enzyme indicators are different formulations, which accounts for the size differences. Control of the dimensions and aspect ratio of a printed microdot to a given specification is obtained by adjusting the following variables: (a) the surface tension of the polymer formulation (e.g. controlled using surfactants, and (b) the surface energy of the polished optical array surface (e.g. controlled using silanization method functionalization or low-wet coatings). The pH and enzyme sensing capabilities of this multianalyte sensor are described in Section 5.

3.4 Conclusions

The newly developed, contact-based microdispensing system is a viable tool for fabricating fiber-based imaging sensors. As demonstrated, we can print single and multiple indicator chemistries on slides or optical fibers with good morphology in contrast to dip coating and other photopolymerization techniques. The uniformity is excellent for the examples shown on slides but slightly less reproducible for examples printed on fibers. The difference is due to the increased difficulty when working with small fibers coupled to our inability to prepare fibers (see Appendix A), under ideal clean room and inert dry atmosphere conditions, which would require a large and dedicated glove box setup. Even so, we have achieved comparable printing results compared to the work in Section 2, which utilized a non-contact system. It is also important to note that the work in Chap 2 utilized a chemical coating as opposed to a chemically functionalized surface (Note: slides used as printing substrates in this paper were chemically coated and not functionalized). The epoxy-based chemistry used for that work was a well-characterized formulation to which an indicator dye was immobilized via trapping (non-covalent attachment). Furthermore, the contact-based demonstrated approach is much simpler than the non contact based system approach described in Section 2 (Figure 1b), which requires a much greater effort to optimize the printing parameters for a given indicator chemistry. We have also demonstrated the ability to print multianalyte sensor arrays using the contact-based approach. (single indicator chemistries were demonstrated in Chap. 2 only). Finally, and perhaps most importantly, sensors fabricated using the contact-based approach do not have issues of cross sensitivity or chemical compatibility

since each indicator chemistry can be attached to the fiber surface independently (i.e. microdots are never exposed to other chemistries).

3.5 References

[1] Peterson, J.I., Goldstein, S.R., Fitzgerald, R.V., Buckhold, D.K., 1980. Fiber optic pH probe for physiological use. Anal. Chem. 52, 864-869.

[2] Saari, L.A., Seitz, W.R., 1982. pH sensor based on immobilized fluoresceinamine. Anal. Chem. 54, 821-823.

[3] Gehrich, J.L., Lubbers, D.W., Opitz, N., Hansmann, D.R., Miller, W.W., Tusa, J.K., Yafuso, M., 1986. Optical fluorescence and its application to an intravascular blood-gas monitoring system. IEEE Trans. Biomed. Eng. 33, 117-132.

[4] Munkholm, C., Walt, D.R., Milanovich, F.P., Klainer, S.M., 1986. Polymer modification of fiber optic chemical sensors as a method of enhancing fluorescence signal for pH measurements. Anal. Chem. 58, 1427-1430.

[5] Jordan, D.M., Walt, D.R., 1987. Physiological pH fiber optic chemical sensor based on energy-transfer. Anal. Chem. 59, 437-439.

[6] Nivens, D.A., Zhang, Y., Angel, S.M., 1998. A fiber optic pH sensor using base-catalyzed organo-silica sol-gel. Anal. Chim. Acta 376, 235-245.

[7] Zhujun, Z., Seitz, W.R., 1984. A fluorescence sensor for quantifying pH in the range from 6.5 to 8.5. Anal. Chim. Acta 160, 47-55.

[8] Nivens, D.A., Schiza, M.V., Angel, S.M., 2002. Multilayer sol-gel membranes for optical sensing applications: single layer pH and dual layer CO_2 and NH_3 sensors. Talanta 58(3), 543-550.

[9] Fuh, M.R.S., Burgess, L.W., Hirschfeld, T., Christian, G.D., Wang, F., 1987. Single fibre optic fluorescence pH probe. Analyst 112 (8), 1159 – 1163.

[10] Wolfbeis, O. S., (Ed.), 1991. Fiber-Optic Chemical Sensors and Biosensors Volume 1, CRC Press, Boca Raton, FL, pp. 77.

[11] Schiza, M.V., Nelson, M.P., Myrick, M.L., Angel, S.M., 2001. Use of a 2D to 1D dimension reduction fiber-optic array for multiwavelength imaging sensors. Appl. Spectrosc. 55(2), 217-226.

[12] Healey, B.G., Foran, S.E., Walt, D.R., 1995. Photodeposition of micrometer-scale polymer patterns on optical imaging fibers. Science 269 (5227), 1078-1080.

[13] Healey, B.G., Walt, D.R., 1997. Fast temporal response fiber optic chemical sensors based on the photodeposition of micrometer-scale polymer arrays. Anal. Chem. 69, 2213-2216.

[14] Barnard, S.M., Walt, D.R., 1991. A fiber optic chemical sensor with discrete sensing sites. Nature 353 (6342) 338-340.

[15] Ferguson, J.A., Healey, B.G., Bronk, K.S., Barnard, S.M., Walt, D.R., 1997. Simultaneous monitoring of pH, CO_2 and O_2 using an optical imaging fiber. Anal. Chim. Acta 340, 123-131.

[16] Wallace, D.B., Cox, W.R., Hayes, D.J., 2002. In: Pique, A., Chrisey, D.B., (Eds.), Direct Write Using Ink-Jet Techniques, Academic Press, New York, Chapter 7.

[17] Carter, J.C., Egan, W.J., Nair, R.B., Murphy, C.J., Morgan, S.L., Angel, S.M., 1999. Fiber-optic imaging for in-situ chemical measurements. SPIE Proceed. 3540, 210-221.

[18] Cox, W.R., Hayes, D.J., Chen, T., Ussery, D.W., 1995. Fabrication of micro-optics by microjet printing. SPIE Proceed. 2383, 110-115.

[19] Cox, W.R., Chen, T., Ussery, D., Hayes, D.J., Tatum, J.A., MacFarlane, D.L., 1996. Microjetted lenslet-tipped fibers. Optics Communication 123(4-6), 492-496.

[20] Chen, T., Cox, W.R., Lenhard, D., Hayes, D.J., 2002. Microjet printing of high precision microlens array for packaging of fiber-optic components. SPIE Proc. 4652, 136-141.

3.6 Figures for Section 3

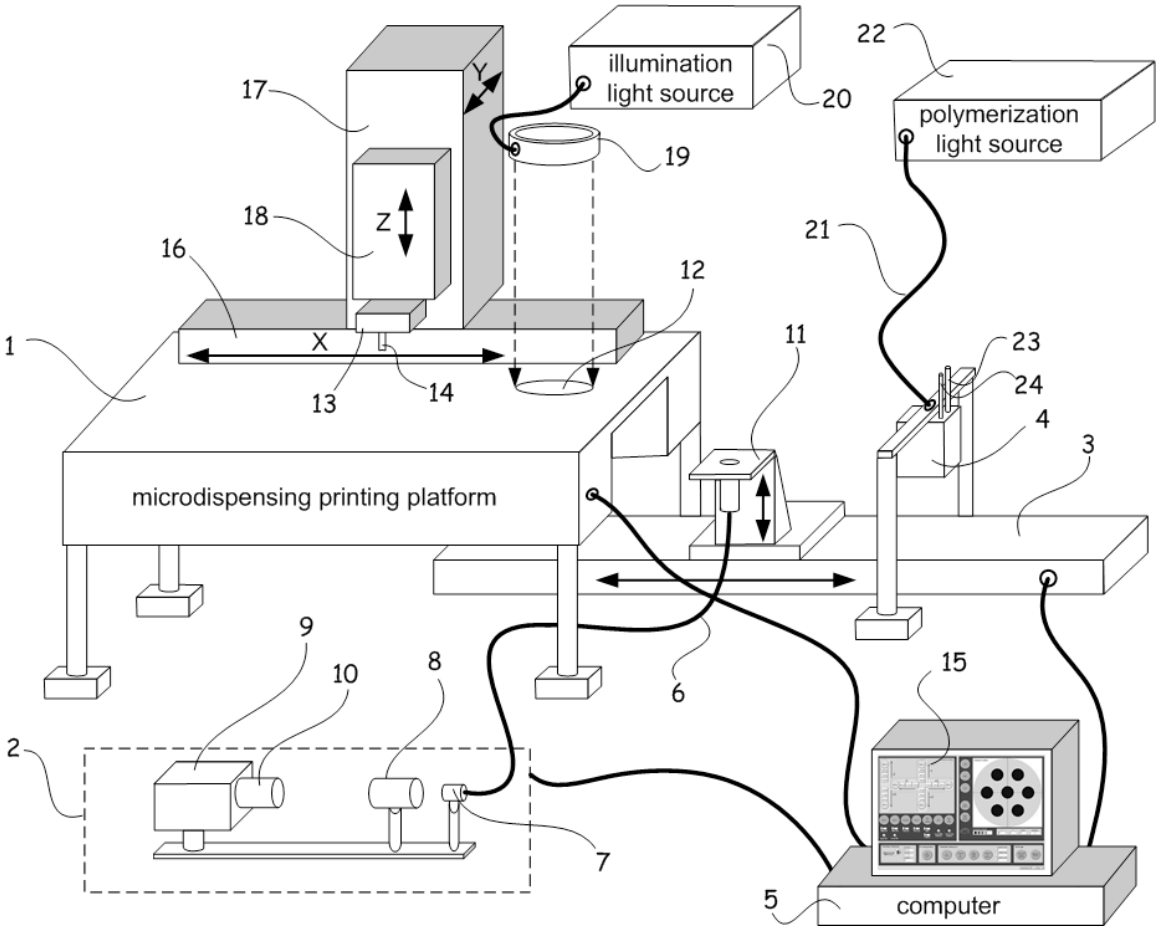

Fig. 3.1 Schematic design of the microdispensing system for printing sensing arrays on optical fiber image guides. The following describes each system component:

1) microdispensing printing platform
2) imaging vision system
3) horizontal translating stage
4) photo-polymerization chamber
5) computer/custom software
6) optical fiber image guide
7) fiber fixture (proximal end)
8) collimating microscope objective
9) CCD camera
10) camera lens
11) translating fiber fixture (distal)
12) optical fiber printing position
13) print head
14) rigid pin printing tool
15) graphical interface control
16) X positioner translation stage
17) Y positioner translation stage
18) Z positioner translation stage
19) ring light
20) light illumination source
21) liquid light guide (for UV)
22) intense UV light source
23) relative humidity probe
24) inlet for N_2 purge

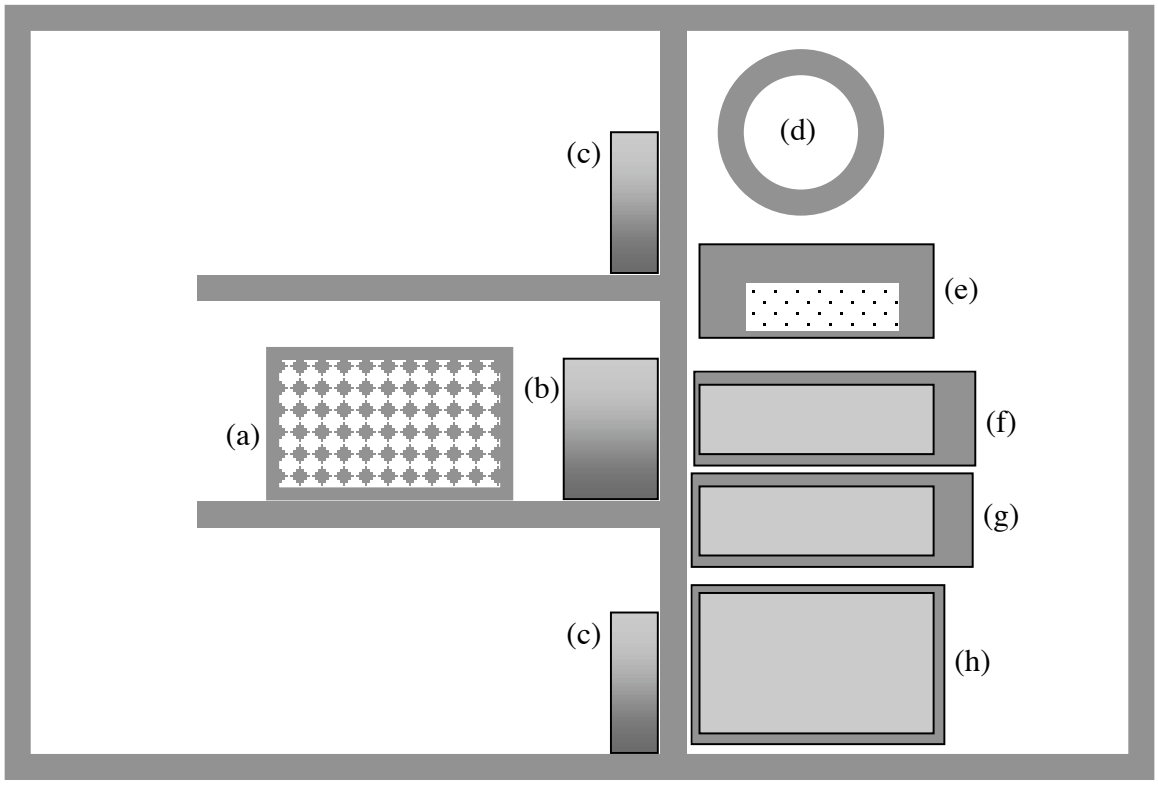

Figure 3.2 Schematic diagram of the microdispensing printing platform chamber showing stations for (a) sample loading via a 96, 384, or 1576 well plate, (b) pin blotting (glass substrate), (c) dispensing on slides, (d) dispensing on a fiber, (e) pin vacuum cleaning (f) pin cleaning via wash station #1, (g) pin cleaning via wash station #2, and (h) pin sonicating.

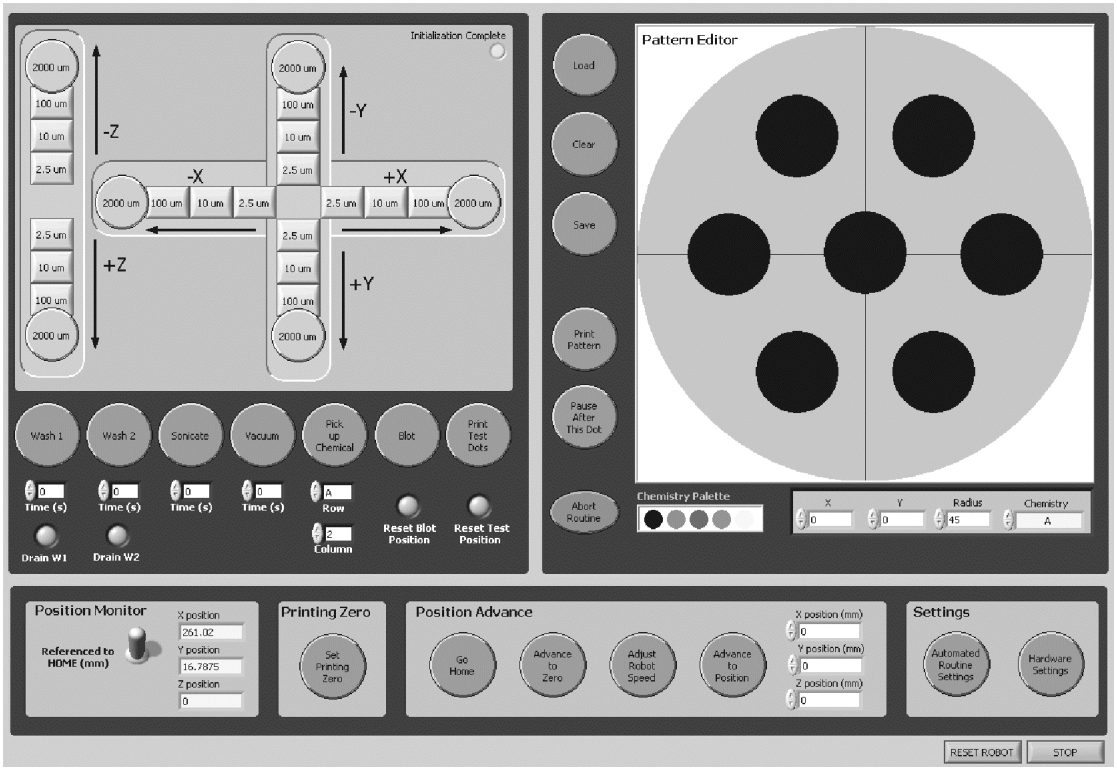

Figure 3.3 Custom user interface with key features including (a) software joystick control, (b) the fiber diagram, and (c) color-coded indicator chemistry palette.

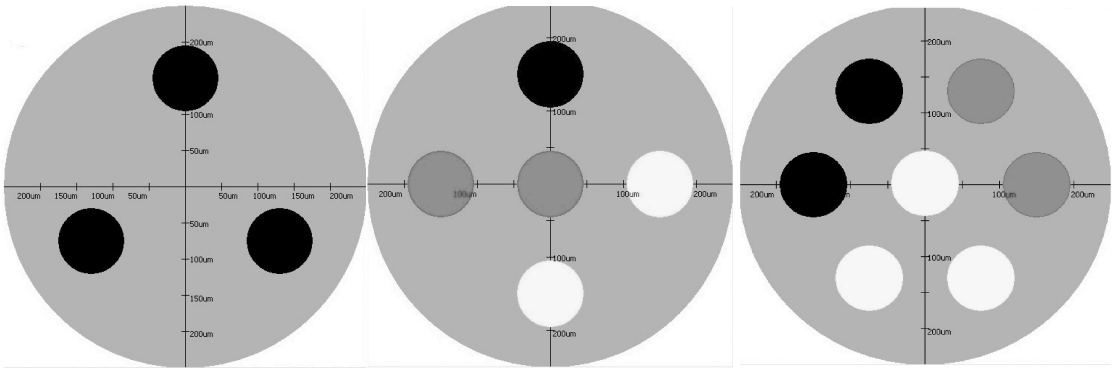

Figure 3.4 Examples of different printing patterns for printing (a) single or (b,c) multiple indicator chemistries on optical fibers or other waveguide substrates. A rigid pin printing tool is programmed to dispense indicator chemistries in the exact positions represented, in this case, on the surface of an optical fiber template. Each indicator chemistry is color coded and the different colors represent different indicator chemistries.

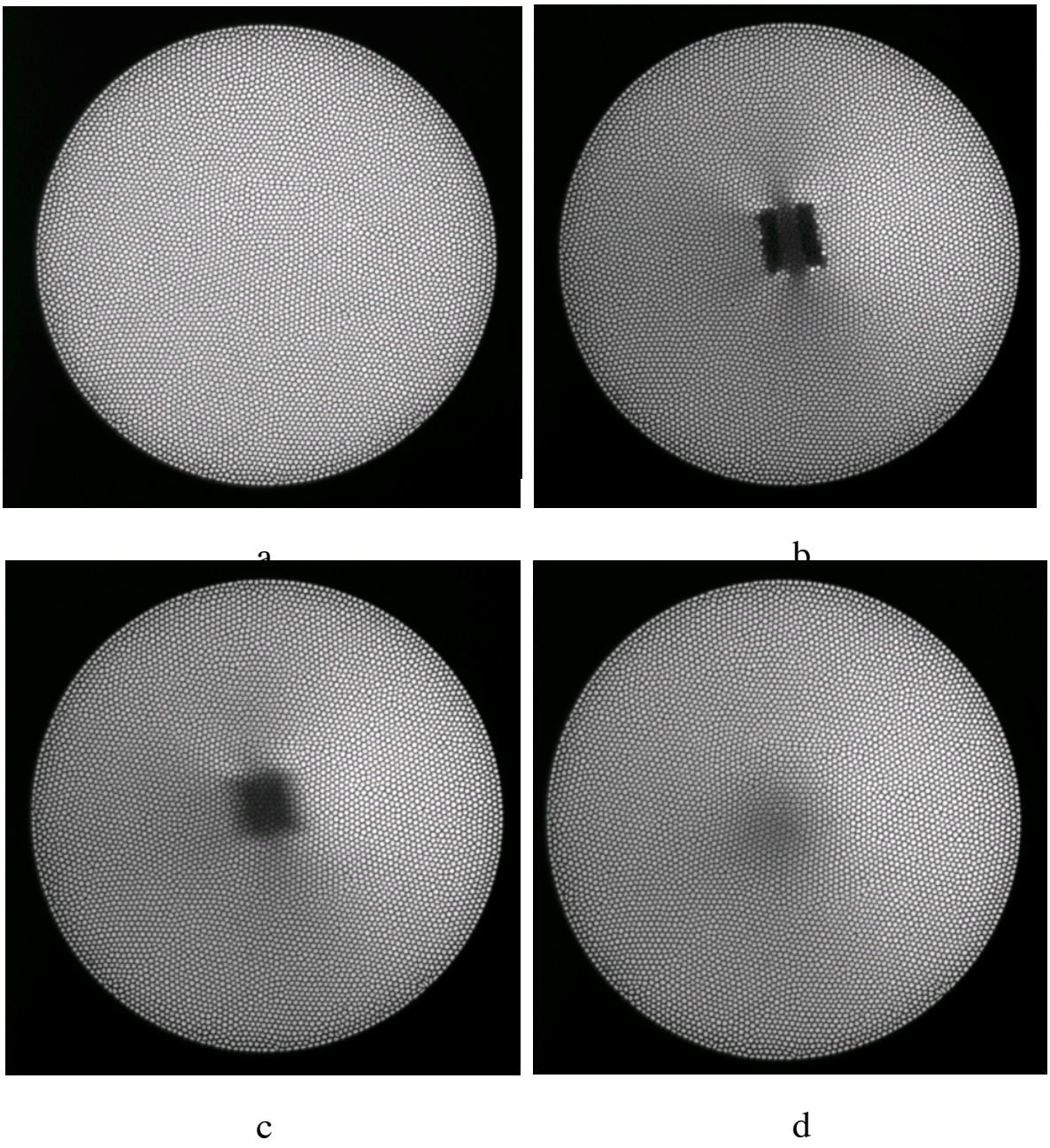

Figure 3.5 Images acquired through the image guide fiber (a) before and (b) after the rigid pin printing tool is positioned in direct contact with the fiber surface, and images of the rigid pin printing tool at (c) 10 and (d) 100 microns above the fiber surface. In image (b) the center portion of the rigid pin printing tool tip is open forming the capillary from

which indicator chemistries are dispensed. The chemistries are actually "stamped" onto the surface of the fiber.

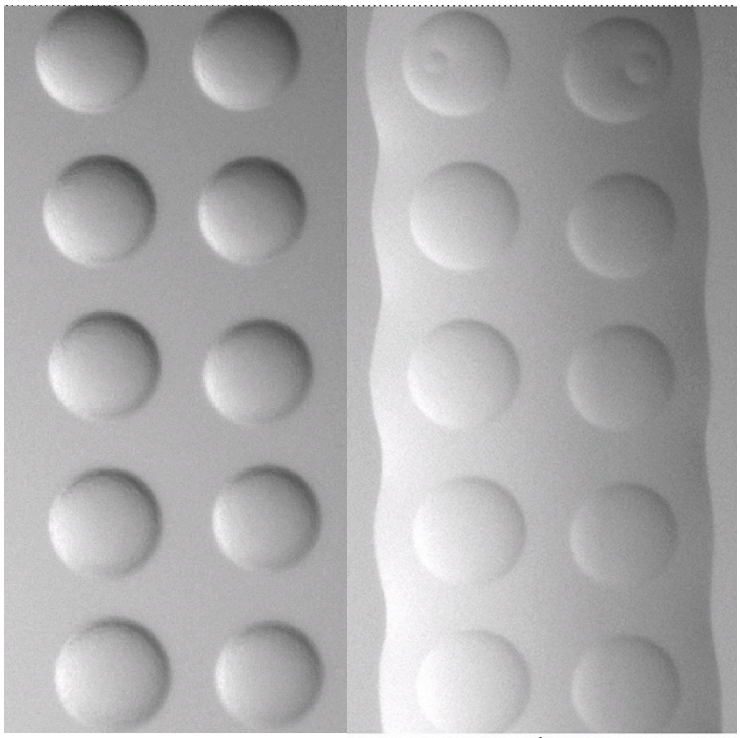

Figure 3.6 An image of (a) sensing elements (~100 micron diameter each) printed and photopolymerized as a linear array on a microscope slide and subsequently (b) exposed to a droplet of water. The water is visible in (b).

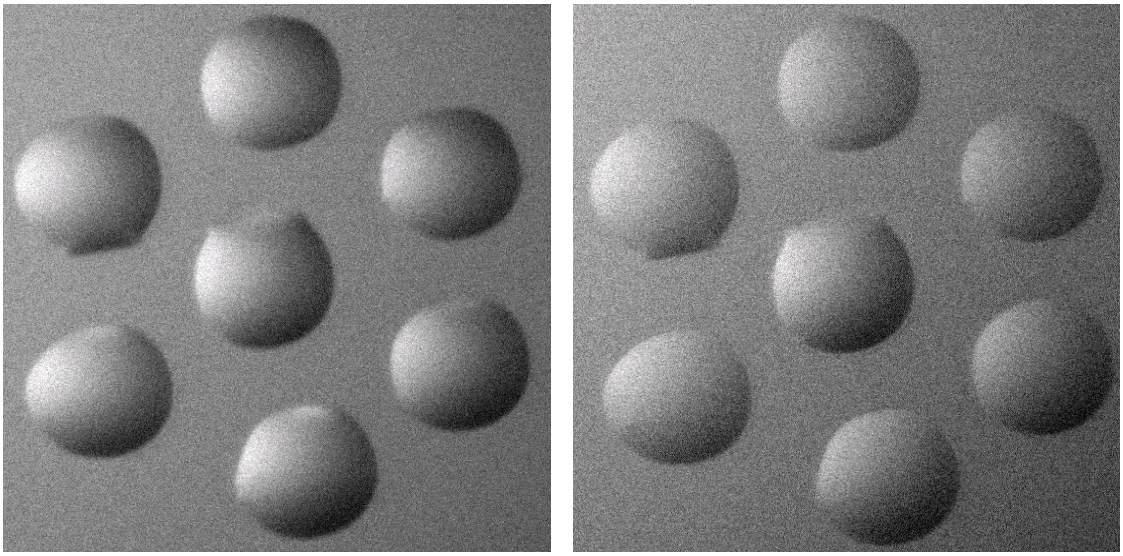

a b

Figure 3.7 An image of a (a) 6-around-1 pattern of sensing elements (~100 micron diameter each) printed and photo-polymerized on a microscope slide and subsequently (b) exposed to a droplet of water. The water has evaporated and is not visible in (b).

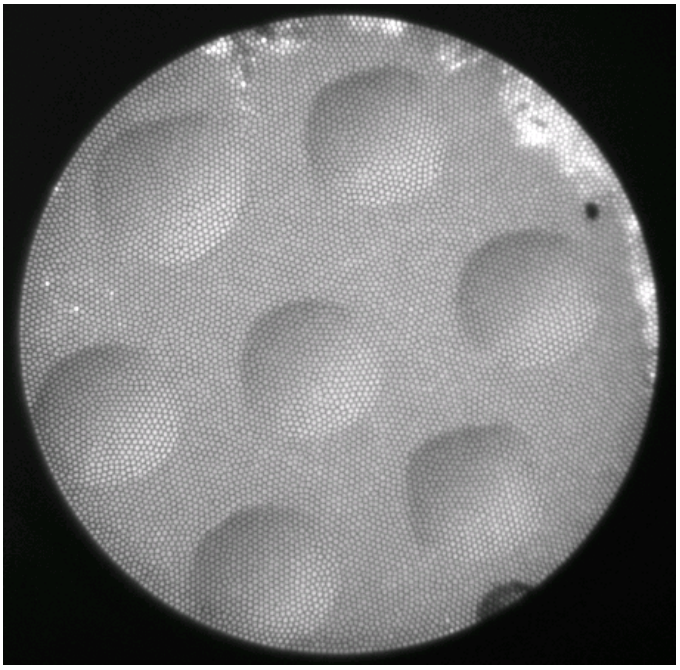

Figure 3.8 A 6-around-1 pattern of sensing elements printed and photopolymerized on the surface of a 500 micron diameter optical fiber image guide. The brighter areas around the edge of the image guide fiber are contaminants introduced during fiber functionalization and printing preparation. Each sensing element is ~100 microns in diameter.

Chapter 4

Chemistry Development for Contact-based Inkjet Printing

4.1 Introduction

All sensors developed during this work, whether single or multianalyte, are of the type known as immobilized indicator-based optical fiber chemical sensors. The concept of immobilized indicator-based involves indirect sensing of target analytes via optical changes (e.g. absorption or fluorescence) in an indicator chemistry immobilized (e.g. covalently, etc.) in a medium (e.g. polymer, etc.) that can be attached (e.g. covalently, etc.) to the optical fiber surface. This section details the development of these sensing chemistries (i.e. indicators and the polymers in which indicators are immobilized) for contact-based microdispensing using rigid pin printing tools [a discussion of non-contact microdispensing chemistries is included in Section 2, the only section devoted to that approach]. Although a portion of the information included in this section is contained in others, the focus here is an in depth discussion of sensing schemes, indicator chemistry design criteria, hydrogel chemistry design, enzyme activation, and photopolymerization considerations. The chemistries that are included here are the fluorescence-based indicator chemistries for pH and enzymes and the acrylamide-based hydrogels for immobilizing the indicator chemistries on the tips of optical fiber image guides.

4.2 Fluorescence Resonance Energy Transfer Substrate Development for Enzyme Detection

The sensing scheme for detecting enzymes in solution involves monitoring changes in the fluorescence intensities of indicator chemistries using fluorescence resonance energy

transfer (FRET). Fluorescence is a type of photoluminescence spectroscopy in which a molecule absorbs energy from a photon and subsequently re-emits a photon at a longer wavelength than the exciting photon. More specifically, fluorescence involves emission between electronic states in the molecule. Typically, a molecule is excited via energy from an incident photon from the singlet ground state into an electronic excited singlet state. Some vibrational energy loss in this excited singlet state usually occurs prior to the molecules return to the ground singlet state, resulting in photon emission.

Fluorescence resonance energy transfer (FRET) is a process involving at least two molecules, commonly referred to as the (1) donor and the (2) acceptor molecules. The donor molecule absorbs energy from a photon (i.e. ground singlet state to excited singlet state) as described above for fluorescence, however, the donor molecule does not re-emit a photon but rather transfers the energy to the acceptor molecule. This energy transfer process between two molecules is known as FRET. FRET depends on several factors, which include the overlap between the donor molecule emission band and the acceptor molecule absorption, the dipole orientation of each molecule with respect to the other, and the physical separation distance between the donor and acceptor molecules (typically 10-100 nm is required) [1-3]. Since FRET is dependent on the donor/acceptor pair physical separation distance, it is a useful methodology for enzyme detection since substrates can be designed with enzyme cleavage sites between the donor/acceptor pair. Finally, the efficiency of FRET is dependent on the inverse sixth power of the intermolecular separation.

A new class of fluorescence resonance energy transfer (FRET) based indicator chemistry was developed for detecting enzymes, in situ. This chemistry, based on short chain (7-10 amino acid sequences) polypeptide substrates, utilizes two innovations: (1) the use of donor/acceptor dye pairs that absorb and fluoresce in the visible region of the spectrum, (2) and a unique "handle" for covalently binding the substrate to a surface (e.g. waveguide) or within a polymer network. Although there are numerous commercially available FRET-based substrates for detecting various enzymes, a survey revealed that nearly all incorporate the use of FRET donor/acceptor pairs with optical properties (i.e. absorption and emission) in the ultraviolet region (UV). The most commonly used FRET donor molecules are coumarin-based dyes. Acceptors include molecules that undergo both radiative or nonradiative quenching. These commercially available substrates are limited to solution-based analyses only, having no means for direct covalent attachment to a waveguide surface (e.g. optical fiber) or within a polymer matrix attached to a waveguide surface. Even if immobilization were possible, commercially available substrates are not amenable to fiber-based sensing because optical fibers (particular optical image guide fibers) do not transmit light efficiently in the UV.

The following are four principal issues involved in developing FRET substrates:

- selectivity
- sterrics
- reaction rates
- energy transfer efficiency
- solubility

Selectivity refers to the ability of the enzyme to recognize and bind to a specific substrate and subsequently catalyze a reaction. The binding of the relatively large enzyme

biomolecules (~20-30 kDaltons for the enzymes in this study) to the substrate can be limited by sterric hindrance in the substrate design. For example, fluorescent dyes with optical properties in the visible region of the spectrum are typically large aromatic pi-pi bonding species (e.g. fluorescein and rhodamine). These dyes tend to be relatively large compared to their UV counterparts (e.g. coumarin-based dyes) and thus more likely to interfere with the enzyme/substrate interaction. Another concern involves reaction rates, which may also be affected by the same sterric hindrance issues. The addition of a "handle" for covalently linking the substrate is also a concern since it can potentially interfere with the enzyme/substrate interaction by altering the electronics of the donor or acceptor molecule, thereby, shifting the optical properties and effecting the transfer efficiency of the donor pair. Lastly, the individual solubilities of the molecules (i.e. donor, acceptor, amino acids, linker) that form the FRET-based substrate determine the dissolution characteristics. Dye molecules with optical properties in the visible spectrum tend to be large aromatic species and are more hydrophic than hydrophilic. Therefore, it is necessary to compensate for this in other ways such as choosing amino acids and a linker that is hydrophilic.

The first custom substrate for detecting MMP enzymes was designed at LLNL but outsourced to SynPep Corporation (Dublin, CA) for synthesis using standard industry peptide procedures and purification. The polypeptide sequence for this substrate is shown in Table 4.1a. The peptide sequence contained the Leu/Ala pair, which has been reported to be the cleavage site for the target enzyme, MMP-8 (matrix metalloprotease 8, collagenase family). This substrate was designed using carboxyfluorescein (FL) and

tetramethylrhodamine (TMR) as the donor/acceptor pair. This pair has been widely used for FRET measurements because of their individually high molar absorptivities and superior energy transfer optical properties compared to other dye pairs [4]. A polymerizable linker (e.g. reactive carbon-carbon double bond "handle") for covalent attachment to a hydrogel or other polymer was not designed as part of this substrate since initial work was aimed at evaluating whether large aromatic dyes could be used for solution-based enzyme detection (relatively smaller coumarin-based dyes are typically used). All MMP enzymes were purchased from Calbiochem and activated using the manufacturer protocol [5-6].

For the experiments involving the custom peptide shown in Table 4.1 sequence 1, a stock solution of the peptide was first prepared in Tris buffer (with a few 100 microliters of DMSO for dissolution purposes). Aliquots of this peptide solution were incubated with the individual MMP enzymes including the target, MMP-8. The solution-based fluorescence emission spectra (ex: 440nm/ex: 515nm) of the various aliquots, after incubating for 17 hours with APMA-activated Calbiochem enzymes, are shown in Figure 4.1 (a-f). All data was recorded using a Perkin-Elmer LS55 fluorimeter at room temperature. The broad bands at 515 and 580 nm show the carboxyfluorescein (donor molecule) and tetramethylrhodamine (acceptor molecule) emission, respectively. The substrate is designed such that excitation radiation, corresponding to a shoulder on the absorption band of the donor, excites the donor molecule (carboxyfluorescein), which then transfers energy through a non-radiative process to the acceptor molecule (tetramethylrhodamine), having a partial overlapping absorption band with the donor

emission band. It is important to note that in FRET applications, exciting the donor molecule at the absorption maximum does not always produce the best results. For example, if carboxyfluorescein is excited at its absorption maximum, the excitation radiation will also directly excite the tetramethylrhodamine shoulder, resulting in tretramethylrhodamine emission that is not solely due to energy transfer from the fluorescein. For this reason, the excitation radiation (~440 nm) used in these experiments does not correspond to the absorption maximum (~480 nm) of carboxyfluorescein. This is a very important consideration when performing FRET with fluorescent dye donor and acceptor molecules.

When the energy transfer is broken (i.e. when the enzyme cleaves a site between the donor and acceptor molecules causing a separation in distance between the molecules), the donor no longer transfers energy to the acceptor molecule but rather emits at its characteristic emission wavelength (emission max ~515 nm). Figure 4.1f shows the emission spectra with no enzyme added and serves as an experimental control. Because FRET is not 100% efficient, there is some observable emission from the carboxyfluorescein donor molecule (there is also some fluorescence observed from tetramethylrhodamine). Figure 4.1a-c shows a noticeable increase in the emission observed at 515 nm, the emission max for carboxyfluorescein. This indicates that the target enzymes, MMP-9, MMP 8, and MMP 3, have cleaved the FRET-based substrate to varying degrees. This also shows that the custom peptide design does not have the desired selectivity toward the target enzyme, MMP-8). The emission spectra (d, e) resulting from incubation with MMP-1 and 2 do not show any significant differences

from the control spectra (f), indicating that these enzymes did not cleave the substrate. The spectra for MMP-1 (d), MMP-2 (e) and the control (f) are superimposed in Figure 4.1(d-f). Because of the extremely long incubation time required to observe cleavage of the substrates with the enzymes and the target enzyme MMP-8, it was impractical to conduct fluorescent time scans (i.e. monitoring the donor or acceptor emission wavelength versus time) of the cleavage process. It is also important to note that the substrate had limited solubility in aqueous solution, requiring the addition of DMSO to completely dissolve the substrate. One possibility for such slow reaction rates is steric effects related to the insolubility of the molecule in water. The varying degree of reactivity between MMP-9, MMP8, and MMP-3 is also attributed, at least in some part, to steric effects, although this was not fully investigated.

The data in Figure 4.2 is a repeat of experiments previously described above (Figure 4.1) with one exception. The enzymes used to obtain the data in Figure 4.1 were prepared and used the same day, whereas, the data for Figure 4.2 was obtained with 1 day old enzymes which had been frozen and thawed. In comparing the fluorescent intensity data of Figures 4.1 and 4.2, there is a clear difference in response, which is attributed to the relative activity of the enzymes. The effect of a freeze/thaw cycle reduces the activity of MMP-8 as shown in Figure 4.2, resulting in lower fluorescence intensity counts over the same incubation time (17 hours) as experiments in which enzymes were fresh. The enzymes MMP-3 and 9 show no response in Figure 4.2, which indicates that a single freeze/thaw cycle has deactivated these enzymes. It is important to note that long-term refrigerated storage of the stock peptide solutions does not degrade the peptide.

The next iteration involved designing an MMP-1 specific substrate based upon the published work of Geoghegan and coworkers [7]. Table 4.1 (sequence 2a) lists the sequence that was synthesized based upon their work. Another variation of this sequence was synthesized as shown in Table 4.1 (sequence 2b) with a carbon-carbon double bond linker for covalently attaching the peptide sequence to a polymer network. Following the work of Geoghegan and coworkers, all enzymes (i.e. MMP-1, MMP-2, MMP-3, MMP-8, and MMP-9) were activated with chymotrypsin and individual enzymes incubated in aliquots of the stock peptide solutions in the same manner described above for Table 4.1, sequence 1. The experimental control for these experiments contained the buffer solution and the chymotrypsin activator but no MMP enzyme. This control, as well as all MMPs activated with chymotrypsin, cleaved the peptide substrate indicating that the chymotrypsin (an enzyme activator) was specific for the substrate. Figure 4.3a,b show the fluorescence emission time scan (monitored at 515 nm) and fluorescence emission spectra, respectively, before and after chymotrypsin is added to the solution containing the peptide substrate. Although the results from the initial MMP experiments using chymotrypsin as an activator were inconclusive, we learned from this that chymotrypsin is a very useful enzyme for testing the viability of the refrigerated stock peptide solutions. Since chymotripsin is readily available and relatively low cost compared to MMPs, we also began using chymotrypsin as our test enzyme for new peptide substrates. As an example, Figure 4.4a,b shows comparisons of the fluorescence emission time scans (monitored at 515 nm) and fluorescence emission spectra, respectively, of the sequences containing “no handle” (Table 4.1, sequence 2a) and a “handle” (Table 4.1, sequence 2b).

In both cases, all things being equal (substrate and chymotrypsin concentration, incubation time, etc.) the presence of the "handle" (sequence 2b) does affect the reaction rate and overall fluorescence intensity during and after enzyme cleavage of the substrate.

At the beginning of this project, pre-activated MMP enzymes (1,2,3,8,9) were not commercially available, which required a parallel effort on our part aimed at understanding the MMP activation process. This effort was hindered by the fact that there was a wide discrepancy between manufacturer activation protocols and published literature protocols. For example, one published report [8] specified incubating with an organomercurial activator concentration of 1.5mM for 16hr, whereas, the Calbiochem protocol [5] calls for 10-50 mM for 2-3hrs. Enzyme activation studies were conducted using APMA (4-aminophenyl mercuric acetate), a commonly used organomercurial enzyme activator. The commercially available peptide substrate shown in Table 4.1, sequence 3, was chosen for these studies since it responds to most MMPs (except MMP-3). This substrate utilizes a FRET donor/acceptor pair with excitation and emission properties in the UV region. All enzyme activation studies were conducted in cuvettes (i.e. non-fiber) using a Perkin-Elmer LS55 fluorimeter. These studies focused on understanding and optimizing MMP activation such as the activator concentration, the incubation time of the enzyme and activator, and buffers.

Figure 4.5 a-e shows the fluorescence emission time scans of the peptide sequence in Table 4.1, sequence 3 before and after addition of MMP enzymes activated with APMA using our optimized protocol of 1mM APMA incubated for 30 min in Hepes buffer. The

emission time scan shows the baseline intensity before adding each enzyme and the resulting increase in fluorescence intensity monitored at 390 nm. A decrease in fluorescence intensity is observed at the point of enzyme addition, a result of peptide concentration dilution. Hepes buffer provided superior results compared to Tris buffer (data not shown). Hepes had been recommended [11] over other buffers for enzyme storage since it best preserves enzyme activity over several freeze/thaw cycles. In addition, some of the commercially available MMP kits (e.g. biomol) utilized Hepes buffer as well.

Using the optimized APMA activation protocol, Table 4.1 sequence 2a was retested. Figure 4.6 shows the fluorescence emission scans of before and after addition of MMP-1 and MMP-8. The rate of enzyme cleavage is nearly the same but very slow. Figure 4.7 shows the fluorescence emission spectra of the peptide substrate in solution before and after 5 hr incubation with MMP1.

Although we achieved improvements in enzyme activation by modifying the published protocols, we struggled with reproducibility. Fortunately, Biomol (Plymouth Meeting, PA) began selling commercially available pre-activated MMPs during the second year of this project. We soon abandoned activating enzymes in house and began purchasing pre-activated MMP enzymes.

The final set of substrates developed during this work are shown in Table 1 (sequences 4a and b). Sequence 4a contains no “handle” for covalently linking within a polymer matrix. Sequence 4b contains a carbon-carbon double bond “handle” attached to a

hydrophic long chain polyethylene glycol (PEG) linker (X=COCH2-$(OCH2CH2)_2$NHCOCH2$CH_2CH_2CH_2$=CH2). The use of a longer chain linker was based on experimental work involving the Table 4.1, sequence 2b in which unsuccessful attempts were made to co-polymerize the substrate with an acrylamide-based hydrogel. We attributed the lack of success to the relatively short and unreactive methacrylic acid linker used in that substrate. The details of this last substrate are the subject of Section 6.

Table 4.1 Enzyme substrate sequences.

Substrate number and sequence	
1. TMR-Gly-Pro-Leu-Ala-Tyr-Lys-(Fl)-Ala-Arg-NH_2	no handle
2. a) LY-Gly-Pro-Leu-Gly-Leu-Arg-Ala-Lys-(5-carboxylTMR)-COOH	no handle
b)LY-succinyl-S-Lys(Acryloyl)-Gly-Pro-Leu-Gly-Leu-Arg-Ala-Lys-(TMR)-COOH	handle
3. Mca-Pro-Leu-Gly-Leu-Dpa-Ala-Arg-NH_2.AcOH	no handle
4. a) 5-FAM-Lys-Pro-Leu-Ala-Nva-Dap(5/6-TMR)-Ala-Arg-NH_2	no handle
b) 5-FAM-Lys(X)-Pro-Leu-Ala-Nva-Dap(5/6-TMR)-Ala-Arg-NH_2	handle

4.3 pH sensitive indicator synthesis

Fluorescein and its derivatives have been widely studied and are effective for aqueous measurements in the neutral pH range. The pH-dependent ionic equilibria of fluorescein and its derivatives have been described.[9] Although numerous fluorescein dyes are commercially available, the fluorescein derivative, acryloyl fluorescein, was synthesized using the following modified procedure from published reports.[10-11] To a solution of

0.9g (2.6 mmol) of fluoresceinamine in 30ml of distilled THF was added 0.2 ml (2.6 mmol) of acryloyl chloride. The solution was stirred in dark at 0o C for four hours. Evaporation of the solvent gave almost pure acryloylfluorescein as dark brown powder. HNMR (DMSO, 300MHZ), _: 5.800- 5.834 (d,1H), 6.288-6.888 (m, 8H), 7.205-7.2333 (d, 1H), 7.902-7.929 (d, 1H), 8.418 (s, 1H), 10.79 (s, 1H). CNMR (DMSO, 100MHZ), -: 69.833, 102.308, 110.670, 113.738, 114.820, 125.390, 126.075, 127.399, 127.780, 129.323, 131.616, 140.888, 144.375, 152.876, 152.876, 161.174, 163.845, 168.340. ES-MS: m/z 401.

4.4 UV Curable pin printable hydrogel formulations

In this work we developed UV curable water-based monomer formulations to immobilize the indicator chemistry (absorbing dye) in hydrogel microdots on the ends of optical fiber bundles. In this section we discuss the development of those formulations in view of the many functional requirements placed on them in terms of their printability, polymerization, and sensor application specific properties. These functional requirements are discussed first, followed by a detailed discussion of the roles and specific chemistry of hydrogel formulation components.

4.4.1 Sensor specific properties

The conceptual basis for an optical fiber based multianalyte sensor was based on the idea of immobilizing the indicator chemistry in matrices with distinct geometry patterns that can be attached to the surface of an optical fiber. Many different types of matrices have been reported including inorganic sol-gels, porous polymer membranes, and hydrogel networks. The choice of matrix depends primarily upon the hydrophilicity of the analyte,

(e.g. whether the analyte of interest requires either a hydrophobic or hydrophilic membrane). Hydrogels, i.e. materials that are composed primarily of water pervaded by a three-dimensional macromolecular or polymer network, offer many advantages for sensing applications in which the target analyte is water-soluble. These advantages include broadly varying chemical composition, compatibility with biological molecules such as peptides, proteins, enzymes, and DNA, a tremendous range of possible network morphologies, and the ability to simultaneously immobilize specific indicator molecules while making them accessible to analytes in solution.

In the case of hydrogels used for the target sensors (pH and enzyme) in this work there are a number of specific requirements. First, the chemistry must be such that the hydrogels are compatible with target biological molecules. This is especially true in the case of the enzyme sensor where the hydrogel cannot promote the denaturing of target enzymes. The sensors are to be used in vivo, hence, these must be biocompatible. Depending on their specific site and duration of use, this may mean invoking no short term cytotoxic, immulogical, or thrombogenic response. The hydrogels must have the appropriate network structure to optimally allow for the diffusive penetration of targeted analytes while excluding as much as possible other molecules. The hydrogel must be capable of immobilizing the indicator chemistry while at the same time allowing for interaction of the indicator chemistry with the analyte. The hydrogel must have sufficient mechanical integrity to withstand handling and/or hydrodynamic forces imposed on it in application. Finally, since the sensors are based on fluorescence techniques, they must be optically clear. Generally, these requirements were accomplished through choice of type

and concentration of monomer and crosslinker, immobilization through either physical entrapment of indicator molecules or by covalently binding them to the hydrogel network during photopolymerization, and by the inclusion of surfactants, choice of photoinitiator, and use of co-solvents.

The next set of hydrogel formulation issues to be considered regards the process for placing geometric patterns of differnent hydrogel/analyte composites onto the end of an optical fiber. While the decision to use pin printing for this process is discussed elsewhere, here we consider the pin printing process and requirements placed by it on the printable pre-polymer formulation. This process is illustrated in Section 3. A robotic arm with 3 axis mobility is used to hold a metal pin and successively move the pin to dip into a formulation source 96 well plate, move the pin to a glass blotting substrate which is contacted a number of times to remove excess formulation and establish a pseudo-steady pattern, move the pin to positions above the desired print substrate and contact the pin onto the substrate the required number of times, then take the pin through a cleaning process to be ready for the next pre-polymer formulation. The pre-polymer formulation must have the appropriate physical properties to be taken up by the capillary pin and be deposited reproducibly as approximately hemispherical microdots onto the substrate during impacts between the capillary pin and substrate. In this process the key relevant forces acting on the pre-polymer fluid include surface tension (relative to pin surface energy and substrate surface energies), fluid inertia, and fluid hydrodynamics. In particular, there must be a delicate balance between surface energy of the capillary pin, surface tension of the formulation, and surface energy of the substrate. Once printed, the

pre-polymer dots must be geometrically stable until they are polymerized. Formulation properties that must be controlled to achieve proper printing are then surface tension, fluid rheology, and formulation volatility. Additionally, it is necessary to modify the surface energy of the substrate through surface modification (e.g. functionalization).

Once printed, the pre-polymer formulation must be capable of being set into the final hydrogel morphology. Gel networks can be formed by both physical and chemical processes, and in chemical processes by both condensation and step (e.g. free radical) types of polymerization. In radical polymerization, initiation can be accomplished thermally, through photoinitiation, ionization, plasma methods, and electroionization methods. Of these thermal or photo-initiated free radical polymerizations have been most widely used for microjet processes. In particular UV intitiated free radical polymerization allows for the rapid and uniform polymerization of printed microdots and was thus chosen.

4.4.2 Hydrogel pre-polymer formulation components

A summary of the prepolymer formulation compositions is given in Table 2 for the pH and enzyme sensors. These formulations were then mixed 1:1 with a solution of the indicator chemistry in water just prior to printing. The selection and purpose of individual components and their concentrations are described below in more detail.

Table 4.2 Typical Sensor pre-polymer formulations (in Weight Percent)

Component	Function	pH sensor formulation	Enzyme sensor formulation
Water	solvent	53.47	84.93
Acrylamide	monomer	44.34	14.51
Bisacrylamide	crosslinker	0.92	0.148
BEE	initiator	0.20	0.065
Ciba 2959	initiator	0.98	0.316
FC-430	surfactant	0.10	0.035
Acrylamide/ Bisacrylamide	monomer/crosslinker	49:1	24:1

4.4.3 Monomer and concentration

As previously discussed, there are a large number of factors involved in the selection of an appropriate hydrogel chemistry, including water solubility, biocompatibility, biodegradeability, interaction with analyte molecules, crosslinkability, ability to incorporate indicator molecules into network, isoelectric point, process for polymerization, ability to control network structure, etc. Suitable candidates can be derived from the extensive list of water soluble polymers (reference) and include acrylamide, water soluble acrylics (e.g. hydroxyethylmethacrylate), phosphazene polymers, polysacharides, cellulosics, poly(ethylene oxide), poly(methylene oxide), water soluble polyesters, etc. Poly(acrylamide) was quickly chosen as the primary candidate due to its high solubility, excellent compatibility with enzymes and DNA, rapid

polymerization kinetics in water, and extensive literature on the use of acrylamide hydrogels for DNA separations.

Acrylamide monomer concentration was optimized for the different types of sensors (pH enzyme) based on the individual application requirements. Factors affecting the optimization process include size of analyte versus the size of undesirable molecules in the media being examined, rate of polymerization, and solubility of initiator. Polymerization rate and initiator solubility increased with monomer concentration, while diffusivity of analyte molecules into the polymer network degree with monomer concentration.

4.4.4 Crosslinker

The selection of crosslinker mainly involves choosing one, which has both water solubility and has reactivity as similar to the monomer as possible to form as uniform a network structure as possible within the constraint of a statistical polymerization process. While several crosslinkers were considered the selection was rapidly narrowed to N,N'-methylene bisacrylamide (bisAcrymaide)and ethylene glycol dimethacrylate (EGDMA). In the end bisAcrylamide was chosen based on reactivity and the preponderance of prior art in its use with acrylamide to make hydrogels for DNA separations.

The ratio of crosslinker to monomer determines the modulus of the hydrogel network as well as the size of openings within the network through which analyte will pass. A higher crosslinker concentration provides for a hydrogel with higher mechanical modulus

and strength, lower swellability in analyte solution, smaller network openings, and faster gelation on polymerization. Studies was varying ratios were used to optimize the crosslinker level with respect to allowing for immobilization of the indicator chemistry while allowing for diffusion of the analyte into the network. Values are given in Table x.

4.4.5 Photoinitiator type and concentration

The determination of an optimal coctail of photoinitiators for the UV induced initiation of radical polymererization involved the consideration of photoinitiator solubility, absorption spectra, and thermal stability. Concentration of initiator needs to be high enough to promote polymerization (after burning off residual oxygen and inhibitor), while too much will adversely affect the molecular weight of the polymer and hence the finished network structure. A number of initiators were tried including benzoin, benzoin ethyl ether, camphorquinone, AIBN, and 1-[4-(2-Hydroxyethoxy)-phenyl]-2-hydroxy-2-methyl-1-propane-1-one (Irgacure 2959®) . Benzoin ethyl ether (BEE) was found to be an excellent initiator but suffered from limited solubility in water (<0.1% at 25% monomer). It was found that a combination of the Irgacure 2959® (2.2 wt% based on monomer) and BEE (0.4wt% based on monomer) provided near optimal polymerization and hydrogel formation.

4.4.6 Issue of O_2 inhibition for free radical polymerization

The prepolymer formulations used here were polymerized by free radical polymerization with UV intiators into a hydrogel network after printing. Oxygen is known to be a powerfull inhibitor to the free radical polymerization of vinyl monomers at lower

temperatures, where it scavenges radicals to form relatively stable peroxides. In this work care was taken to minimize the amount of dissolved oxygen in sensor formulations at each step of the process prior to their polymerization. The formulations were mixed using water which had been nitrogen sparged for 12 hours or more. Printing was carried out in a moist nitrogen environment and the printed sensors were keep in a moist nitrogen atmosphere up to and during UV curing. In this way the UV intensity and exposure time required to polymerize the sensors was minimized, which likewise minimized the photobleaching of the sensor components.

A variety of different polymerization processes are known, including thermal techniques, photoinitiated methods, ionization methods, plasma methods, and electroionization methods. Photoinitiated methods are very clean methods in that no solvents are required. Most importantly this method is also more amenable than the other methods, which are based on wet chemistry. There are numerous commercially available non-water soluble photoinitiators. One of the most often used is benzoin ethyl ether, which has very limited solubility in water. Initial experiments in which microdots were printed and photopolymerized revealed problems. Polymerization occurred at the interface of the fiber surface and not in the bulk. One potential reason for this may have been due to the surfactant utilized. As previously discussed, a surfactant was required to adjust the surface tension of the printable formulation to allow pin printing. A search for a water-soluble photoinitiator with absorption properties similar to benzoin ethyl ether revealed only one suitable, 2959. Hydrogels formulated with both the water soluble C2959 and non-water soluble benzoin ethyl ether were easily polymerized using UV light.

4.4.7 Surfactant

A key parameter in the effective printing of prepolymer formulation is the surface tension of the formulation. In the printing process, the formulation must spontaneously wet (zero advancing contact angle) the surface of the capillary pin in order to both load properly and to ensure that there is a reproducible bead of liquid at the tip for contact to the substrate. In the case of the substrate, the formulation must simultaneously be able to wet the substrate surface but not in a spontaneous manner. More precisely, the formulation must have a contact angle with the substrate less than 90 degrees or else liquid will retract with the pen and not form reproducible dots. However, the contact angle must be higher than approximately 30 degrees or spreading of the printed liquid will occur and both result in irreproducible dots as well as the coalescence of closely printed dots into larger droplets. In the end it was found that surfactant modification to achieve a contact angle in the range of 60 degrees was nearly optimal. For this purpose a number of surfactants were tested and of those it was found that 0.1% by weight of Fluorad FC-430 (3M Specialty Materials, St.Paul, MN), a fluoroaliphatic ester surfactant, provided effective modification of both concentrated monomer solutions (pH) and was still effective down to 0.016% in dilute monomer formulations (enzyme).

4.4.8 Rheology Modifier

The viscosity of the prepolymer formulation is a key variable in the process of rigid pin printing. Viscous forces resist the impact of the pin against the substrate squeezing out the fluid pendent on the tip of the pin and causing splattering around the impact site.

Likewise, hydrodynamic forces present during as the pin is raised resist the removal of the fluid from the substrate surface. At the same time, if the viscosity is too high there is not enough time for the formulation to re-establish a pendent drop on the pin tip nor for surface tension to cause the droplet to become round (print drops are initially rectangular due to pin geometry) after printing and before polymerization. In this work it was found that the viscosity of the prepolymer formulation should be roughly in the range of 2 to 5 centipoise and Newtonian (rate independent viscosity, no elasticity) in order to achieve best print results. It turns out that the acrylamide monomer based formulations designed for other purposes fit within this range. However, it was found that in cases where substrate surface energy was exceedingly low (e.g. teflon) achievement of good droplets required viscosities in the range of 50 to 200 centipoise, achieved through the use of in-house synthesized linear polyacrylamide with molecular weight in the range of 100,000 g/mole and at loadings of approximately 1% by weight.

4.4.9 Co-solvents to control Volatility

After pin printing the droplets of prepolymer formulation must maintain a relatively constant composition prior to and during polymerization; otherwise, demixing of the components can occur. The main change likely to occur is the evaporation of water. Initially, the use of co-solvents with water was investigated as a method of inhibiting solvent evaporation. A number of cosolvents were looked at including ethylene glycol, glycerol, and dimethyl sulfoxide (DMSO). While the use of high-boiling cosolvents decreased formulation volatility, it was also found to adversely affect polymerization. Therefore, it was abandoned in favor of the use of a high relative humidity atmosphere.

4.4.10 Surface Modification of substrate

Surface modification techniques were applied to the optical fiber ends in order to control both fiber surface energy and to provide adhesion of the hydrogels to the fibers by covalent bonding. The optical fibers used in this work are based on silican, and a number of silica surface functionalization techniques have been reported in the literature (references). Among these, silanization techniques are the most common and were used in this work. A detailed procedure developed for this project based on the use of allyl trimethoxysilane, chosen as optimal both for surface energy and its ability to couple to the polymer network, follows. Specifically, first the optical fibers were cleaved and polished. Following polishing, the fiber ends were

4.5 Conclusions

A new class of fluorescence resonance energy transfer (FRET) based indicator chemistry was developed for detecting enzymes. This chemistry, based on polypeptide substrates, utilizes two innovations: (1) the use of donor/acceptor dye pairs that absorb and fluoresce in the visible regions of the spectrum, (2) and a unique "handle" for covalently binding the substrate within the polymer based microdot.

Reproducibility is a problem with the enzyme substrates. There are many factors that affect this. Foremost is the ability to reproducibly activate enyzymes. As we observed in our studies quality control is key. It is much more beneficial in a developmental project such as this to purchase preactivated and tested enzymes rather than perform this in

house. Another issue is the enzyme preparation. Freeze/thaw cycles reduce the activity in enzymes and, in some cases, completely deactivates the enzyme. Certain buffers are better than others for storing enzymes. We achieved best results using Hepes buffer.

Acrylamide-based hydrogels have proven to be excellent candidates for contact-based printing applications. Acrylamide hydrogels are very reactive relative to other classes of hydrogels (e.g. methacrylates) and can be polymerized rapidly (i.e. 10s of seconds). Furthermore, These hydrogels have biocompatible properties and can be polymerized as transparent microdots (i.e. limited scattering due to turbidity). The ability to rapidly polymerize is critical to minimize photobleaching of the indicator chemistries.

4.6 References

[1] Nicholas J. Turro. *Modern Molecular Photochemistry*. The Benjamin/Cummings Publishing Co., Inc., Menlo Park, California, 1978.

[2] B. Wieb Van Der Meer, George Coker, III, and S.-Y. Simon Chen. *Resonance Energy Transfer: Theory and Data*, VCH Publishers (Now Wiley-VCH), Inc., New York, 1994.

[3] Discussions of the Faraday Society. *Energy Transfer with Special Reference to Biological Systems*, The Aberdeen University Press Ltd, Aberdeen, Scotland, 1959.

[4] B. Wieb Van Der Meer, George Coker, III, and S.-Y. Simon Chen. *Resonance Energy Transfer: Theory and Data*, VCH Publishers (Now Wiley-VCH), Inc., New York, pg. 280, 1994.

[5] Calbiochem protocol

[6] Stricklin et al, 1983, Biochemistry 22, 61

[7] Kieran F. Geoghegan, Michael, J. Emery, William H. Martin, Alexander s. McColl, and Gaston O. Daumy, 1993. Site-directed double fluorescent tagging of human rennin and collagenase (MMP-1) substrate peptides using the periodate oxidation of N-terminal serine. An apparently general strategy for provision of energy-transfer substrates for proteases. Bioconjuate Chemistry, 4, 537-544.

[8] Nagase

[9] conversations with Dr. Stetler-Stevenson at NIH.

[10] R. Sjoback, J. Nygren and M. Kubista. Absorption and Fluorescence Properties of Fluorescein, Spectrochimica Acta A 51, 7 (1995).

[11] Jane A. Ferguson, Brian G. Healey, Karen S. Bronk, Steven M. Barnard and David R. Walt, *Anal. Chim. Acta*, 340, 123-131 (1997).

[12] Brian G. Healey and David R. Walt, *Anal. Chem*., 67, 4471-4476 (1995).

4.7 Figures for Section 4

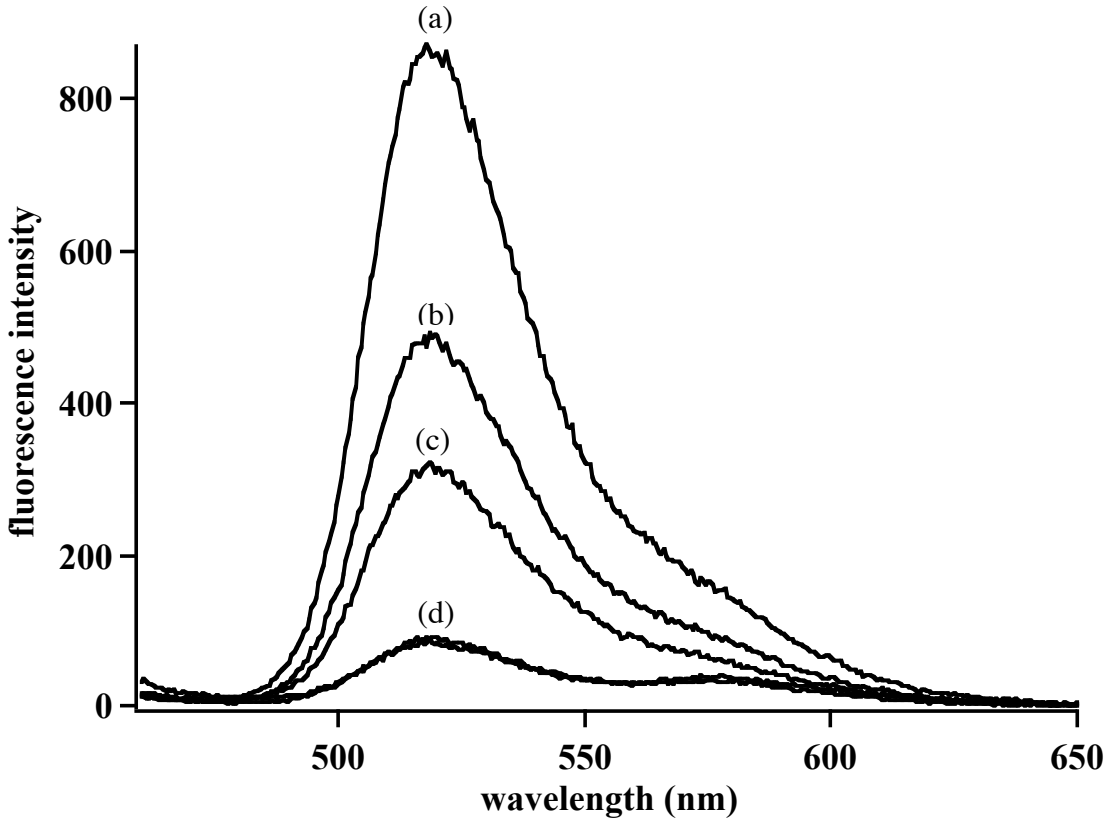

Figure 4.1: Fluorescence emission spectra of the peptide sequence in Table 4.1a after incubating with the target enzymes (a) MMP-9, (b) MMP-8, (c) MMP-3, (d) MMP 1, and (e) MMP 2. The spectra corresponding to (f) served as a control and contained the enzyme buffer solution and all constituents but without any enzyme. MMP 9, 8, and 3 show varying degrees of reactivity with the substrate, wherea,s MMP1 and 2 are identical to the control spectra (f) indicating no reaction with the substrate. The enzymes used in these experiments were prepared fresh and used the same day (i.e. no freeze/thaw cycles).

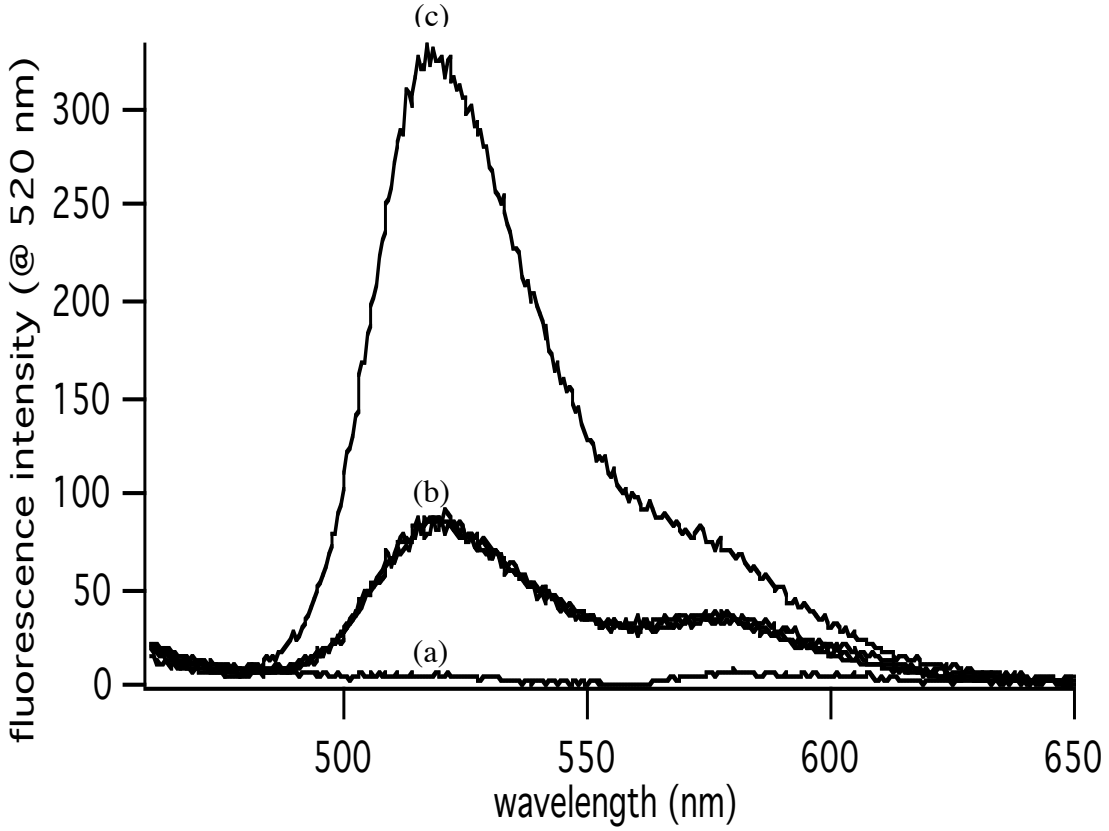

Figure 4.2: Fluorescence emission spectra of the peptide sequence in Table 4.1a after incubating with the target enzymes (a) MMP-9, (b) MMP-8, (c) MMP-3, (d) MMP 1, and (e) MMP 2. The spectra corresponding to (f) served as a control and contained the enzyme buffer solution and all constituents but without any enzyme. MMP 9, 8, and 3 show varying degrees of reactivity with the substrate, wherea,s MMP1 and 2 are identical to the control spectra (f) indicating no reaction with the substrate. The enzymes used in thes experiments were not prepared fresh but rather had gone through one freeze/thaw cycle.

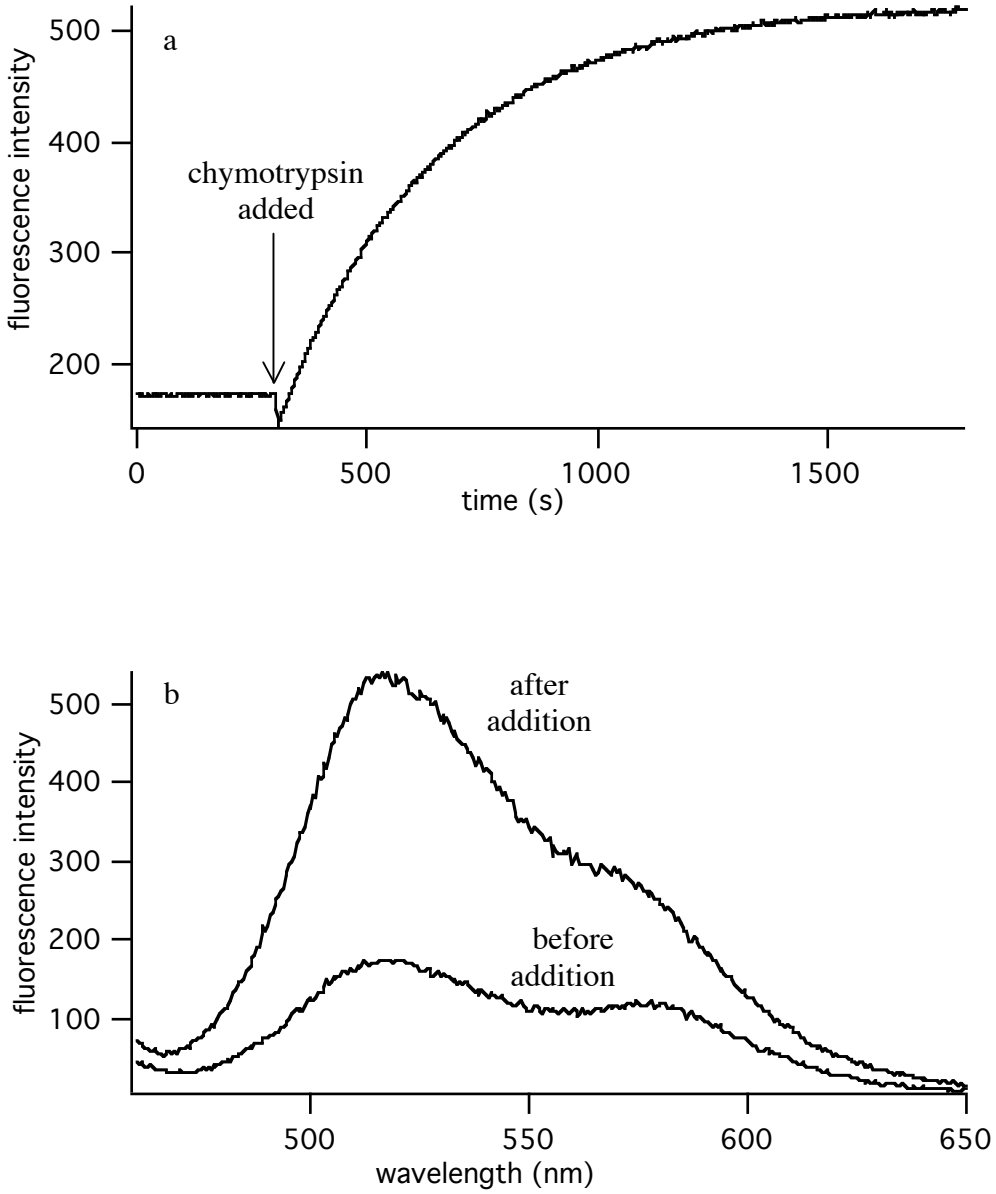

Figure 4.3: Fluorescence (a) emission time scan and (b) emission spectra of the peptide sequence in Table 4.1, sequence 2a before and after addition of chymotrypsin. The (a) emission time scan shows the baseline intensity before adding chymotrypsin and the resulting increase in fluorescence intensity monitored at 520nm. A decrease in fluorescence intensity is observed at the point of chymotrypsin addition, a result of peptide concentration dilution. The (b) emission spectra represent before and after chymotrypsin addition.

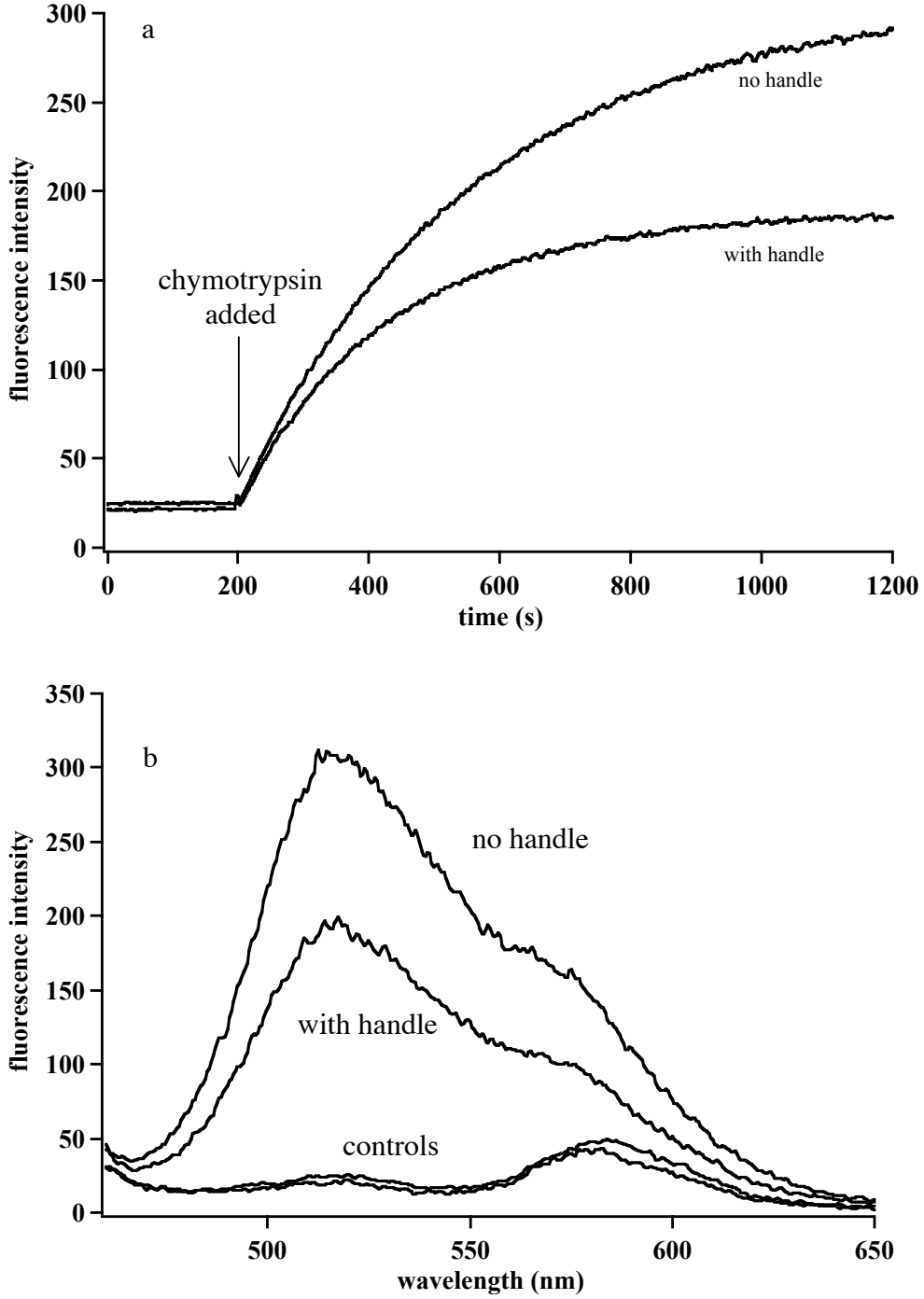

Figure 4.4: Fluorescence (a) emission time scans and (b) emission spectra of the peptide sequence in Table 4.1, sequence 2a and b before and after addition of chymotrypsin. The (a) emission time scans shows the baseline intensity before adding chymotrypsin and the resulting increase in fluorescence intensity monitored at 520nm. The (b) emission spectra represent before and after chymotrypsin addition.

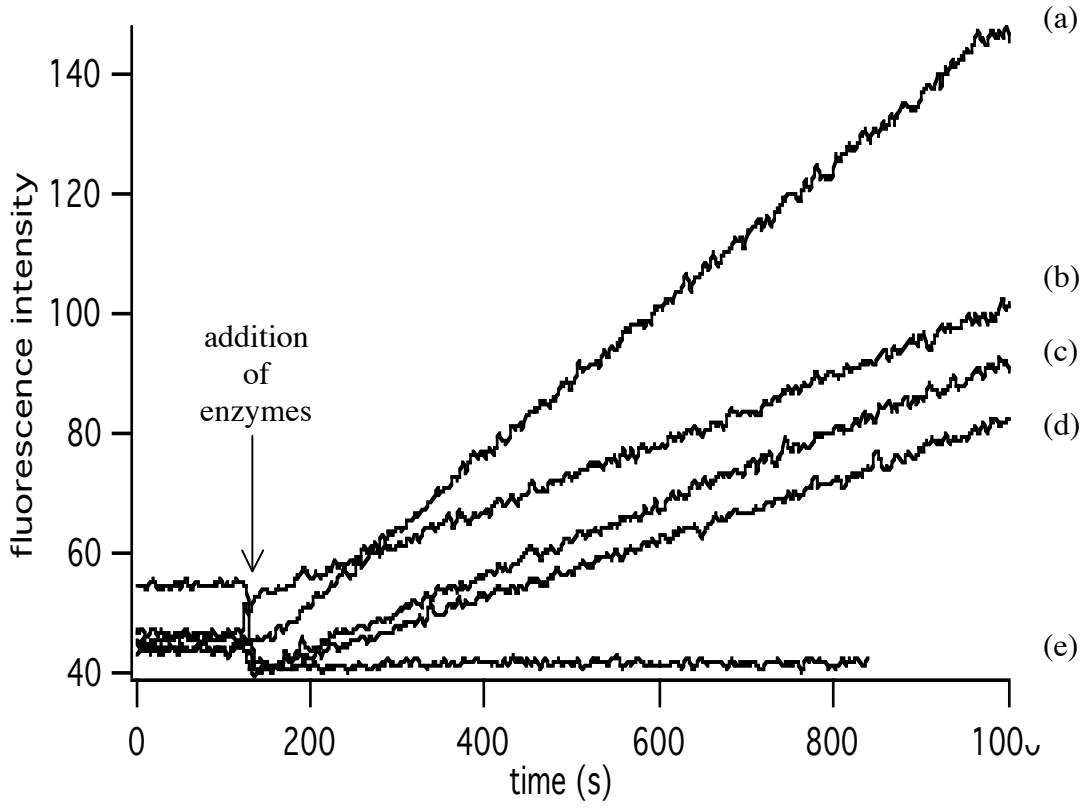

Figure 4.5: Fluorescence emission time scans of the peptide sequence in Table 4.1, sequence 3 before and after addition of the following enzymes activated with APMA using our optimized protocols: (a) MMP-1, (b) MMP-8, (c) MMP-2, (d) MMP-9, and (e) MMP-3. The emission time scan shows the baseline intensity before adding each enzyme and the resulting increase in fluorescence intensity monitored at 390 nm. A decrease in fluorescence intensity is observed at the point of enzyme addition, a result of peptide concentration dilution.

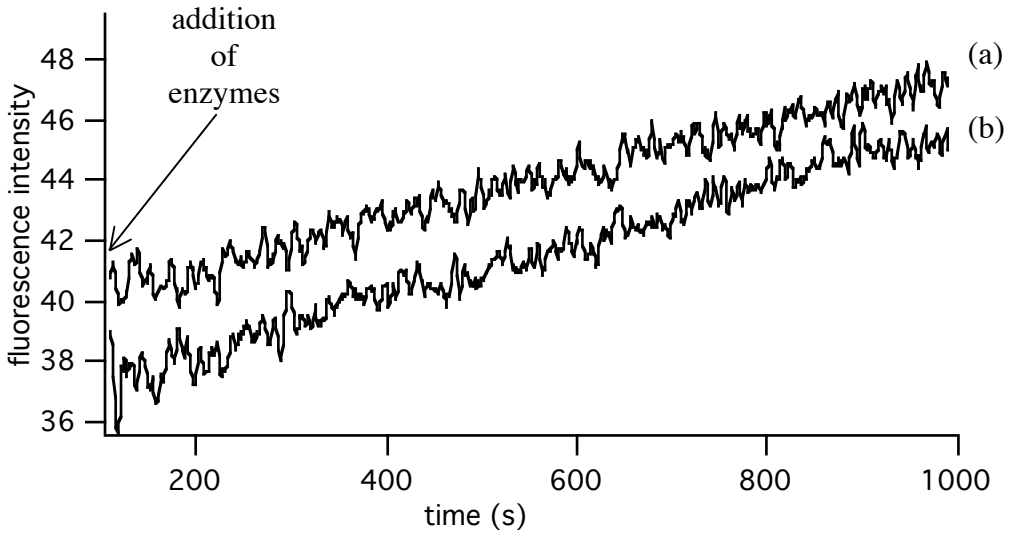

Figure 4.6: Fluorescence emission time scans (monitored at 515 nm) of the peptide sequence in Table 4.1, sequence 2a before and after addition of (a) MMP-8 and (b) MMP-1 (each activated with 1mM APMA for 30 min).

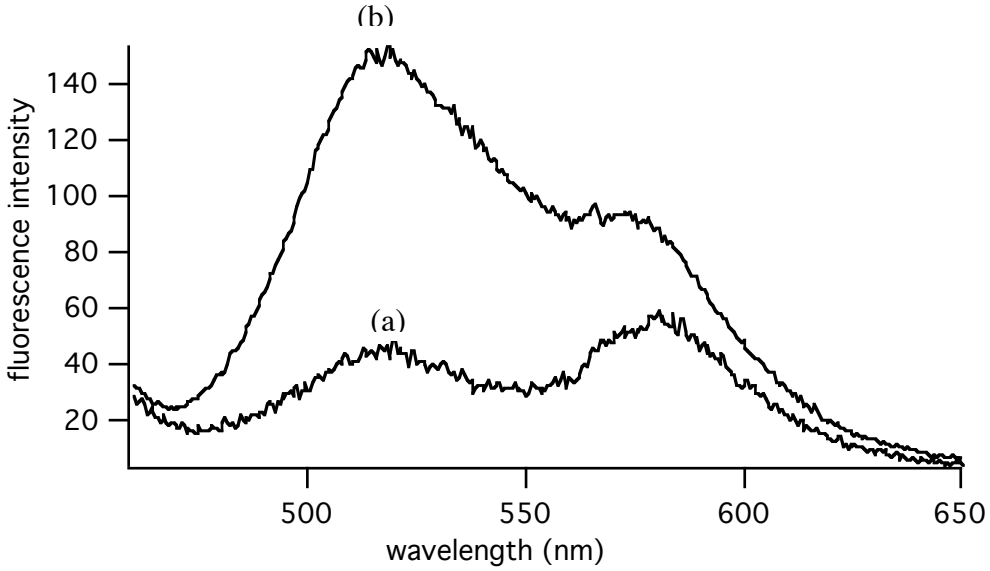

Figure 4.7: Fluorescence emission spectra of the peptide sequence in Table 4.1, sequence 2a (a) before and (b) after 5 hr incubation with MMP-1 (activated with 1mM APMA for 30 min).

Section 5

Development of a FRET-based Enzyme Sensor

5.1 Introduction

There are numerous publications in the optical sensor literature that describe enzyme-based sensors. However, the "enzyme-based sensor" nomenclature can be somewhat misleading for two reasons. First, in all reported examples, the enzyme is not the target to be detected but rather an integral part of the sensing scheme for detecting some other analyte. Generally, the active enzyme is immobilized within a matrix (e.g. polymer) attached to the surface of an optical waveguide (e.g. fiber). Typically, the target analyte diffuses into the matrix and interacts with the immobilized active enzyme, which catalyzes a reaction, producing a bi-product that changes the optical properties of another indicator co-immobilized in the matrix. Changes in the optical properties (i.e. absorption, fluorescence, etc.) of the co-immobilized indicator serve as the transducer. Secondly, the term "sensor" has typically referred to a reversible sensing process; non-reversible (i.e. one time use only) sensors have been referred to by some as "probes" rather than sensors. [1] To date, the majority of reported "enzyme-based sensors" are reversible in design since the action of the enzyme in catalyzing reactions is preserved.

5.1.1 Background: Non fiber-based enzyme sensors

The first demonstration of enzyme entrapment in a polymer matrix was by Bernfeld and Wan [2]. In their work, a cross-linked polyacrylamide hydrogel was used to immobilize

the enzymes: trypsin, a-chymotrypsin, papain, a -amylase, b-amylase, ribonuclease, and aldolase. These initial non-fiber sensors had slow response times indicating that the rate of substrate diffusion to the immobilized enzyme was slow. Dong and Hoffman [3] addressed this problem by preparing low cross-linked polymers, which were heated and cooled to increase diffusion of the substrate to the immobilized enzyme. This process increased the mass transfer of solutes in and out of the hydrogel resulting in faster response times. Kokufuta et al. [4] demonstrated the ability to activate an enzyme while immobilized in a low molecular weight polymer matrix. The initial work described above led others to immobilize enzymes on optical fibers

5.1.2 Background: fiber-based enzyme sensors

Walt and coworkers demonstrated the first fluorescence-based optical fiber enzyme sensor, which utilized an immobilized enzyme for detecting penicillin [5]. This method was based on the photopolymerization technique of Walt and coworkers [6], in which polymer matrices are photodeposited on selective sites on the tip of the optical fiber image guide. Walt et al. [7] created a dual-analyte sensor using this technology, a sensor to detect penicillin and pH. In their work, the enzyme Penicillinase was immobilized in a polymer matrix at discrete sites on the image guide surface along with a pH-sensitive indicator at other discrete sites on the same fiber. Recently, an in-vivo enzyme-based sensor was reported for detecting acetylcholine and choline [17]. Enzyme immobilization has been widely used by researchers since the early 90s. Typically, enzymes are immobilized on inorganic materials and covalently bound to surfaces. Table

5.1 shows some of the most popular enzymes that have been immobilized by researchers to describe different “enzyme sensors”.

In this paper we describe the first optical fiber-based sensor for detecting enzymes in solution. This sensor design is completely different from prior art described above, which sought to immobilize the active enzyme and utilize it as part of the sensing scheme. In these preliminary studies, the proof-of-concept is demonstrated by detecting the presence of a matrix metalloproteinase (MMP-3) and chymotripsin enzymes in solution using novel FRET-based substrates immobilized in a polymer matrix. As the enzyme diffuses into the polymer, it binds to the immobilized substrate and cleaves the substrate producing an optical change in the FRET-based substrate. Included in the discussion are design elements for a new class of fluorescence resonance energy transfer (FRET) based indicator chemistry developed for this work. The two primary innovations are (1) the use of donor/acceptor dye pairs that absorb and fluoresce in the visible regions of the spectrum, (2) and a unique “handle” for covalently binding the substrate within the polymer based microdot.

5.2 Experimental

5.2.1Enzymes

Pre-activated matrix metalloproteinase enzymes, MMP-1,2,3,8,9, (Biomol Research Laboratories, Plymouth Meeting, PA) and chymotrypsin (Sigma (St Louis, MO) were used without further purification.

5.2.2 Reagents

The following reagents were used as received: a natural pig collagenase substrate (Molecular Probes, Eugene, OR), HEPES buffer (Fluka, Switzerland), pH hydrion buffers (VWR), dimethysulfoxide (DMSO) and n-propanol (Sigma), acrylamide, bisacrylamide.

5.2.3 Indicator chemistries

Indicator chemistry development for detecting enzymes is describe in detail in section 4 along with the pH indicator chemistry. Briefly, the pH sensitive indicator, acryloylfluorescein was prepared by reacting fluoresceinamine with acryloyl chloride. The custom FRET-based substrate [5-FAM-Lys(X)-Pro-Leu-Ala-Nva-Dap(5/6-TMR)-Ala-Arg-NH_2] for detecting enzymes was designed at LLNL and outsourced for synthesis and purification to Anaspec (Santa Clara). The carbon-carbon double bond linker was attached to a hydrophic long chain polyethylene glycol (PEG) linker (X=COCH2-$(OCH2CH2)_2$NHCOCH2$CH_2CH_2CH_2$=CH2) and covalently linked to a lysine (Lys).

5.2.4 Instrumentation

All solution based fluorescence measurements were made using a Perkin-Elmer, LS-55 Luminescence spectrometer (Wellesley, MA). The excitation and emission slits widths were, 2.5 nm and 3.0 nm, respectively. For fiber-based measurements, a custom fluorescence imaging system was used which utilizes a liquid nitrogen cooled, charge-coupled device (Princeton Instruments, Model LN/CCD-512TKB/1) photodetector and a high intensity blue light-emitting-diode (LED) for excitation.

5.2.5 Optical fibers

Optical fiber image guides (Sumitomo, IGN-05/06) were polished (1 micron finish) and cleaned and functionalized as described in Appendix A.

5.2.6 Sensor fabrication

The custom contact-based microdispensing system for printing indicator chemistries on optical fiber image guides is described in detail in section 3.

5.2.7 Hydrogel formulation/indicator chemistry

The printed enzyme indicator chemistry was comprised of a two-part solution mixed in a 1:1 ratio. The first solution was a 15% (w/w) acrylamide-based hydrogel with a bisacrylamide crosslinking of 100:1 (acrylamide/bysacrylamide). The formulation contained BEE and Ciba 2959 as initiators and FC-430 as surfactant. The second solution contained the FRET-based substrate dissolved in Hepes buffer and n-propanol for total dissolution. The resulting final formulation contained 0.254 mM FRET-based indicator and overall 7.5% (w/w) solids. Indicator chemistry development is described in detail in section 4.

5.3 Results and Discussion

5.3.1 Solution-based experiments using commercial kit for optimizing monomer formulation

Initial FRET-based enyzyme/substrate studies were conducted using commercially available kits. These solution-based studies allowed key data to be acquired for designing the polymer formulations and custom peptide synthetic substrates. The natural

collagenase with fluorescein dyes such that it acts as both the donor and acceptor pair. Figure 5.2 shows fluorescence spectra of two solutions containing the same substrate concentration (0.002 mg/mL dissolved in deionized water) with varying enzyme activities (0.1 U/ml and 0.025 U/ml, 2 hr incubation), the same solution before the addition of enzyme, and a 1X Reaction Buffer (10X Reaction Buffer: 0.5 M Tris-HCl, 1.5 M NaCl, 50 mM $CaCl_2$, 2 mM sodium azide, pH 7.6) only solution. The spectrum of the substrate before enzyme was added shows a peak at 520nm, which corresponds to the expected emission of fluorescein dye. The spectrum of the buffer serves as a control and does not show an observable emission band from 500 to 650 nm. Figure 5.3 shows the change in fluorescence intensity with time for two of the same substrate and enzyme concentrations shown in Figure 5.2 (the 0.4U/ml fluorescence spectrum does not appear in Figure 5.2 because this concentration saturated the detector). The baseline fluorescence intensity is shown for the first 200 s at which point the enzyme is added to the cuvette as indicated by the sudden rise in the intensity, which was monitored at the emission maximum for fluorescein at 520nm. The lower concentration substrate produces a linear response indicating that the reaction rate is second order according to the Michaelis-Menten equation (i.e. limited enzyme/substrate binding occurs). The higher concentrations of enzyme produce a large enzyme/substrate binding resulting in a first order reaction rate.

First order Michaelis-Menten equation: $$v_o = \frac{V_{\max}[S]}{K_M + [S]}$$

Second order Michaelis-Menten equation: $v_o = \frac{k_{cat}}{K_M}[E][S]$

One of the main reasons the Molecular probes kit was chosen for initial studies was due to the relatively large size of the natural collagenase substrate compared to the synthetic peptides sequences found in other kits, which allowed entrapment of the natural substrate in a polymer membrane (i.e. smaller synthetic substrates simply leach out). Figure 5.4 illustrates how this was used to study the ability of the enzyme to penetrate the polymerized droplet. A concentrated (0.5 mg/mL) solution of natural collagenase substrate was prepared and added to different acrylamide-based monomer formulations of varying weight percent and crosslinker ratio (experiments showed that formulations consisting of 7.5% (w/w) and 50:1 crosslinker ratios are near the limits of the formulations that can be photopolymerized on a fiber and remain attached). Figure 5.5 shows the fluorescence emission as a function of time after addition of enzyme for two different polymer droplets containing the same concentration of collagenase substrate. Not surprisingly, the most porous droplet shows the highest intensity for a given time due to the ability of the enzyme to diffuse into the collagenase substrate immobilized in the polymer. A series of leaching experiments were conducted to remove all non-immobilized collagenase substrate. Polymerized droplets of polymer containing immobilized collagenase were placed in 1 mL volumes of buffer and soaked for varying periods of time. The first wash involved soaking for 17 hrs and subsequent washing for 1 hr each. The fluorescence intensity of the supernate of each wash was measured following the leaching to indicate the presence of remaining collagenase substrate. Figure 5.6 shows fluorescence spectra of the supernate solutions of the first, second,

third, fifth, and seventh washes including the control buffer only spectrum. Figure 5.6 shows that most of the substrate was released into the solution in the first wash. There was also a significant amount of substrate released into solution in the second wash. After the third wash though, there were just traces of the substrate released into the solution and their spectra were very close to that of the buffer alone. Figure 5.7 shows plots of fluorescence intensity monitored over time for the enzyme added to the supernate solutions for the third, fifth, and seventh washes. Here we can see that the fluorescence intensity increased more slowly for the later washes and this is due to the fact that there is less and less substrate to be cleaved by the enzyme. The seventh wash shows no traces of substrate in the solution since the fluorescence intensity measured is the same both before and after adding the enzyme. From the spectra shown in Figure 5.2 for substrate before enzyme was added, it is expected that the substrate alone has very observable background fluorescence due to unquenched fluorescein. Even so, an additional step was taken to insure that the leaching had successfully removed all remaining substrate.

5.3.2 Solution-based experiments using chymotrypsin enzyme with custom substrates

The first synthetic substrate was not designed to be immobilized in a polymer substrate. Our first approach was to design a substrate specific for a particular enzyme before adding additional functionality to the substrate for attaching to a polymer membrane. The first custom peptide (see Table 5.2) was designed for MMP-8 and contained the sequence shown in Table 5.2, substrate 1; the FRET pair was fluorescein and rhodamine. Figure 5.8 shows the fluorescence spectrum of our first custom peptide design before and

after addition of the enzyme chymotrypsin. Although the intended application for this work was the detection of MMPs, chymotripsin was used during the development stage to test our custom designed substrates because it will cleave most substrates and because the cost was much less than the MMPs. Chymotrypsin also provided a positive control to show that the custom peptides were synthesized properly. The Figure 5.8b spectrum shows to emission bands for fluorescein and rhodamine, respectively, before enzyme is added. These bands appear in the spectrum because the FRET process is not 100% effective (i.e. most of the energy from excitation is transferred but a small fraction is undergoes radiative decay).

Figure 5.9 shows the fluorescence emission as a function of time before and after the enzyme, chymotrypsin (0,01 mg/mL), is added to a solution containing the custom peptide (1 □M concentration). The hyperbolic curve indicates again the nature of enzyme kinetics as described by the first order Michaelis-Menten equation. When the same tests were performed on the custom peptide using other enzymes as shown in Figure 5.10, the response time was found take as much as 18 hours to show cleavage for MMP-9, 8, and 3. MMP-1 and 2 did not show any response. The custom peptide was not very soluble in water as indicated by the need to first dissolve in dimethylsulfoxide (DMSO) prior to addition of water. This is due to the hydrophobic nature of the donor/acceptor dyes and the water solubility of the amino acid sequences chosen for this design. It is likely that the custom peptide in aqueous solution was inaccessible do to steric hindrances resulting from its highly hydrophic structure.

Several more iterations (detailed in section 4) were required before arriving at a custom peptide design that was specific for a target MMP enzyme (MMP-3) and one, which could be covalently linked in polymer matrix printed on a fiber using the contact-based microdispensor system described in section 3.

5.3.3 Solution based MMP-3

Figure 5.11 shows the fluorescence emission as a function of time after the enzymes, MMP-1, 2, and 3 are added to a solution containing the FRET-based substrate (sequence 4b, Table 5.2). In all cases, the substrate was used at 0.8-mM concentration. For comparison the enzymes have been normalized to have the same activity (3.75 U/□L). The substrate is selective for MMP-3 and not MMP-1 and 2. The errors bars are small for this figure because we found that by slowly stirring the solution, we achieved better mixing.

5.3.4 Chymotrypsin study on fibers

Figure 5.12 shows a bright-field image of a 6-around-1 microdot array printed on a polished optical fiber image guide (distal end) having a diameter of 500 microns. Of these 7, all but the smaller two microdots contains a FRET (fluorescence resonance energy transfer) based polypeptide sequence [5-FAM-Lys(X)-Pro-Leu-Ala-Nva-Dap(5/6-TMR)-Ala-Arg-NH_2, where X = $COCH_2$-(OCH_2CH_2)-$NHCOCH_2CH_2CH{=}CH_2$] indicator chemistry for detecting select enzymes (e.g. matrix metalloproteinase, MMP-3 and/or chymotrypsin). The two smaller, less noticeable microdots contain no indicator chemistry and serves as an experimental control. Before printing, the image guide fibers were cleaned and functionalized according to the procedures described in Appendix A. Briefly, the fibers were functionalized with allyltrichlorosilane, which provides a carbon-

carbon double bond "handle" for covalently linking the microdot to the fiber surface during the photopolymerization step. The surface energy of the functionalized fiber surface is expected to be ~35 dyn/cm^2 and the surface tension of the formulation is 20-22 dyn/cm^2. Each microdot is about 100 microns in diameter. The polypeptide design is described in detail in section 4. Briefly, the polypeptide sequence contains a unique "handle" [X = $COCH_2$-(OCH_2CH_2)-$NHCOCH_2CH_2CH{=}CH_2$], which provides a carbon carbon double bond for covalently linking the peptide sequence to the polymer microdot during the photopolymerization step. The acrylamide formulations for the pH and enzyme indicators are different formulations, which accounts for the size differences. Control of the dimensions and aspect ratio of a printed microdot to a given specification is obtained by adjusting the following variables: (a) the surface tension of the polymer formulation (e.g. controlled using surfactants, and (b) the surface energy of the polished optical array surface (e.g. controlled using silanization method functionalization or low-wet coatings).

Figure 5.13a,b shows the response of the fiber-based sensor when exposed to the enzyme chymotrypsin in solution. These solutions were leached and supernate measured to insure that all immobilized dye was removed from the microdots. The response of the 5 dots is shown. The two control microdots that do not contain an immobilized indicator do not show any response to the presence of enzyme. The background was data taken from between microdots to show that leaching was not occurring. The error bars show less than 10% variation.

5.3.5 MMP-3 study on fibers

Figure 5.14 shows a bright-field image of a 6-around-1 microdot array printed on a polished optical fiber image guide (distal end) having a diameter of 500 microns. All microdots contain the FRET (fluorescence resonance energy transfer) based polypeptide sequence [5-FAM-Lys(X)-Pro-Leu-Ala-Nva-Dap(5/6-TMR)-Ala-Arg-NH_2, where X = $COCH_2$-(OCH_2CH_2)-$NHCOCH_2CH_2CH{=}CH_2$] indicator chemistry for detecting MMP-3 and/or chymotrypsin. Before printing, the image guide fibers were cleaned and functionalized according to the procedures described in Appendix A. Essentially, these fibers follow the same procedures and results on surface tension and energy described above. Figure 5.15 shows the fluorescence-binned image of Figure 5.14, from which data is acquired.

Figure 5.16 shows the response of the fiber-based sensor when exposed to the enzymes MMP-1, MMP-2, and MMP-3. These solutions were leached and supernate measured to insure that all immobilized dye was removed from the microdots. Response to enzyme presence was observed only for MMP-3. The microdots do not show any response to the presence of MMP-1 or MMP-2. The error bars show a big variation and this is due to several possible factors such as 1) inability to print totally reproducible microdots, 2) possibility of not achieving homogeneous mixing between the substrate and the polymer (polymer might make lumps before mixing), 3) not equally enzyme diffusion through the volume of the polymer matrix. Nevertheless, Figure 5.16 shows that there is some affinity of MMP-3 for this customized substrate. These results are consistent with what was

observed in the solution studies indicating the successful detection of the enzyme MMP-3 by the fiber optic sensor.

5.3.6 Multianalyte biosensor

With the successful proof of concept of both the pH and enzyme single analyte sensors individually the next step was to combine the pH and enzyme sensors to create a multianalyte sensor. Figure 5.17 shows the printed microdots including 4 enzyme microdots (small dots), a control microdot (in the center) and 2 pH microdots (larger dots) to complete the multianalyte sensor. Figure 5.18 is a plot of the pH response for all of the microdots. This figure shows that the pH microdots responded to changes in pH while the enzyme sensors showed a much lower response. There is a slight response of the enzyme sensors to pH changes. This is due to the fact that the enzyme sensors contain fluorescein molecules, which are sensitive to changes in pH. However, the fluorescein in these dots is linked to the polymer and within the Foster distance to the rhodamine molecule and is therefore undergoing FRET, which limits the emission of the fluorescein (the fluorescein donor). Figure 5.19 shows the response of all microdots to the presence of the enzyme MMP-3. Here, it is clear that the enzyme microdots responded while the pH microdots did not. Actually the pH microdot photobleached during the process due to long exposure to light.

5.4 Conclusions

5.5 References

[1] O. S. Wolfbeis, Ed., *Fiber-optic Chemical Sensors and Biosensors,* (CRC press, Boca Raton, FL, 1991). vol. 1.

[2] Bernfeld, P and Wan, J., 1963. Science, vol. 142, 678-679

[2] Steven M. Barnard and David R. Walt, 1991. Antigens and enzymes made insoluble by entrapping them into lattices of synthetic polymers. Science vol.142, 678-679.

[3] Dong, L. C. and Hoffman, A. S. Reversible Polymeric Gels and Related systems; Russo, P., Ed.; American Chemical Society; Washington, DC, 1987; Chapter 16, pp 236-244. Park, T.G.; Hoffman, A. S. Appl. Biochem. Biotechnol. 1988, 19, 1-9.

[4] Etsuo Kokufuta, Yoko Yamaya, Akihiko Shimada, and Isei Nakamura, 1988. Prevention of limiting substrate diffusion in an immobilized enzyme reaction system: lectin-induced activation of gel-entrapped b-D-Galactosidase. Biotechnology Letters, Vol. 10 No 5, 301-306.

[5] Kulp, T. J., Camins, L; Angel, S. M; Munkholm, C.; Walt, D. R., 1987. Anal. Chem., vol. 59, 2849

[6] Steven M. Barnard and David R. Walt, 1991. A fibre-optic chemical sensor with discrete sensing sites. Nature Vol. 353, 338-340.

[7] Brian G. Healey and David R. Walt, 1995. Improved fiber-optic Chemical sensor for penicillin. Analytical Chemistry, Vol. 6, No 24, 4471-4476.

[8] Richard B. Thompson' and Eric R. Jones, 1993. Enzyme-Based Fiber Optic Zinc Biosensor. Anal. Chem., vol. 65, 730-734

[9] K. Taga, S. Weger, R. Gobel, and R. Kellner, 1993. Colorimetric activity assays of enzyme-modified MIR fibers. Sensors and Actuators B, vol. 11, 553-559.

[10] K. Taga' and R. Kellner, 1994. In Situ Attenuated Total Reflectance FT-IR Analysis of an Enzyme-Modified Mid-Infrared Fiber Surface Using Crystalline Bacterial Surface Proteins. Anal. Chem.,66, 35-39.

[11] Zeev Rosenzweig, Raoul Kopelman, 1996. Analytical properties of miniaturized oxygen and glucose fiber optic sensors. Sensors and Actuators B 35-36, 475-483.

[12] Liande Zhu, Yingxiu Li, Faming Tian, Bo Xu, and Guoyi Zhu, 2002. Electrochemiluminescent determination of glucose with a sol-gel derived ceramic-carbon composite electrode as a renewable optical fiber biosensor. Sensors and Actuators B, 84, 265-270.

[13] M. Mascini, 1995. Enzyme-based optical-fibre biosensors. Sensors and Actuators B 29, 121-125.

[14] Zhongpin Chen, D.L. Kaplan, H. Gao, J. Kumar, K.A. Marx, S.K. Tripathy, 1996. Molecular assembly of multilayer: toward the development of a chemiluminescence-based fiber optic biosensor. Material Science and Engineering C4, 155-159.

[15] Xueping Li, Zeev Rosenzweig, 1997. A fiber optic sensor for rapid analysis of bilirubin in serum. Analytica Chimica Acta 353, 263-273.

[16] M.D. Marazuela, M.C. Moreni-Bondi, 1998. Determination of choline-containing phospholipids in serum with a fiber-optic biosensor. Analytica Chimica Acta 374, 19-29.

[17] Kim M. Mitchell, 2004. Acetylcholine and Choline Amperometric Enzyme Sensors Characterized in Vitro and in Vivo. Anal. Chem., 76, 1098-1106.

[18] Ruey-An Doong and Hsiao-Chung Tsai, 2001. Immobilization and characterization of sol gel-encapsulated acetylcholinesterase fiber-optic biosensor. Analytica Chimica Acta 434, 239-246.

[19] M. Mascini, 1995. Enzyme-based optical-fibre biosensors. Sensors and Actuators B 29, 121-125.

[20] Jenna L. Rickus, Allan J. Tobin, Jeffrey I. Zink, and Bruce S. Dunn, 2002. Enzyme-doped thin films and optical fiber sensors for glutamate.

[21] Peter M. Schmidt, Christine Lehmann, Eckart Matthes, and Frank F. Bier, 2002. Detection of activity of telomerase in tumor cells using fiber optical biosensors. Biosensors and Bioelectronics 17, 1081-1087.

[22] Vangelis G. Andreou and Yannis D. Clonis, 2002. A portable fiber-optic pesticide biosensor based on immobilized cholinesterase and sol-gel entrapped bromcresol purple for in-field use. Biosensors and Bioelectronics 17, 61-69.

[23] Kohji Mitsubayashi, Takuo Kon, and Yuki Hashimoto, 2003. Optical bio-sniffer for ethanol vapor using an oxygen-sensitive optical fiber. Biosensors and Bioelectronics 19, 193-198.

5.6 Figures for Section 5

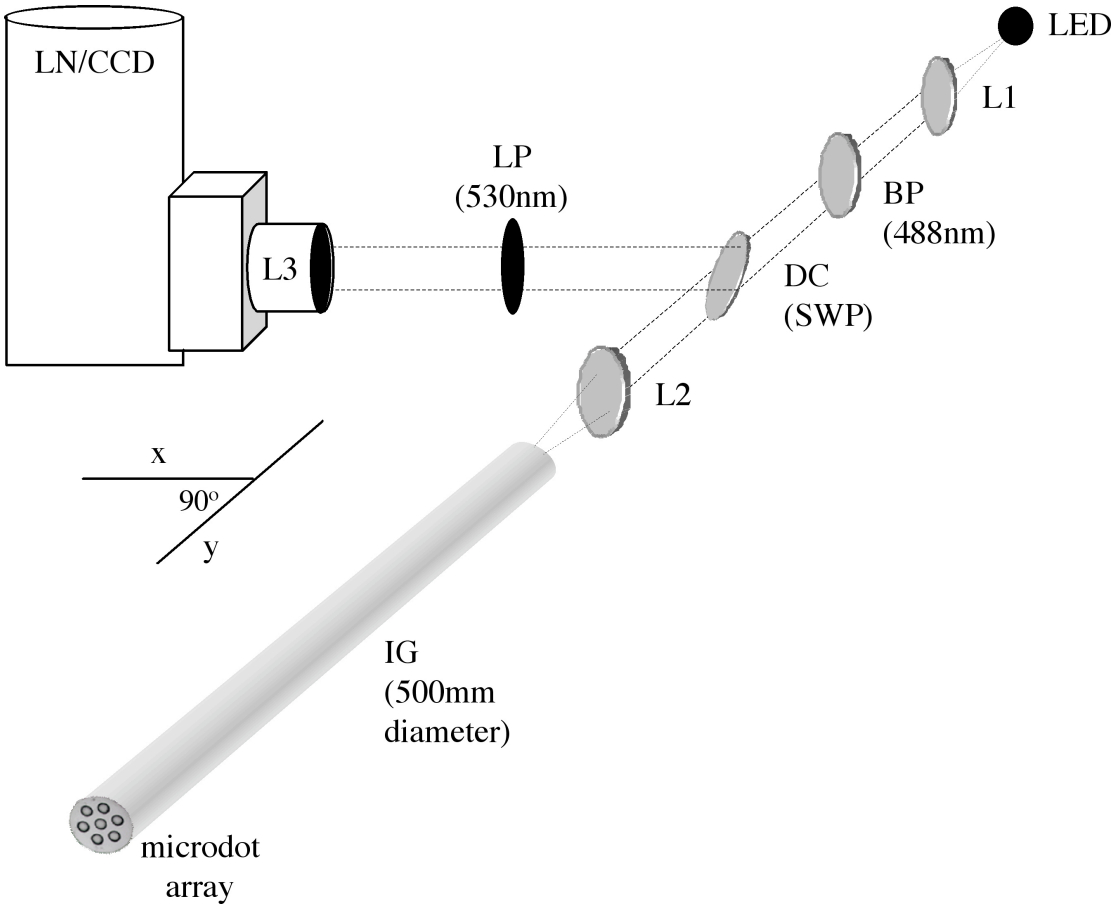

Figure 5.1: Schematic diagram of the custom fluorescence imaging system. Excitation radiation from a light emitting diode (LED) is collimated with a microscope objective (L1) and passed through a bandpass filter (BPF) and dichroic mirror (DCM) before being focusing with a second microscope objective (L2) into the optical fiber image guide. The image guide serves to both illuminate the indicator chemistry and to collect the resulting fluorescence emission, which is collimated by the objective (L2) and reflected off the dichroic mirror (DC) and through a longpass fillter (LPF) and focused (L3) onto the CCD array.

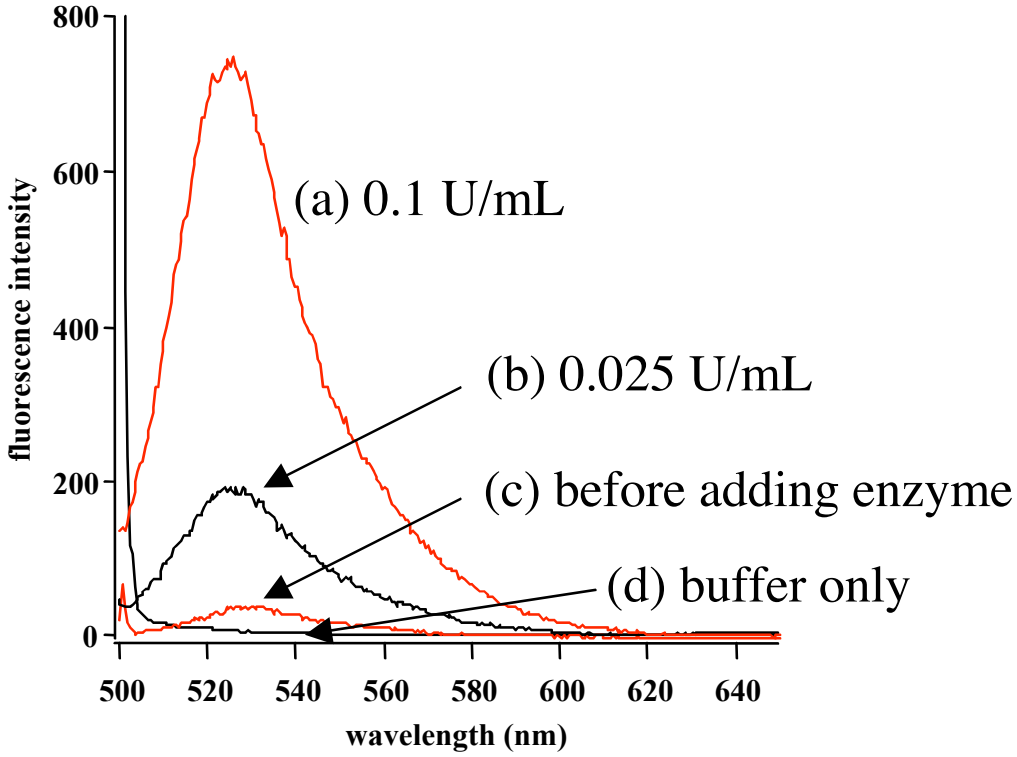

Figure 5.2: Emission spectra of the buffer only, the buffer with the substrate before enzyme was added, and the solutions 2 hours after adding the enzyme at two different concentrations: 0.025 and 0.1 U/ml.

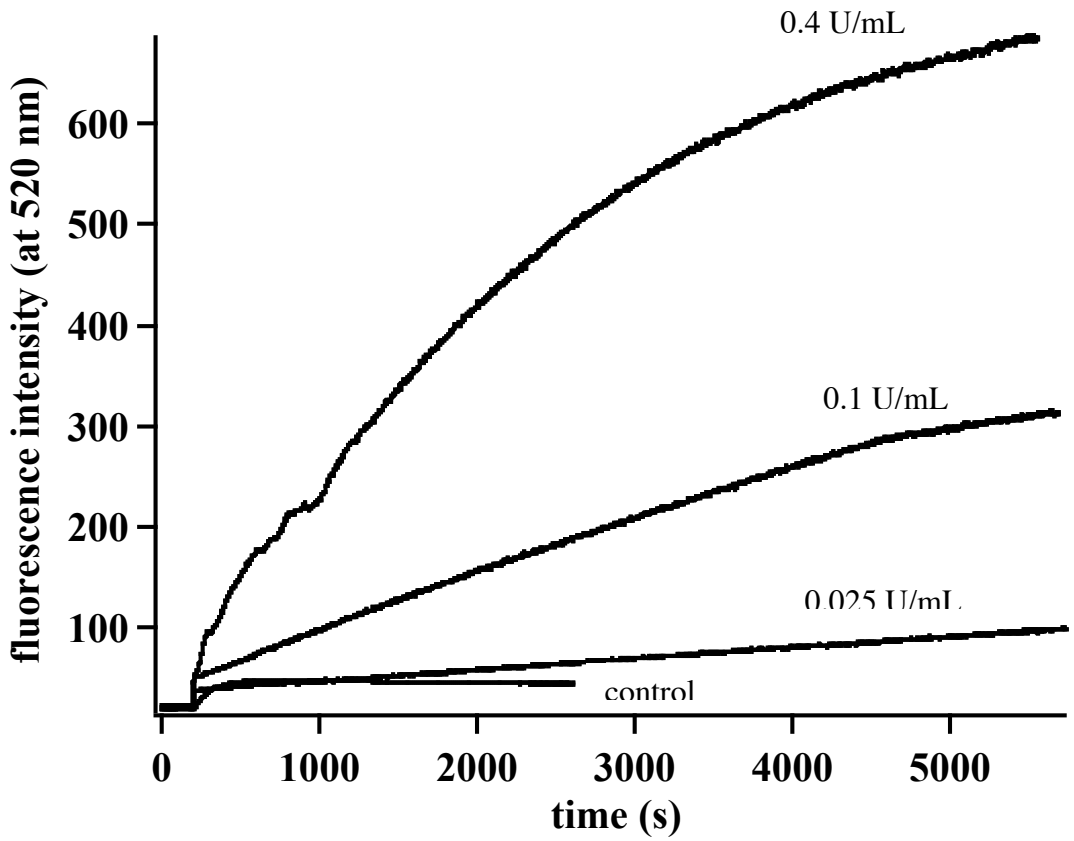

Figure 5.3: Time monitoring of the substrate cleavage by three different concentrations: 0.025, 0.1 and 0.4 U/ml, and control.

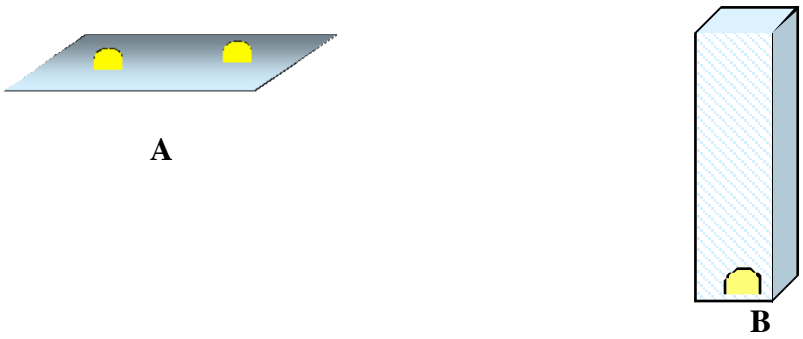

Figure 5.4: A) Dots printed on a glass slide. B) Dot removed from the slide placed in a cuvette filled with buffer solution ready for leaching experiments or to add the enzyme.

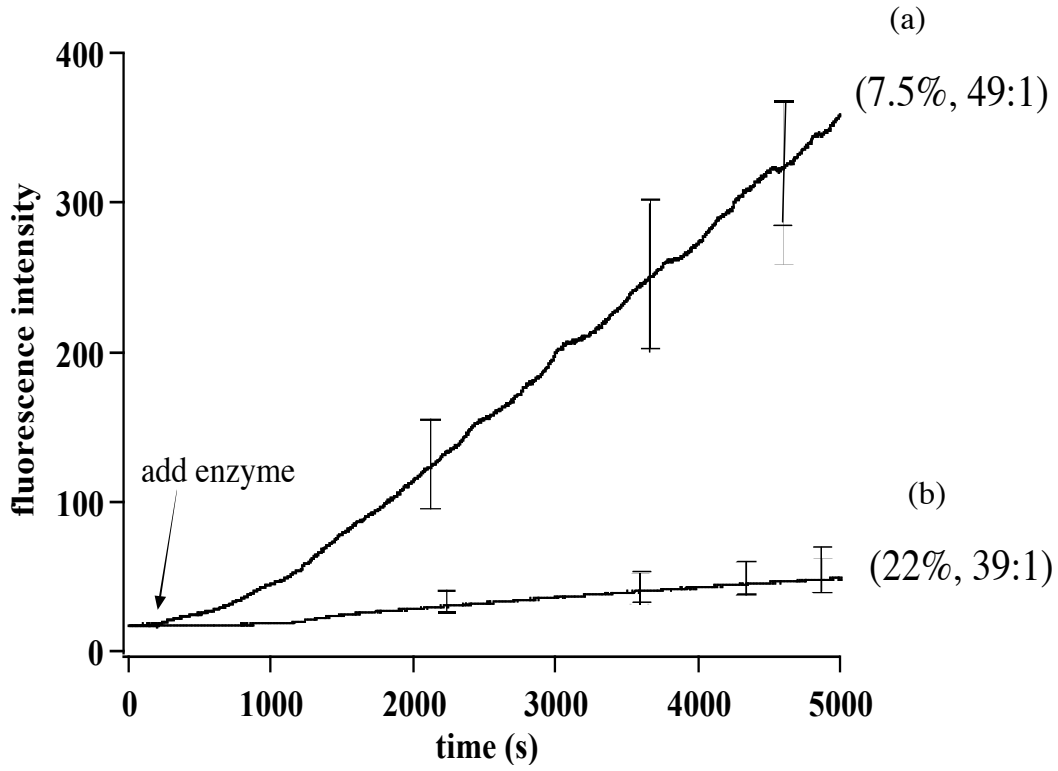

Figure 5.5: First dots showing evidence of enzyme difussion through a polymer hydrogel. The substrate attached inside the polymer matrix is being cleaved by the enzyme. The release of substrate into the solution is shown as a continuos increase in the fluorescence emission. Two different polymer formulations for the diffusion of collagenase through polymer matrices. Enzyme was added at 200 s.

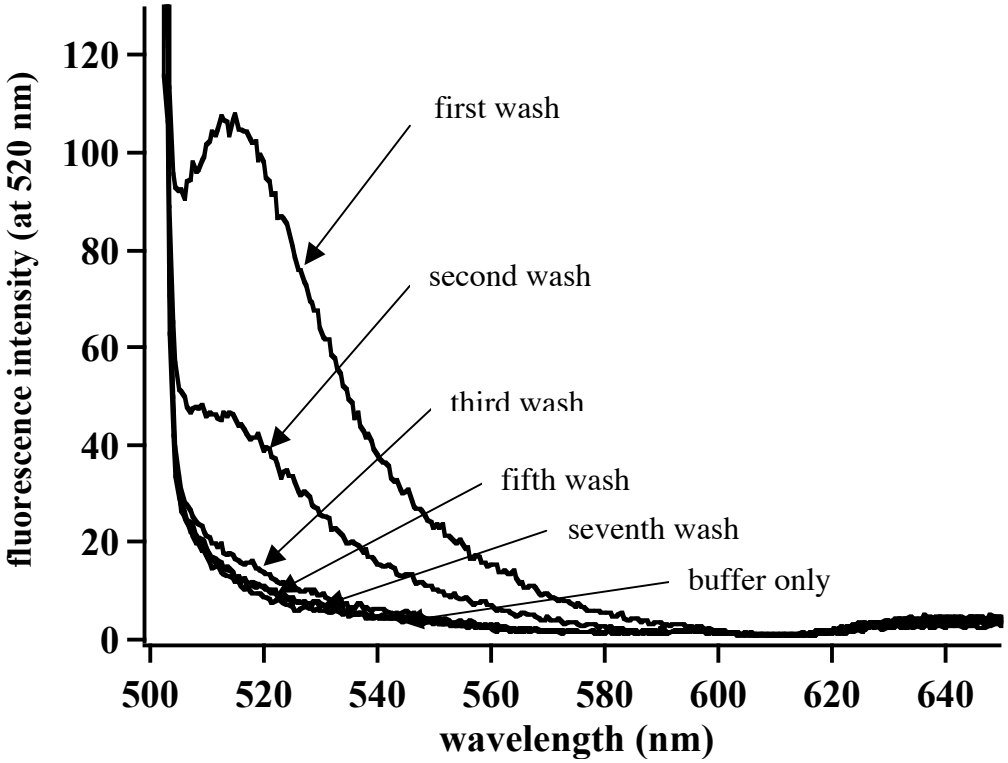

Figure 5.6: Emission spectra of the supernate solutions of the consecutive washes. The first wash was performed after 17 hours of leaching and thereafter consecutive washes were done at 1 hour intervals.

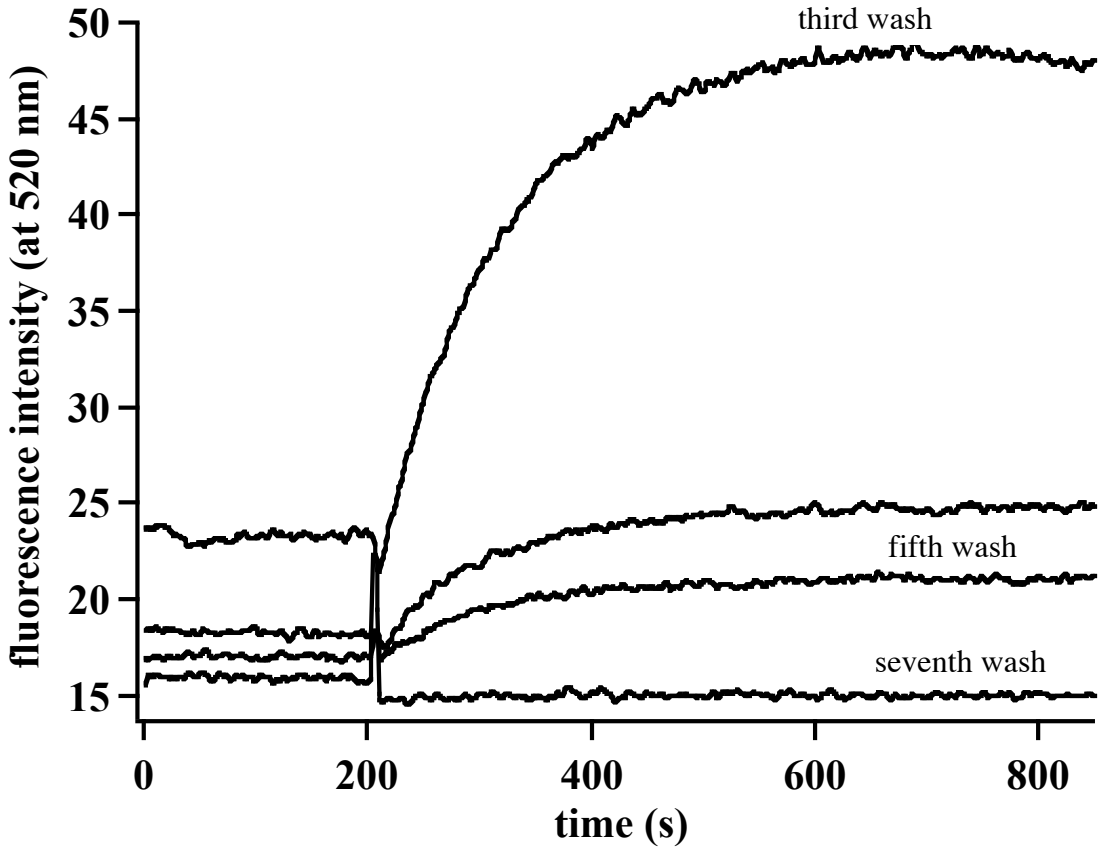

Figure 5.7: Time line monitoring of the fluorescence emission for 4 washes. The enzyme is added at 200 s. The seventh wash shows no traces of substrate in the solution.

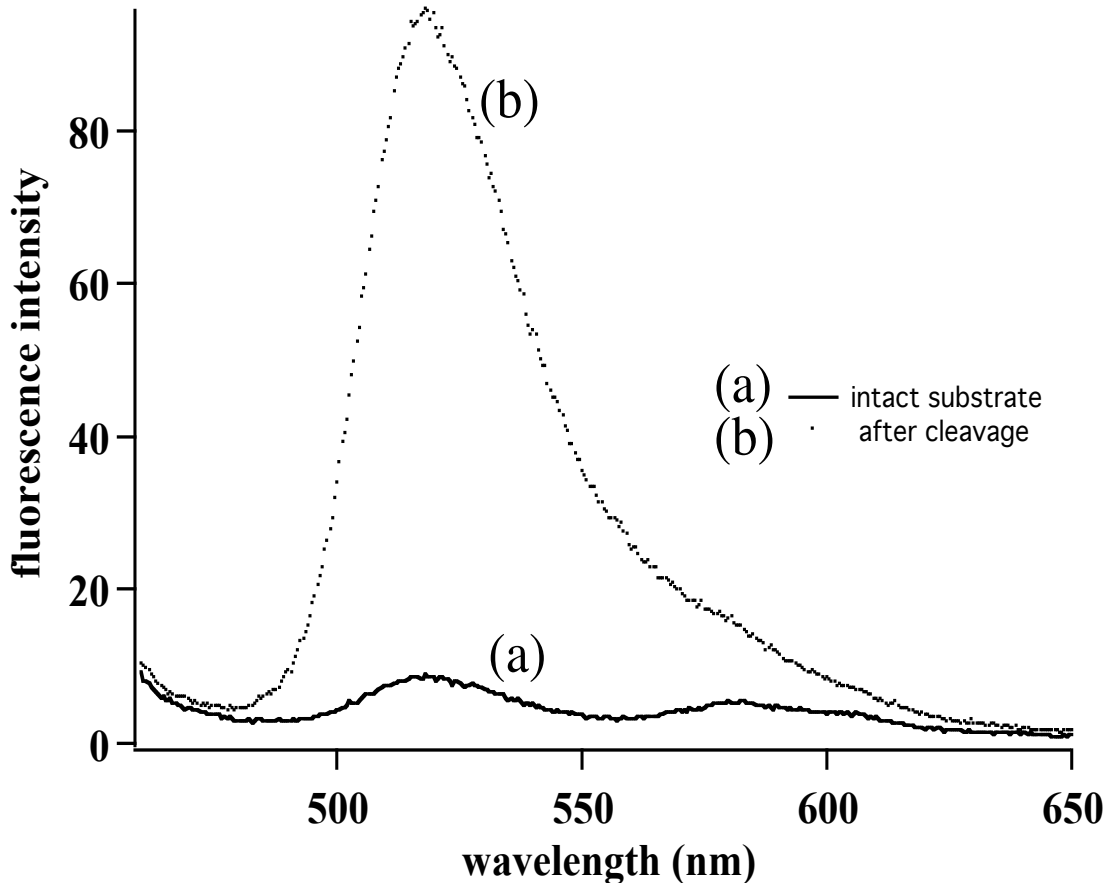

Figure 5.8: Fluorescence emission spectra of (a) buffer solution containing the dissolved substrate only (b) minutes after cleavage by chymotrypsin.

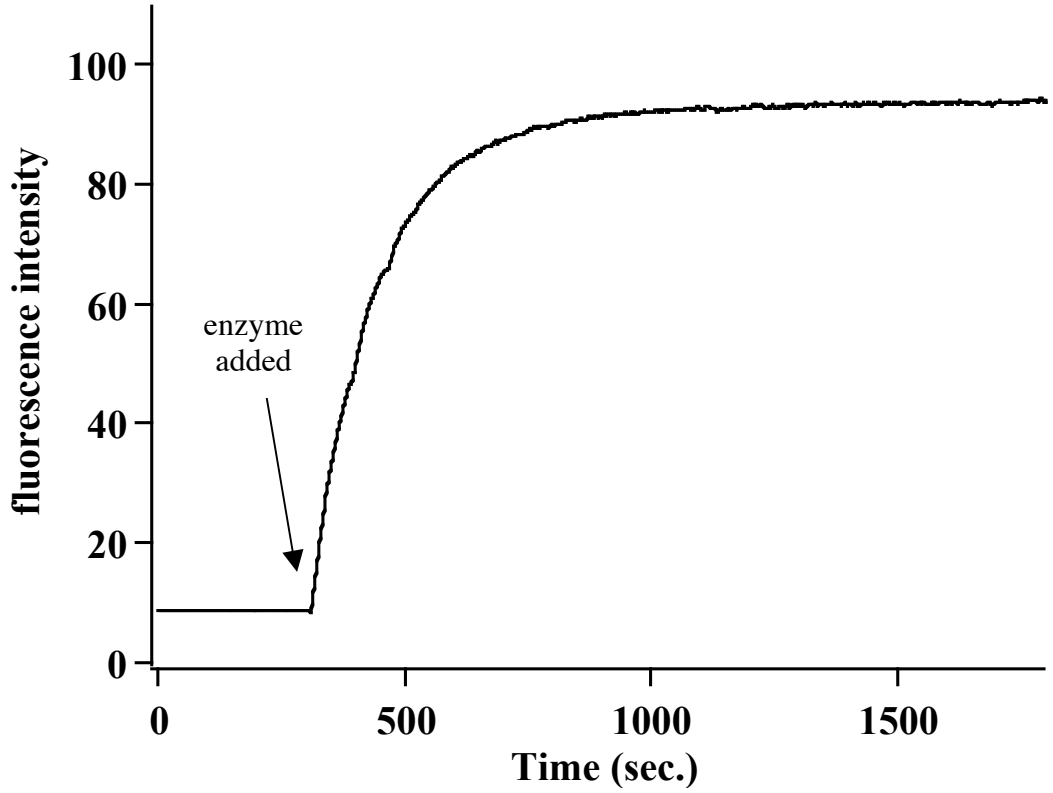

Figure 5.9: Time monitoring of the cleavage of substrate by the enzyme chymotrypsin. The enzyme was added at 300s.
[S] (Fl-TMR)= 1 □M
[E] (chymot) = 10 □L in 1 mL (1 mg/mL)

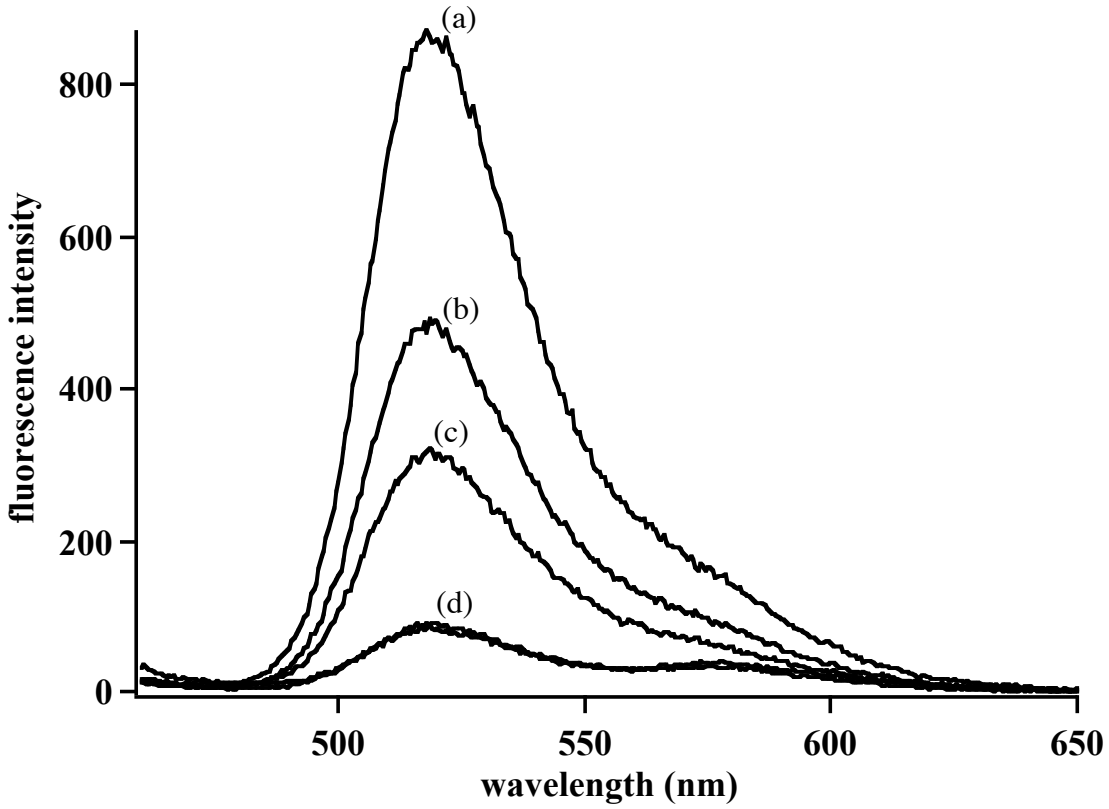

Figure 5.10: Fluorescence emission spectra of the custom peptide 17 hours after reaction started. (a) MMP-9, (b) MMP-8, (c) MMP-3, (d) control (substrate), MMP-1, and 2, which did not respond.

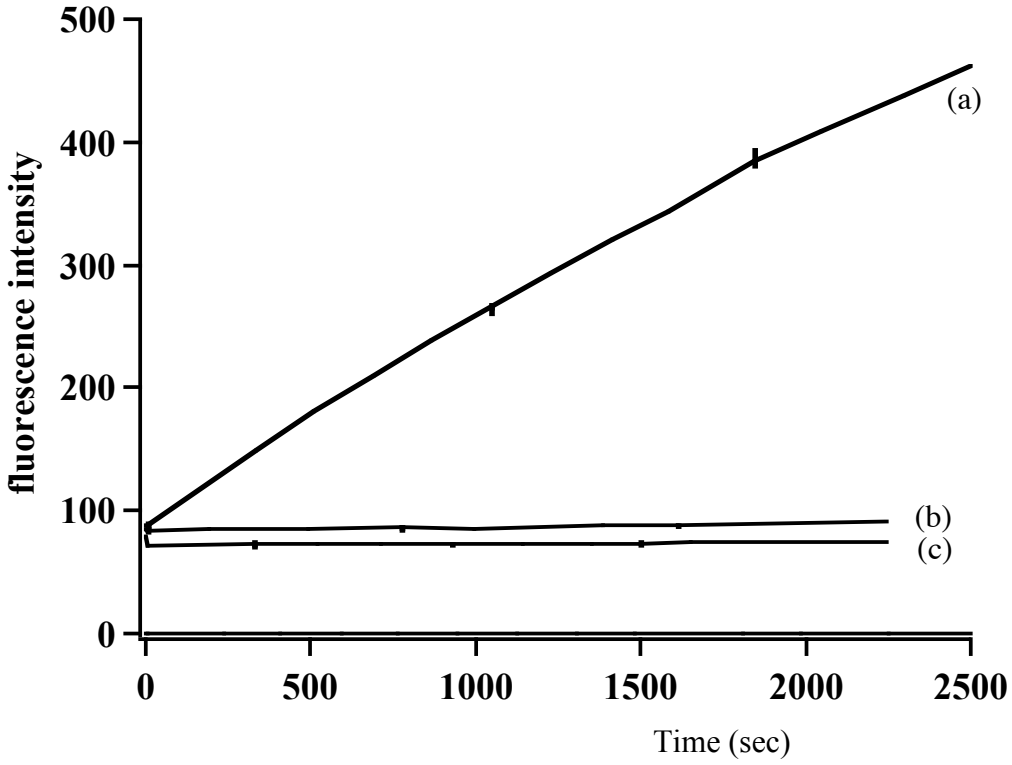

Figure 5.11: Activity of the 3 different enzymes on the substrate (AnaSpec substrate) in solution: a) MMP-3, b) MMP-1, and c) MMP-2.

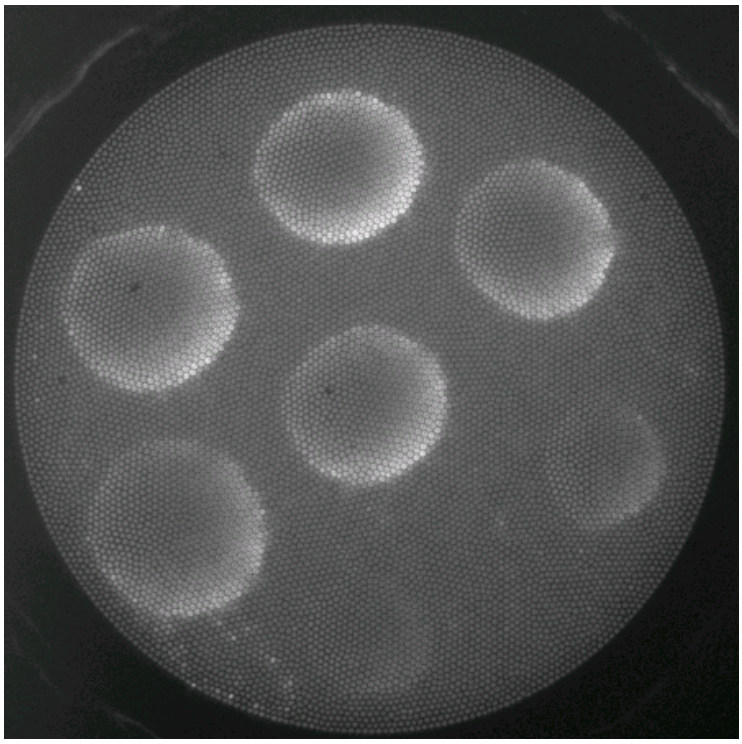

Figure 5.12: printed sensor for the detection of chymotrypsin. The 2 less visible dots are the controls, which are printed microdots containing the polymer formulation only.

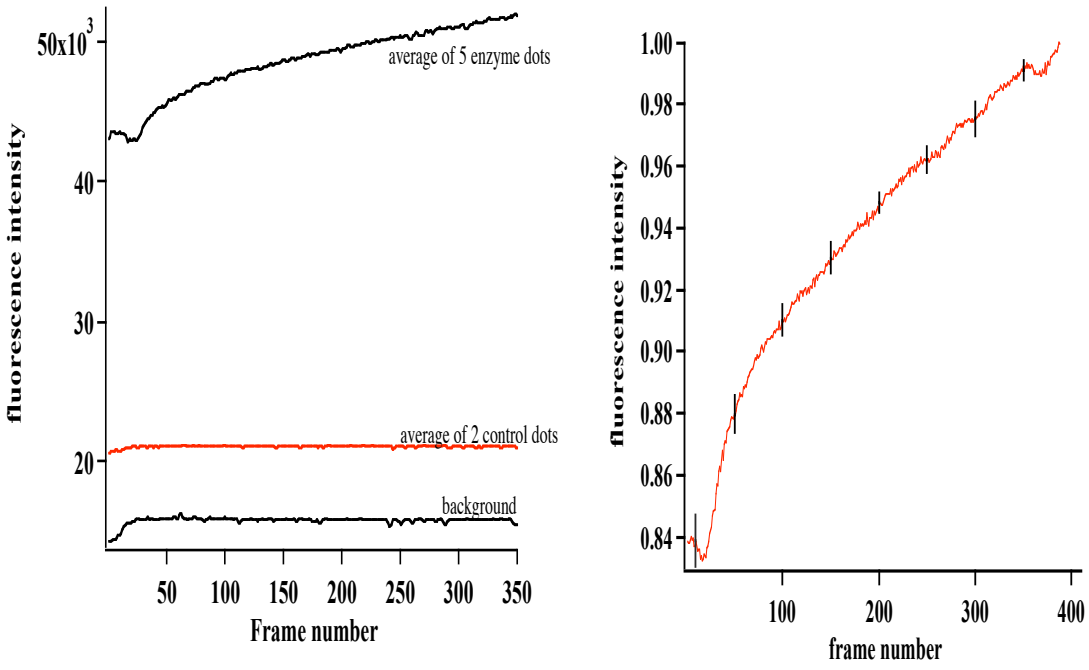

(a) (b)

Figure 5.13: (a) Time-resolved emission of the enzyme sensors as they are cleaved by chymotrypsin, the controls, and the background (area where no polymer microdots have been printed, all exposed to chymotrypsin. (b) enlarged plot of the average of the enzyme sensors with error bars.

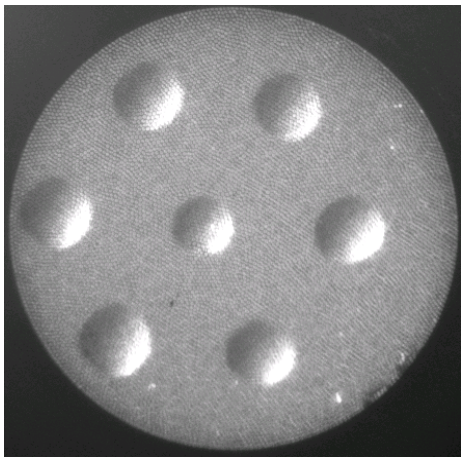

Figure 5.14: MMP-3 enzyme printed sensor. Microdots show similar morphology

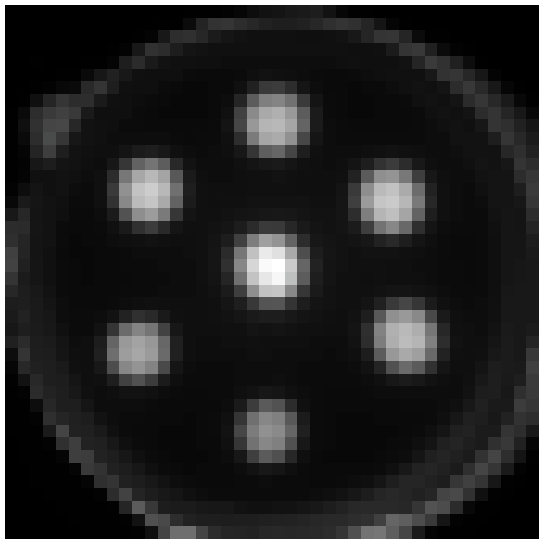

Figure 5.15: 7 X7 binned fluorescence image.

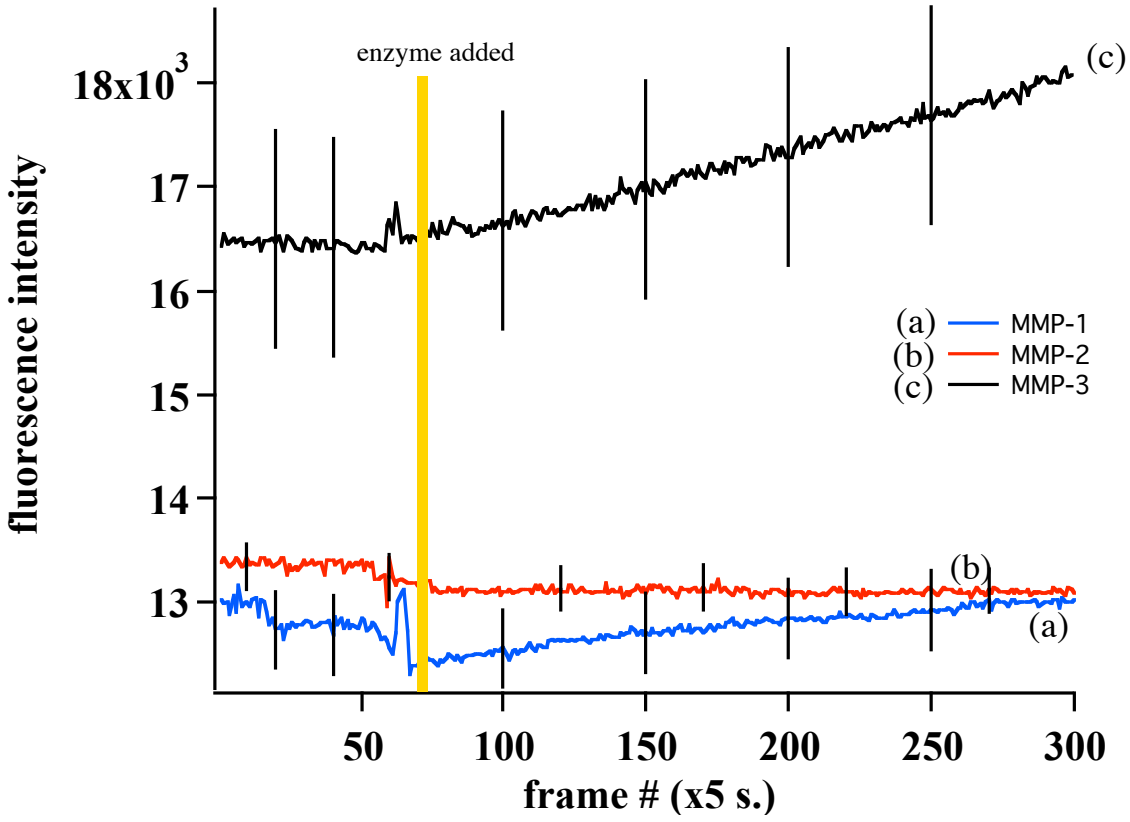

Figure 5.16: Time-resolved fluorescence emission adding the enzyme at the 75th frame for MMP-1, MMP-2, and MMP-3

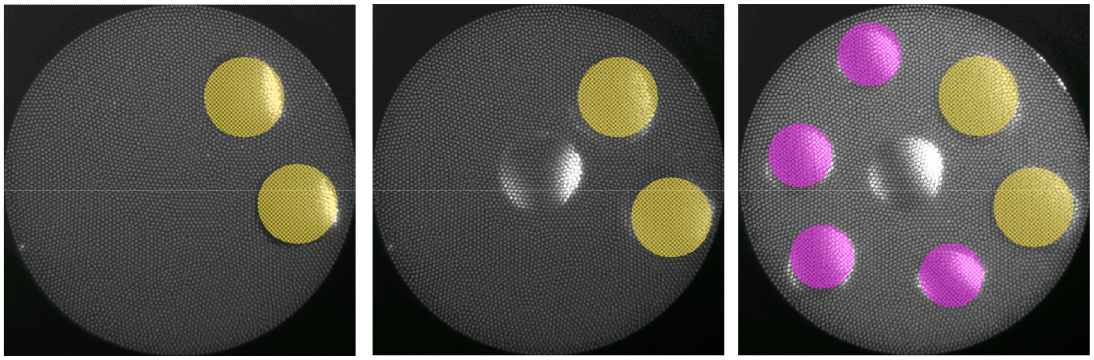

Figure 5.17: Printed multianalyte biosensor: A) 2 pH microdots B) adding a control microdot (center), and C) adding four enzyme microdots

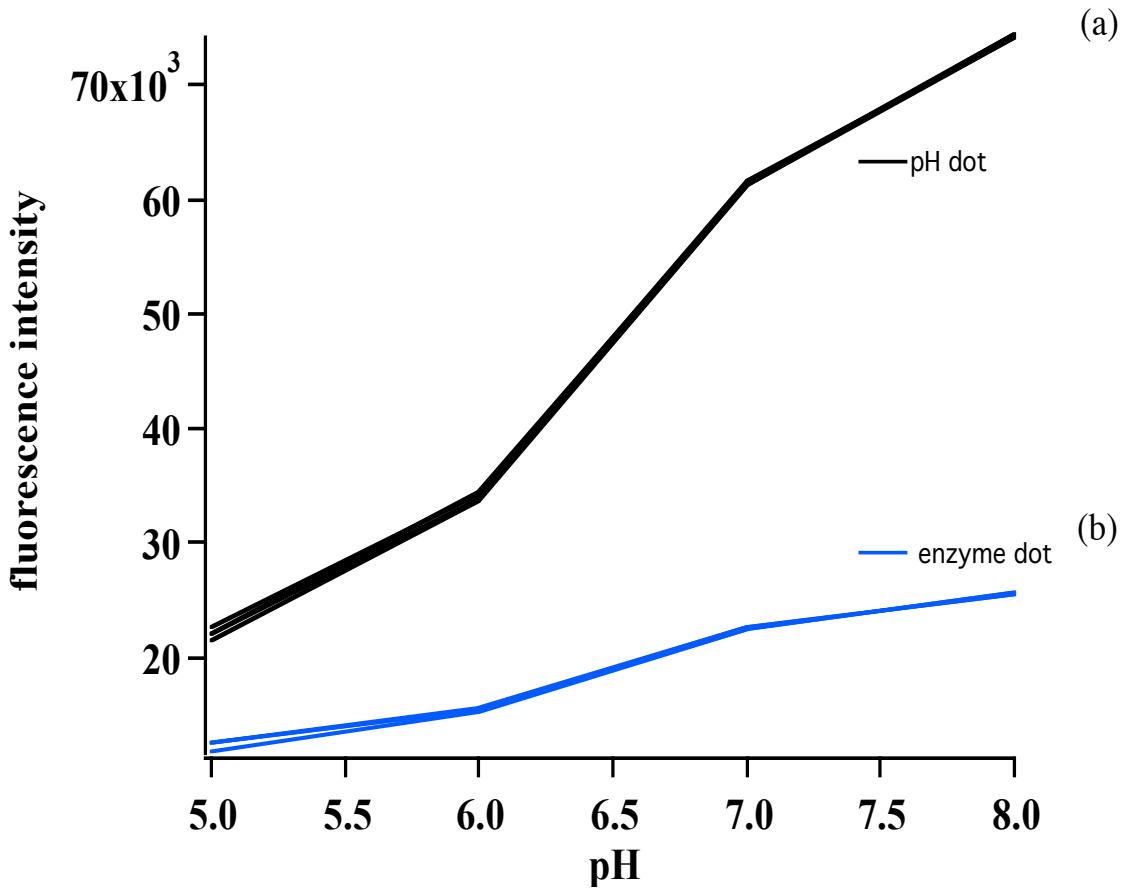

Figure 5.18: pH response of a pH dot and an enzyme dot

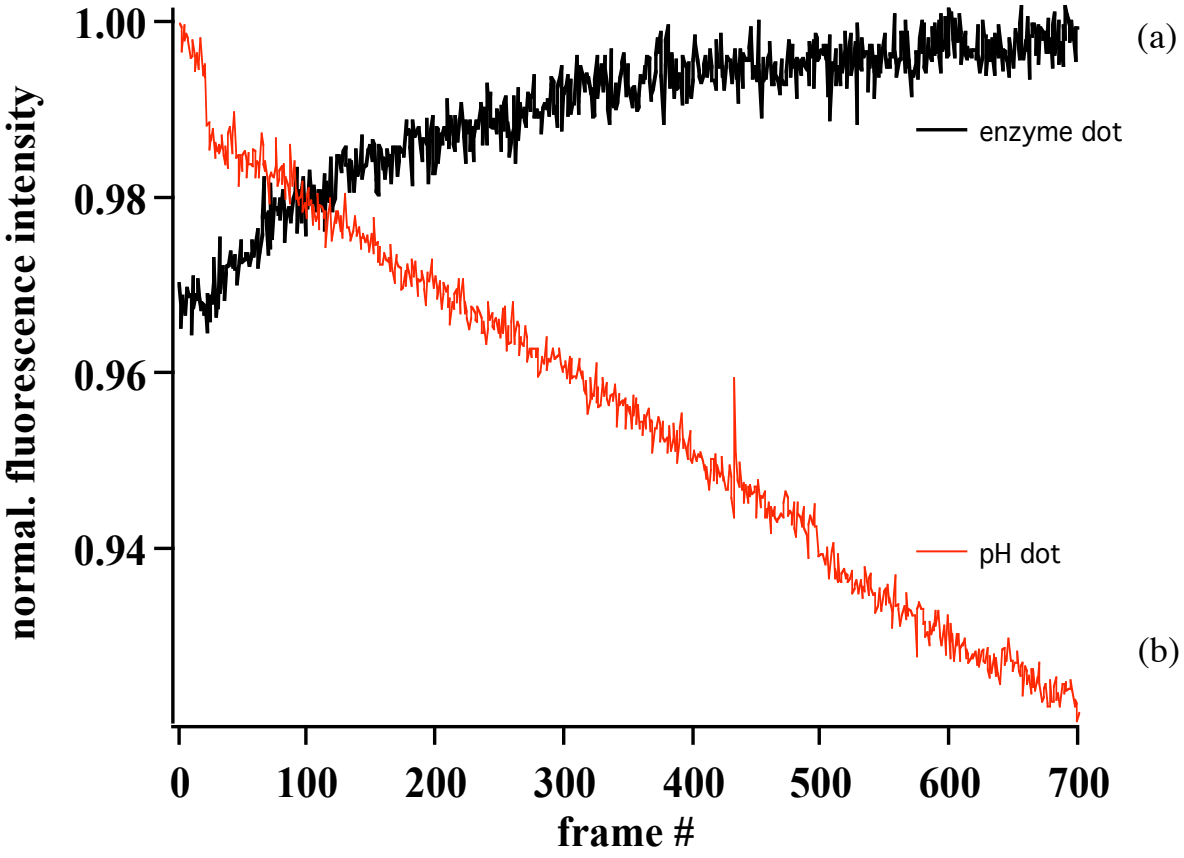

Figure 5.19: Enzyme dot and pH dot in the presence of MMP-3. Enzyme added at the 25 th frame. Enzyme dot responds to the enzyme by cleaving the substrate. The pH dot does not respond to the presence of MMP-3. Instead it shows photobleaching during the exposure to light.

Enzyme	detection method	use fiber	reference
glucose oxidase	total reflectanceFT-IR		[9, 10, 11, 12]
urease			[13]
alkaline phosphatase	chemiluminescence		[14]
bilirubin oxidase	fluorrescence quenching		[15]
choline oxidase			[16]
acetylcholinesterase			[17, 18, 19]
glutamate dehydrogenase			[20]
tolomerase			[21]
cholinesterase			[22]
alcohol oxidase			[23]
acetylcholine and choline	amperiometric		[17]

Table 5.1: enzyme sensor reports

Substrate number and sequence	
5. TMR-Gly-Pro-Leu-Ala-Tyr-Lys-(Fl)-Ala-Arg-NH_2	**no handle**
6. a) LY-Gly-Pro-Leu-Gly-Leu-Arg-Ala-Lys-(5-carboxylTMR)-COOH	**no handle**
b)LY-succinyl-S-Lys(Acryloyl)-Gly-Pro-Leu-Gly-Leu-Arg-Ala-Lys-(TMR)-COOH	**handle**
7. Mca-Pro-Leu-Gly-Leu-Dpa-Ala-Arg-NH_2.AcOH	**no handle**
8. a) 5-FAM-Lys-Pro-Leu-Ala-Nva-Dap(5/6-TMR)-Ala-Arg-NH_2	**no handle**
b) 5-FAM-Lys(X)-Pro-Leu-Ala-Nva-Dap(5/6-TMR)-Ala-Arg-NH_2	**handle**

Table 5.2: Enzyme substrate sequences

Appendix A

Optical Fiber Preparation for Printing/Polymerization

A 5-step procedure was developed for preparing optical fiber image guides for fabricating optical fiber image guide sensors. These steps include glassware cleaning, fiber polishing, fiber cleaning, fiber surface functionalization, and fiber storage. The following is a detailed description of each step (Part 1) along with a materials list (Part II) and description of custom fixtures (Part III).

Part I

Glassware Cleaning

All glassware used for fiber cleaning and fiber surface functionalization are cleaned as follows:

- A 10% (v/v) aqueous solution (tap water) of Alconox is prepared. The inside and outside of all glassware is scrubbed using a sponge and brush followed by a triple rinse (minimum) with running tap water.

- A 10% (v/v) aqueous solution (tap water) of Contrad is prepared. All glassware is filled with this solution and allowed to soak for a minimum of 20 min followed by a triple rinse (minimum) with running tap water.

- All glassware is sonicated for a total of 15 minutes in three steps (5 min each) using three fill solutions, DI water, isopropyl alcohol, and DI water.

    - For the Pyrex dishes, each individual item is carefully placed in a sonicator bath so that the dish floats. The inside of the floating dish is partially filled with a fill solution (so that it does not sink in the sonicator bath) and sonicated for 5 min. The dish is removed and triple rinsed in DI water. This procedure is repeated three times using DI water as the first fill solution followed by isopropyl alcohol as the second and followed by DI water again. [It is important to note that in the case of sonicating with isopropyl alcohol, the dish

is rinsed once in isopropyl alcohol between the triple DI water rinse and placement in the sonicator].

  - The same procedure described above is used for the graduated cylinder with one exception. The base of the graduated cylinder is allowed to rest on the bottom of the sonicator since trying to float this was awkward.

- Each piece of glassware is triple rinsed in DI water.

- All glassware was then placed in a N_2 purged clean oven for 2 hr at 120 degrees Celsius. [see note on Clean Oven Preparation in Part III].

- All glassware remains stored in the oven under N_2 purge at ambient temperature until used. It is not recommended to store glassware for long periods of time before use (i.e. for this work, glassware was re-cleaned if stored beyond 48 hrs).

Fiber Polishing

A requirement for fiber polishing is a sufficiently smooth surface such that high-resolution (4 micron spatial resolution) images are transmitted between the proximal and distal end. The image shown in Figure 1 was acquired by imaging one end of an optical fiber image guide while exposing the opposite end to light. The individually clad fibers within of the optical fiber image guide are clearly visible indicating an ideally polished image guide fiber. To achieve such image quality, both ends of the fiber must be flat, smooth, and perpendicular to the axis of the fiber; otherwise, light will reflect or scatter producing distorted images.

- Image guide fibers (500-micron diameter) are cut to ~18in lengths.

- Both ends of the fiber are coarsely polished (15 or 12 micron grit paper) and viewed with a fiber scope to ensure that any longitudinal fissures in the fiber have been removed. A special fiber chuck, part of the FPH Series (Newport Corporation), allows fibers with diameters ranging from 80 microns to 1millimeter to be removed and replaced repeatedly without damage. More importantly, fibers can be securely held while hand polishing without breaking the fiber and without having to permanently epoxy the fiber tips in connectors.

- One end (herein referred to as the proximal end) of the fiber is connectorized using a standard SMA connector that was predrilled to fit 500 micron image guide fibers. This involves using epoxy to permanently secure the fiber in the connector [refer to manufacturer instructions for epoxy procedure]. Briefly, a bare fiber (18in length) is fed into a transparent plastic tube (~0.03in ID, 16in length) made of fluorinated ethylene/propylene (FEP). Epoxy is then placed in the SMA connector using a syringe. The bare fiber is pushed into the connector until it extends out by a few millimeters. The plastic tubing is then pushed as far as possible into the SMA connector and the epoxy allowed to harden. The FEP tube forms a protective sheath around all but the last 2inches of the distal tip of the fiber. Figure 2 a,b shows the proximal and distal end of a connectorized optical fiber image guide, respectively. [NOTE: SMA connectors were received having a standard pre-drilled diameter of ~125 microns. A standard # 76 drill bit and fiber drill press were used to increase the diameter. The final diameter was achieved using a #78 drill bit].

- Approximately 0.5in polyimide coating is removed from the distal end of each fiber using acetone and a dry Kimwipe [It is only necessary to dip the distal end in acetone for ~10 second or so before the coating can easily be removed with the Kimwipe].

- The proximal and distal ends of each fiber are then polished to a 1-micron finish.

  - The proximal end, having been secured permanently in a SMA connector as described above, is secured to a mechanized fiber polisher using an SMA adapter.

  - The distal end of the fiber is placed in a custom SMA fixture (see Custom Devices/Fixtures, Part III). The fixture is secured to the same SMA adapter (used with the fiber polisher) for polishing the distal end of the fiber.

  It is important to work from higher grit to the desired 1-micron grit finish (e.g. polishing should begin with 12 micron grit paper then 9 micron then 3 micron then 1 micron). This can be accomplished manually if one has the experience and a steady hand; however, a mechanized fiber polisher is more convenient and easier to use. A fiberscope is required for inspecting the progress of fiber polishing.

Fiber Cleaning

Since the fiber preparation process is lengthy, a custom fiber manifold was developed to hold multiple fibers. The manifold (see Custom Fiber Manifold, Part III) was machined from Teflon and allows the cleaning and preparation of up to 20 fibers at a time. The manifold is secured to a swivel base that allows the manifold to be manipulated into different positions for cleaning, functionalization, heating, etc. The cleaning procedure is a modified version found in Bearinger et. al.[1]

- A sonication step is used to clean the distal end of each fiber while secured in the custom fiber manifold. A pre-cleaned Pyrex dish (see Glassware Cleaning above) is carefully placed in the sonicator bath so that the dish floats. The inside of the floating dish is partially filled with a fill solution (so that it does not sink in the sonicator bath). Using the swivel base, the custom fiber manifold is lowered such that the distal ends of the fibers are submerged ~1/2in in the fill solution of the floating dish and sonicated for 5 min. This procedure is repeated three times using DI water as the first fill solution followed by isopropyl alcohol as the second and followed by DI water again.

- A 30% (v/v) piranha solution (i.e. hydrogen peroxide/sulfuric acid) is prepared [place the 100x50 Pyrex dish inside the150x75 dish and partially fill the 100x50 dish with sulfuric acid (~30 ml). Slowly add hydrogen peroxide until reaching 20% (v/v) solution]. The distal ends of the fibers (while secured in the custom fiber manifold manifold attached to the swivel base) are soaked in this solution for no more than 15 min followed by a dip rinse in DI water. [CAUTION - piranha solution is a highly caustic mixture and will initially fume – the reaction is exothermic and must be carried out using appropriate glassware and secondary containers and in an approved hood. Personal protective equipment such as appropriate gloves, lab coat, and eyewear are essential].

- The distal ends of the fibers are sonicated in DI water for 5 minutes as described above in the fiber sonication step.

- The custom fiber manifold is placed in a custom air gun heater (see Custom Devices/Fixtures, Part III) for 45 min at 120 degrees C to dry the distal ends of the fibers. [Once the heating step is complete the heater can be turned off allowing the fibers tips to remain in a N_2 purged environment while awaiting to be functionalized].

Fiber surface functionalization

- A 1.25% (v/v) solution of allytrichlorosilane in toluene (DriSolv) is prepared in a dry N_2 purged glove bag. 75 ml of toluene was decanted into a graduated cylinder using a shlenk line and N_2 purged needle. This was then poured into a Pyrex dish to which 935 microliters of allytrichlorosilane was pippetted.

- The distal ends of fibers (while secured in the manifold) are submerged in this solution for 5 min, all within the N_2 purged glove bag.

- The functionalized fibers are then soaked in toluene (DriSolv) for 1 min. This is repeated a total of three times [it is not necessary to perform this task in the N_2 purged environment].

- The distal fiber tips are then placed back in the custom air gun heater (see Custom Devices/Fixtures, Part III) for 5 min at ~100 degrees Celsius. As soon as the fibers are placed in the heater, the heat source is turned off (and slowly begins cooling) while being purged with N_2. [Once the heating step is complete the heater can be turned off allowing the fibers tips to remain in a N_2 purged environment while awaiting storage].

Fiber Storage

- The custom fiber manifold is designed to be removed from the swivel base. The Telfon fiber holder is then stored in a dry N_2 purged glove bag. [For best results, fibers should be used within several days after functionalization, although fibers could be used after up to 7 days in storage – for this work, this was not studied in detail]. The major risk to long-term storage in a glove bag is the possible exposure to humid air, which can condense on the fiber surface and diminish the ability to print accurately.

Part II

The following sections list the required reagents/materials and describe the custom

devices/fixtures used.

reagents

- Alconox (Alconox, Inc. New York, NY)
- Contrad (Decon Labs, Inc)
- DriSolv toluene (EM Industries Inc., Gibbstown, NJ)
- allytrichlorosilane (Aldrich, St. Louis, MO)
- acetone (Mallinckrodt, Paris, KY)
- DI water
- isopropyl alcohol (EMD Chemical Inc., Gibbstown, NJ)
- hydrogen peroxide (Sigma Chemical Co. St. Louis, MO)

- sulfuric acid (EMD Chemicals Inc. Gibbstown, NJ)

glassware

- 150x75 Pyrex dish
- two 100x50 Pyrex dishes
- four small Pyrex dishes
- 100-ml graduated cylinder.

materials

- optical fiber image guides (Sumitomo, Japan)
- predrilled SMA connectors (SMA 905, Fiber Instrument Sales, Inc., Oriskany, NY)
- fiber optic connector epoxy (Fiber Instrument Sales, Inc., Oriskany, NY)
- epoxy application syringe (Fiber Instrument Sales, Inc., Oriskany, NY)
- epoxy mixer (Fiber Instrument Sales, Inc., Oriskany, NY)
- fiber chuck (Newport, CA, model FPH-DJ)
- bare fiber strain relief (Newport, CA, model FPH-SR)
- drill bits (#76 and #78)
- drill press
- fiber polishing paper (15, 12, 9, 5, 3, 1 micron grit paper) (Buehler, Lake Bluff, IL)
- fiber polisher (Buehler, Lake Bluff, IL)
- Kimwipes (Fiber Instrument Sales, Inc., Oriskany, NY)
- pipettes (Rainin, Oakland, CA)
- sonicator (Bransonic, Danbury, CT)
- glove bag with gas inlet (VWR)
- shlenk line (VWR)
- fiber scope (F1-0111-E, Fiber Instrument Sales, Inc., Oriskany, NY)
- PID controller (Love Controls, series 2600)
- K-type thermocouples (Omega)
- dual channel thermometer (VWR)
- polypropylene tubing (VWR)

Part III

Custom Devices/Fixtures

Custom SMA fixture

The custom SMA fixture, as shown in Figure 3, is a modified FPH series fiber chuck that contains a press-fitted SMA connector on one end and a bare fiber strain relief (black end) on the other end. Part of the longitudinal portion of the modified fiber chuck has been removed to aid the user when introducing a fiber into the device.

Custom fiber manifold

Figure 4 shows a picture of a custom fiber manifold capable of securing 20 optical fiber image guide fibers. The manifold is made from solid Teflon and contains machined channels into which fibers are easily pressed and secured.

Custom air gun heater

A custom heater (Figure 5) was developed using a commercially available hot air gun (Omega engineering). Nitrogen gas is fed (100 SCFH) across the hot filament of the air gun via a 1/4in-diameter polypropylene tube connected to a Prestolok connector as shown in Figure 5. The hot air is directed via a 5/8in-diameter aluminum tube to a custom stainless steel box that disperses the heat. A schematic diagram of the dispersive heater box is shown in Figure 6. A thermocouple positioned perpendicular to the direction of airflow in the 5/8in tube is connected to a PID (Proportional Integral and Derivative) controller for real-time feedback of the temperature. A second thermocouple is placed inside the custom box to monitor, via a dual channel thermometer, the temperature at the coolest point (area furthest from the heater) in the box. Figure 7 shows the custom fiber manifold used in conjunction with the custom heater.

NOTES

Clean Oven Preparation

The silicone rubber gaskets from a newly purchased oven were put through a devolatilization procedure using a custom vacuum pulse and purge oven (developed at LLNL) to prevent degassing and subsequent coating of glassware during heating. The silicone gaskets were removed from the oven and placed under vacuum (20 mTorr) at 200 degrees Celsius for 24hr. At ~4.3 min intervals, nitrogen gas was pulsed into the

chamber thereby raising the pressure to ~1mTorr. This cycle between vacuum pressures of 20 and 1 mTorr was repeated during the entire 24 hr period to remove volatiles from the gaskets. The gaskets were reinstalled in the oven and all surfaces cleaned with isopropyl alcohol including the gaskets). The inside of the oven is periodically cleaned with isopropyl alcohol.

References for Appendix A

[1] J. P. Bearinger, D. G. Castner, S. L. Golledge, S. Hubchak, and K. E. Healy, 1997. P(AAm-co-EG) Interpenetrating Polymer Networks Grated to Oxide Surfaces: Surface Characterization, Protein Adsorption, and Cell Detachment Studies. Langmuir 13, 19, 5175-5183.

Figures for Appendix A

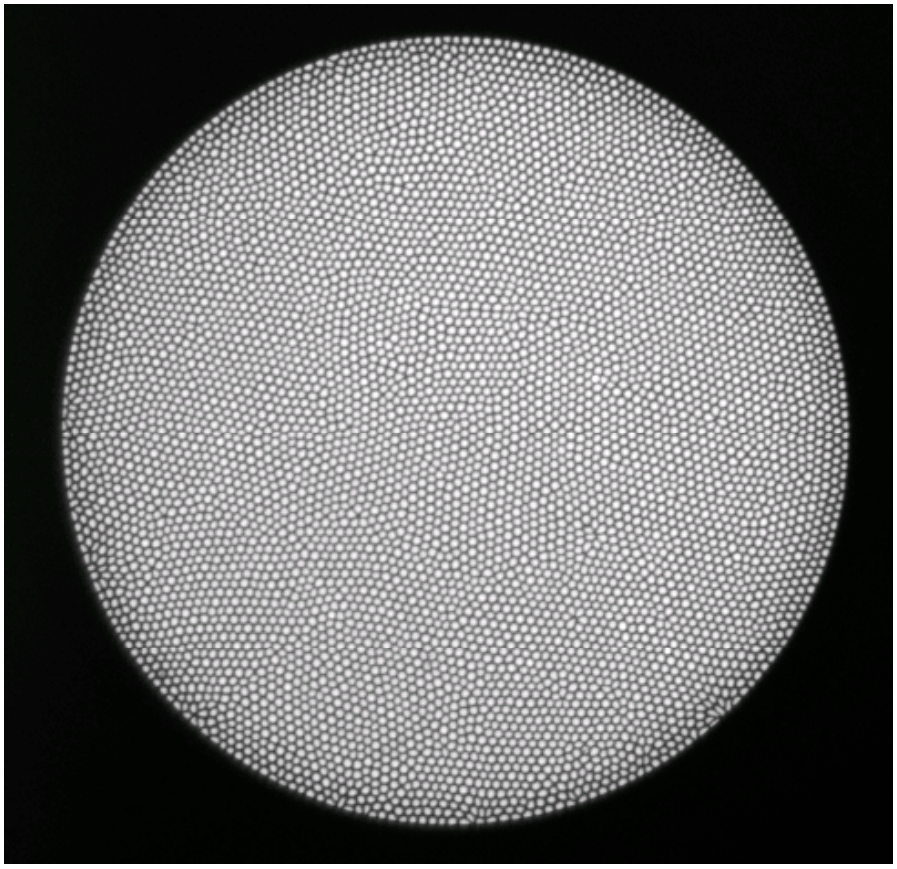

Figure A.1 Image of a 500-micron diameter optical fiber image guide acquired by imaging the proximal end of the fiber while exposing the distal end to light.

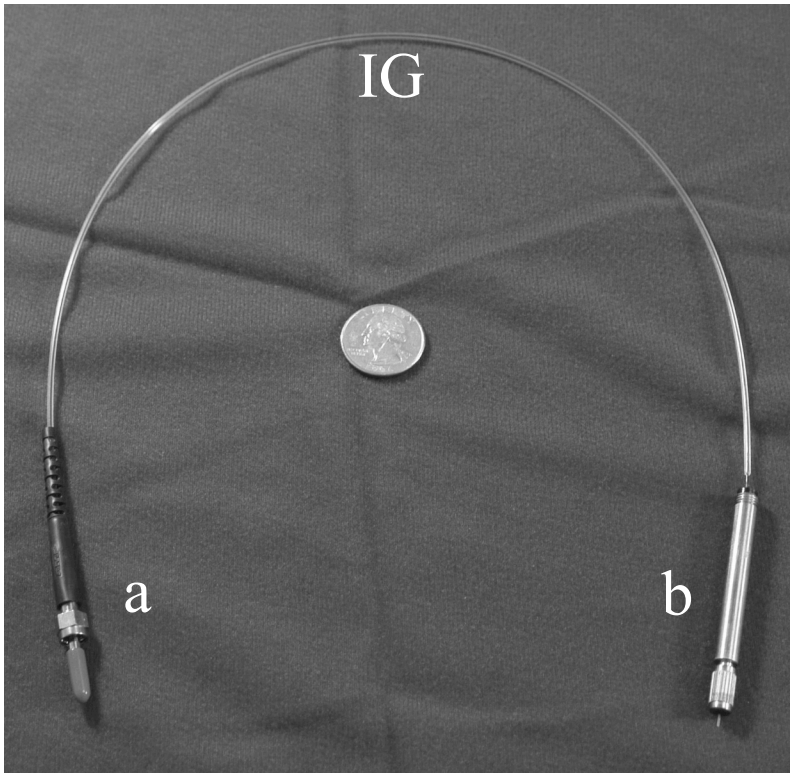

Figure A.2 a,b A 500-micron diameter optical fiber image guide (IG) with (a) a permanent SMA type connector on the proximal end and (2) a removable fiber chuck connector on the distal end, respectively. A quarter is shown for scale.

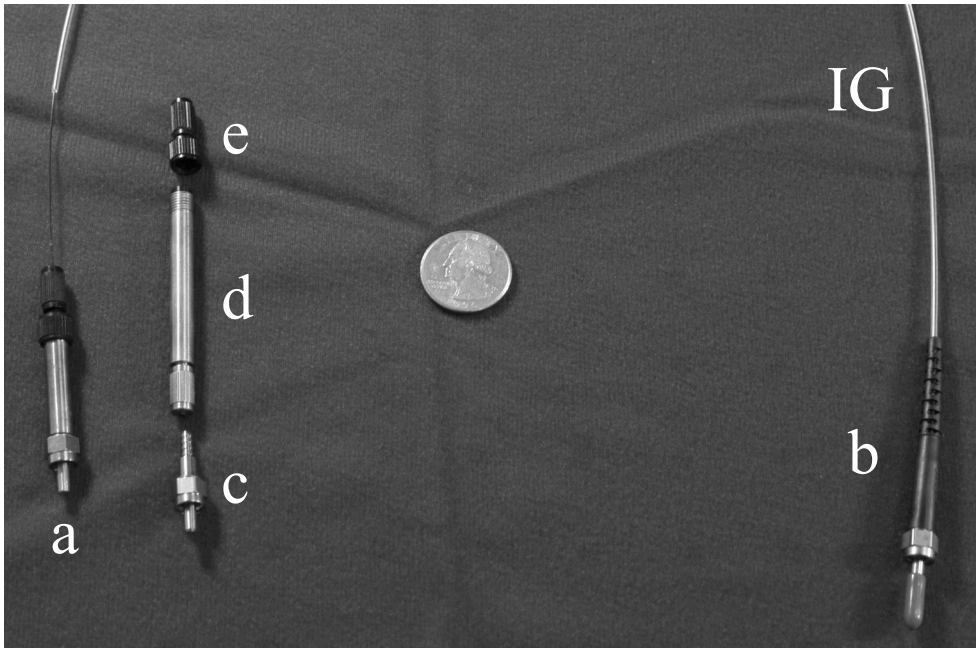

Figure A.3 a,b A 500-micron diameter optical fiber image guide (IG) with (a) a custom fiber chuck connector on the distal end and (b) a permanent SMA type connector on the proximal end, respectively. Adjacent to (a) are the three components used to make the custom connector, (c) the SMA connector, (d) a Newport fiber chuck, and (e) a bare fiber strain relief. A quarter is shown for scale.

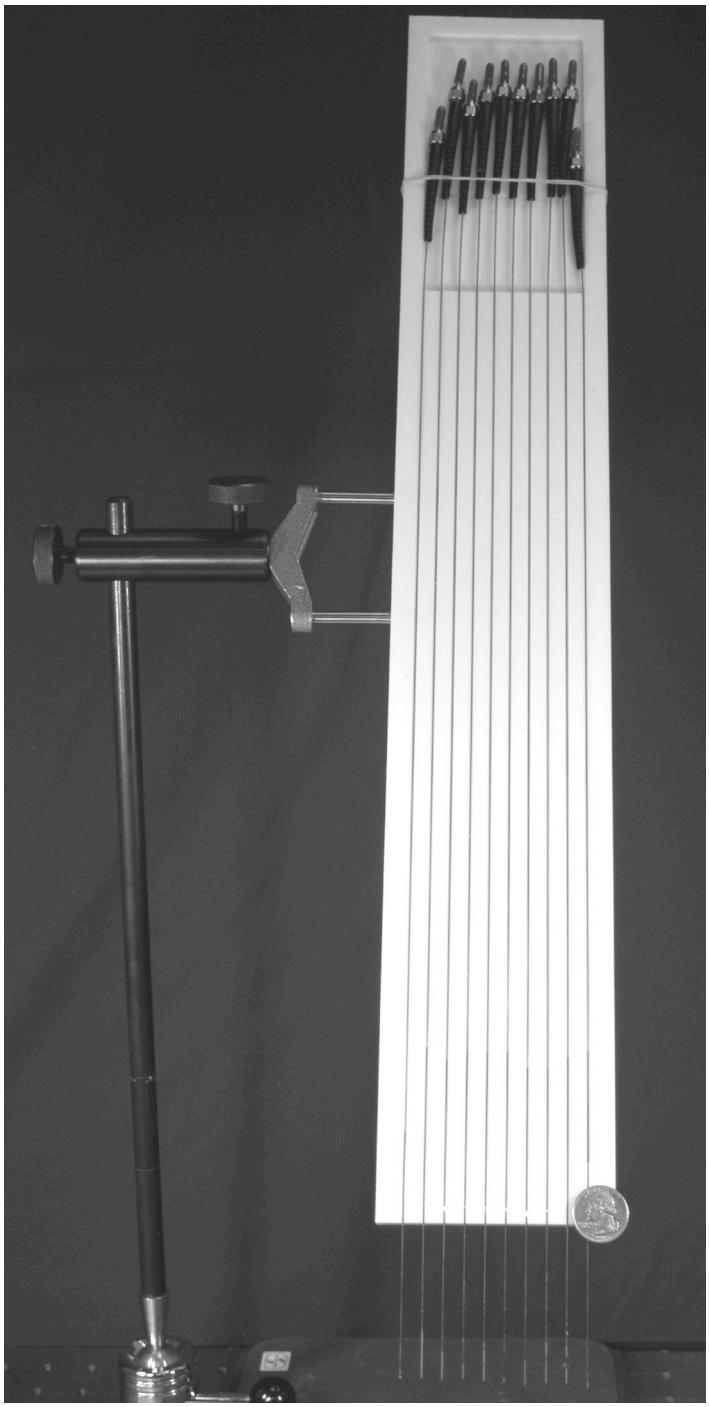

Figure A.4 A custom fiber manifold machined from Teflon for holding up to 20 (10 on the front and 10 on the back side) optical image guide fibers having a 500-micron diameter. All fibers shown are connectorized on the proximal end and bare on the distal end. Only 10 fibers are shown in the picture. A quarter is shown for scale.

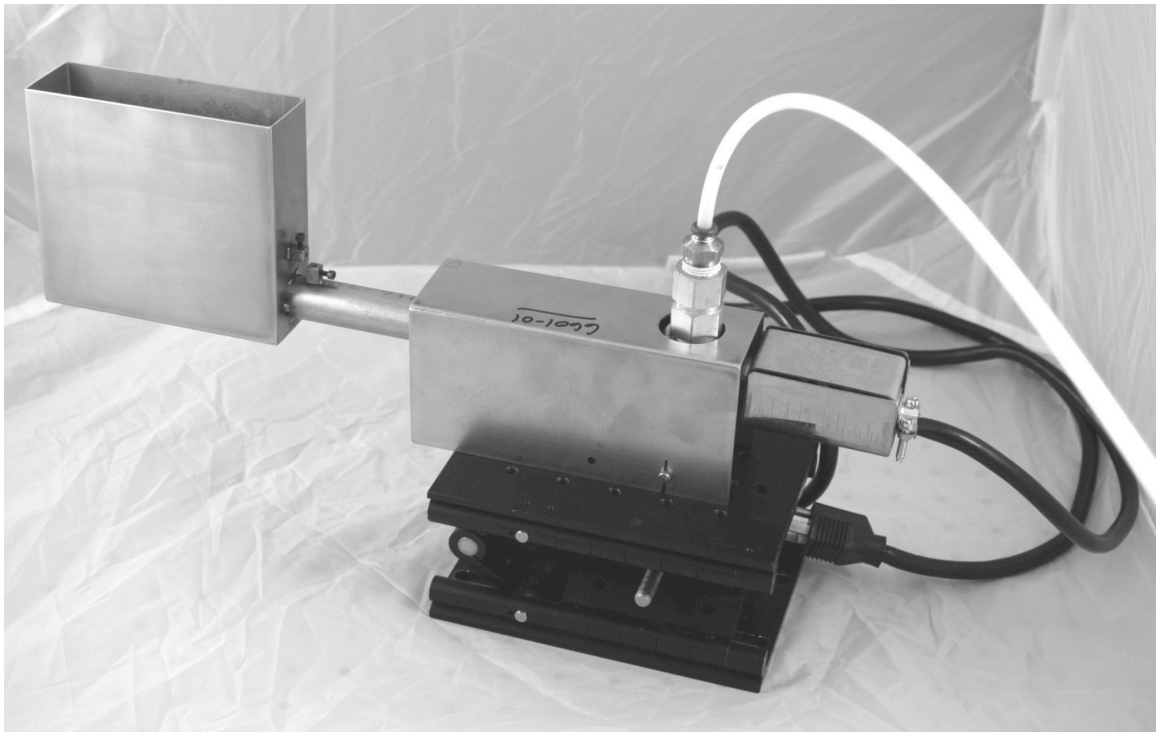

Figure A.5 A custom air gun heater designed to work with the custom fiber manifold for preparing optical fiber image guides.

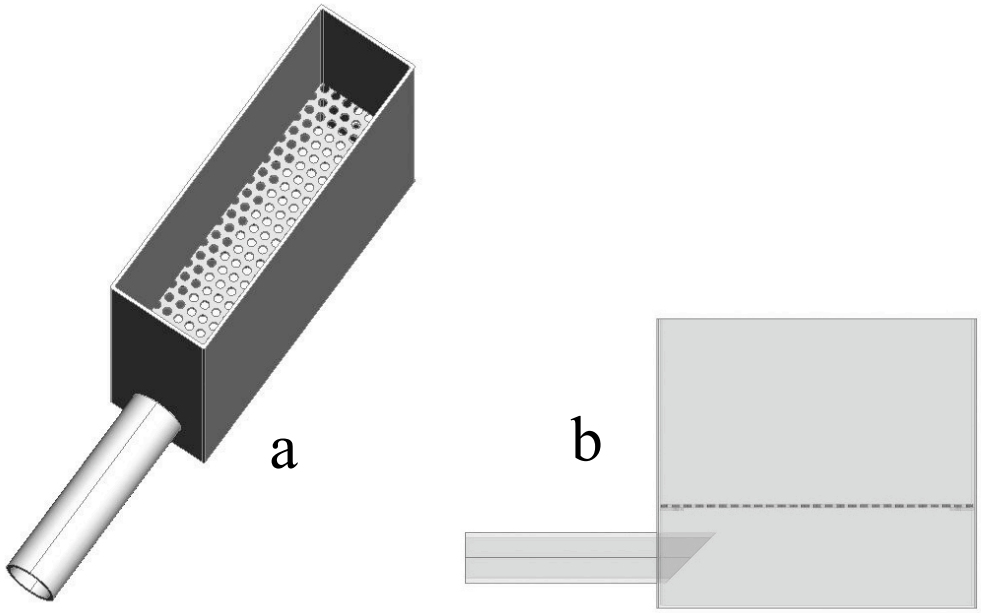

Figure A.6 A schematic illustration of the (a) custom heater box used to disperse heat from the hot air gun. The diagram in (b) shows the relative positions of the stainless steel box, the mesh screen and the gas inlet tube.

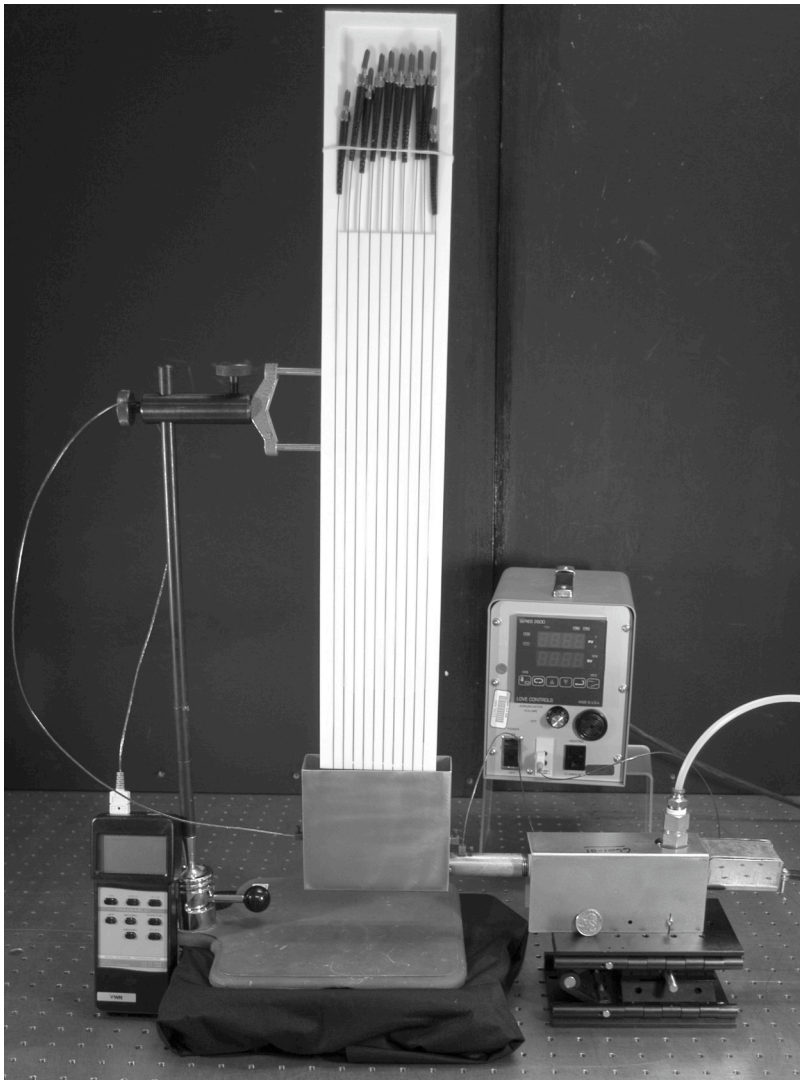

Figure A.7 (a) Custom fiber manifold mated with the (b) custom heater comprised of (c) a dual channel thermometer, (d) a thermocouple for recording the temperature in the heater box, (e) a thermocouple for recording the temperature nearest the tube entrance to the heater box, (f) a PID controller.

Appendix B

Pictures of the Contact-Based Microdispensing Platform

The following pictures are of the contact-based microdispensing platform (described in detail in Section 3) for fabricating optical fiber imaging sensors:

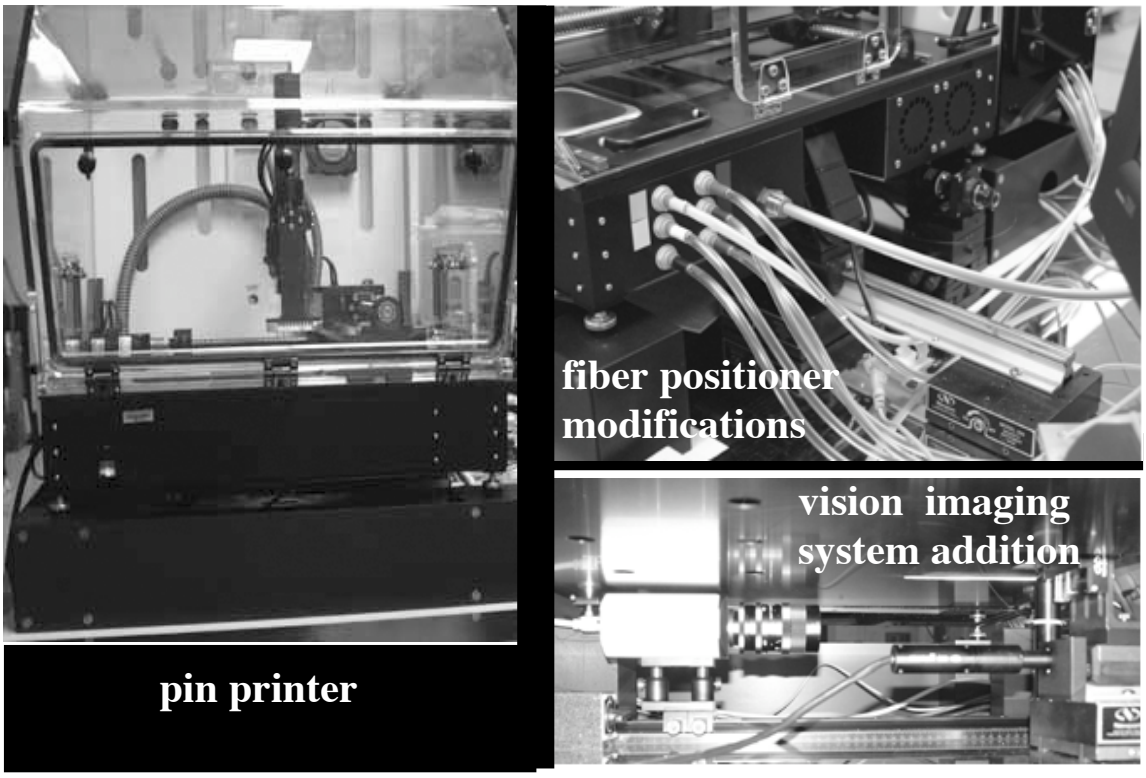

Figure B.1 Pictures featuring the modified contact-based microdispensing system (refer to Section 3.2 for details).

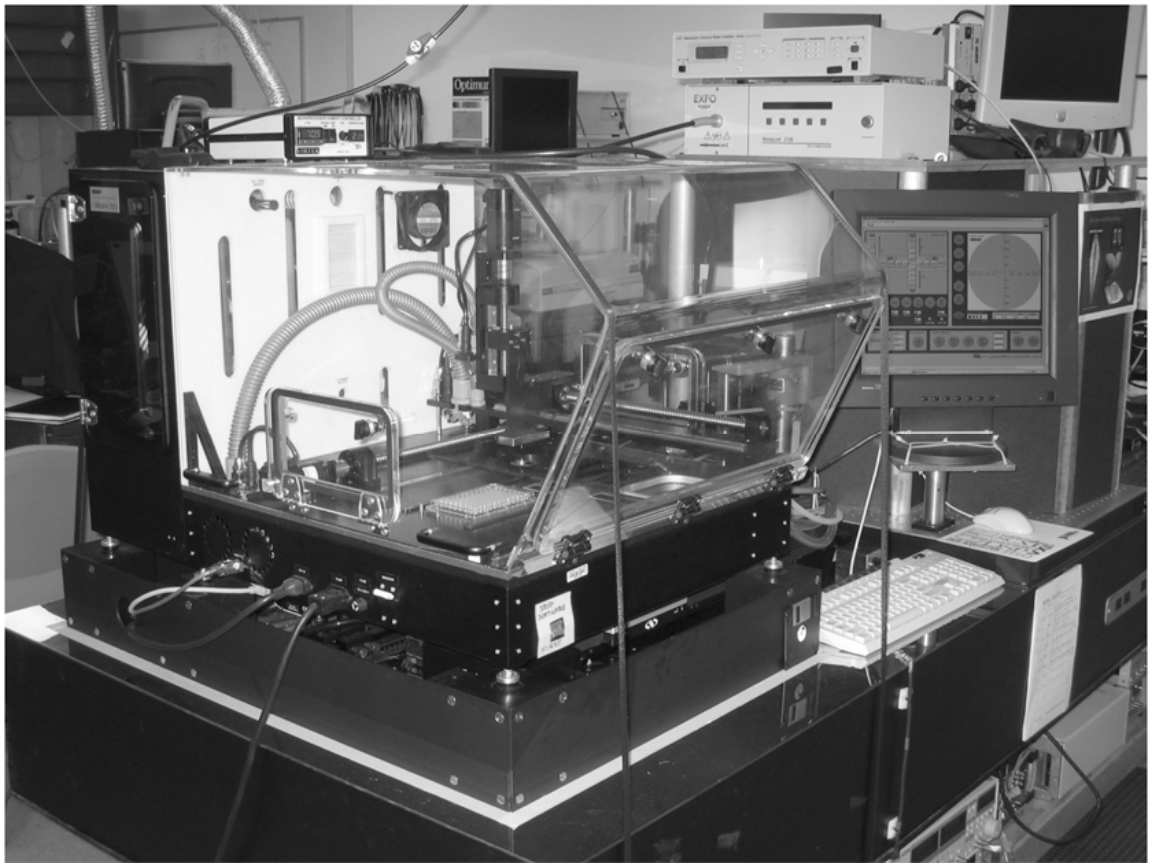

Figure B.2 LLNL's contact based microdispensing system for printing on optical fiber image guides.

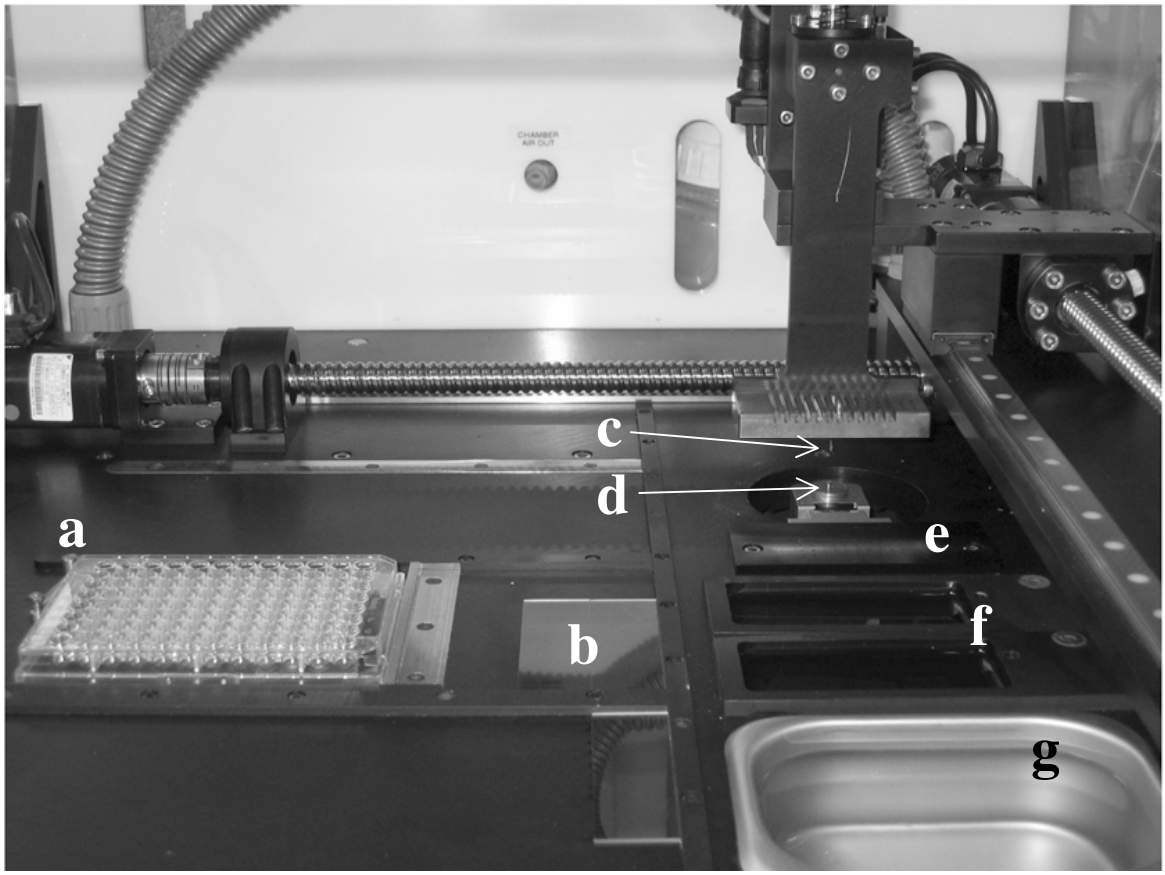

Figure B.3 Internal view of contact-based microdispensing system featuring the (a) sample holder, (b) pin blotter, (c) rigid pin printing tool, (d) optical fiber holder, (e) vacuum, (f) wash stations, and (g) sonicator.

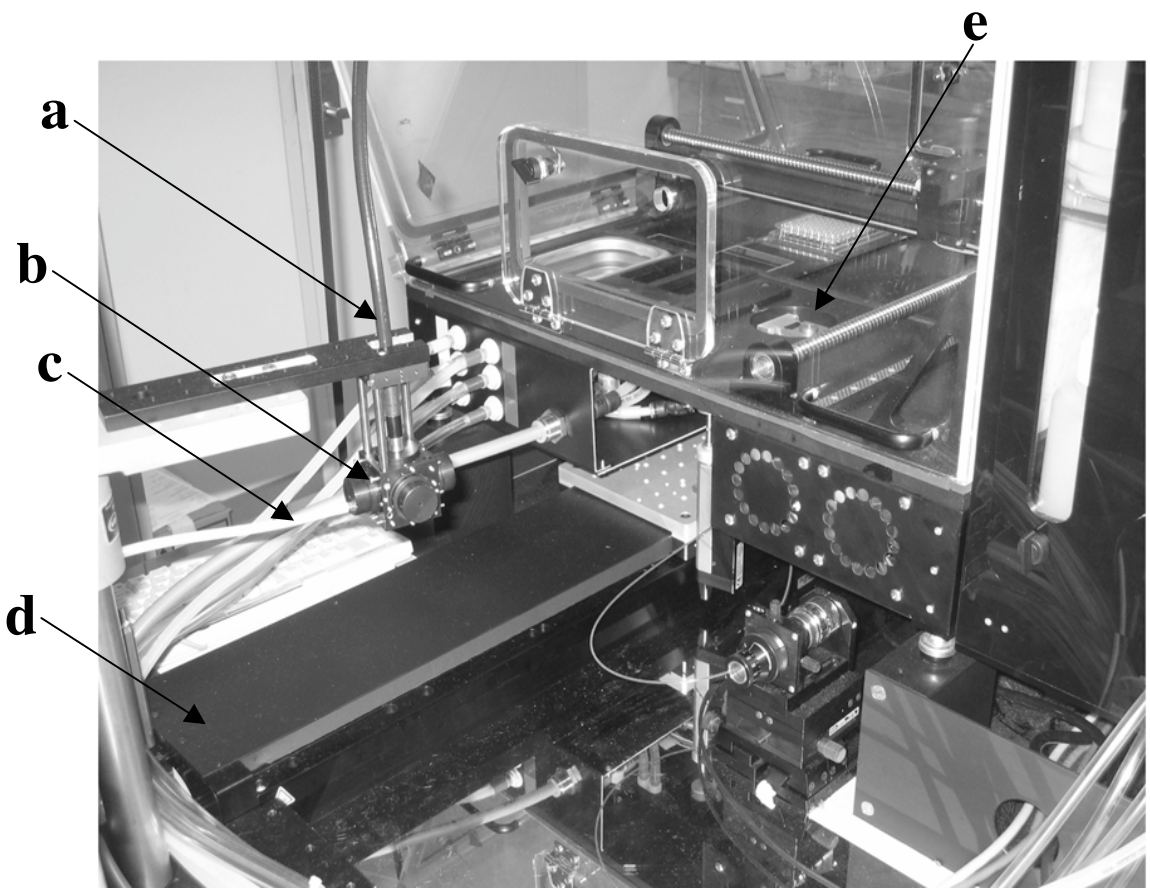

Figure B.4 Picture featuring the (a) uv liquid light guide, (b) polymerization chamber, (c) N gas inlet, (d) horizontal linear stage, and (e) optical fiber holder with fiber.